Hydrogen Storage in Ni/graphene and Pd/graphene Nanomaterials

A Thesis Submitted to the College of Graduate and Postdoctoral Studies

In Partial Fulfillment of the Requirements

For the Degree of Doctor of Philosophy

In the Department of Mechanical Engineering

University of Saskatchewan

By

Chunyu Zhou

PERMISSION TO USE

In presenting this thesis in partial fulfillment of the requirements for a postgraduate degree from the University of Saskatchewan, I agree that the Libraries of this University may make it freely available for inspection. I further agree that permission for copying of this thesis in any manner, in whole or in part, for scholarly purposes may be granted by the Dr. J. A. Szpunar who supervised my thesis work or, in their absence, by the Head of the Department or the Dean of the College in which my thesis work was done. It is understood that any copying or publication or use of this thesis or parts thereof for financial gain shall not be allowed without my written permission. It is also understood that due recognition shall be given to me and to the University of Saskatchewan in any scholarly use which may be made of any material in my thesis.

Requests for permission to copy or to make other use of material in this thesis in whole or part should be addressed to:

Head of the Department of Mechanical Engineering

57 Campus Dr.

University of Saskatchewan

Saskatoon, Saskatchewan (S7N 5A9)

ABSTRACT

Hydrogen is a promising energy carrier that could be an alternative to the traditional carbon based fuels. Hydrogen storage in the Ni/graphene and Pd/graphene systems was investigated in the present work using Thermogravimetric Analysis (TGA).

A laboratory apparatus was designed, built and applied for hydrogenation under pressure. Novel synthesis methods were developed to synthesize the graphene-based composites. Multiple characterizations have been performed to understand the sorbent structures, including the component determination and distribution, chemical state, electronic structure and metal-graphene interfaces. The hydrogen storage behavior was determined, and a hypothesis was proposed to explain the hydrogen performance in the sorbents.

The Ni/graphene (5 at.% Ni, atomic percentage; 100 at.% : Ni + C) composite, charged with H_2 pressure under 1 and 60 bar desorbed 0.14 wt.% H_2 and 1.18 wt.%, respectively, in a TGA apparatus under a flow of argon, at room temperature. The hydrogen release could occur at an operating temperature below 150°C and was completed at 250°C.

The Pd/graphene (1 at.% Pd, 100 at.% : Pd + C) composite, charged under H_2 pressure of 50 and 60 bar released 6.7 and 8.67 wt.% H_2, respectively, in a TGA apparatus under a flow of argon, at room temperature. The 5%Pd/graphene (5 at.% Pd, 100 at.% : Pd + C) composite charged under 60 bar H_2 and dehydrogenated under the same conditions in a TGA apparatus, released 7.16 wt.% H_2. The composites could discharge hydrogen below 100°C and complete the process up to 200°C. The Pd/graphene system releases relatively high hydrogen storage capacity in TGA.

ACKNOWLEDGEMENTS

I would like to express my sincere gratitude to my supervisor, Dr. Jerzy A. Szpunar for being a wonderful mentor, for all his continuous guidance, enthusiasm, support, inspiration and patience throughout the research. Besides, his passion and curiosity for life, energetic attitude also motivate me towards a positive lifestyle.

I greatly acknowledge the advisory committee members: Dr. Hui Wang, Dr. Yongfeng Hu, Dr. Ikechukwuka Oguocha and Dr. Szyszkowski Walerian for the constructive comments. I thank external examiner, Prof. Robert Varin, for his insightful points.

My great thanks go to Mr. Fan Fan and Mr. Xu Wang for the experimental discussions and operations, and for offering kind assistance whenever they could. My special thanks go to Mr. Siyamak Javadian for his kind advice in scientific attitude and methods at my starting phase of project. I also appreciate the beamline scientists Dr. Jian Wang and Dr. Xiaoyu Cui for their kind comments on my research and help with the data collections.

I would like to thank the staff and students from various departments for their friendly, effective assistance and support. The list goes to Mr. Blair, Mr. Dung, Ms. Helen Yin, Mr. Rob Peace, Dr. Daniel Chen, Dr. Ajay Rajaram, Ms. Heli Eunike, Mr. Richard Blondin, Mr. Qunfeng Xiao, Mr. Guosheng Liu and Mr. Bei Yan.

I thank Mr. Tedric Soh, Dr. Nilesh Gurao, Dr. Razavi Tousi, Seyed Salman, Ravikiran Siripurapu and other colleagues in the Advance Materials and Renewable Energy (AMRE) research team.

I acknowledge the Natural Sciences and Engineering Research Council of Canada (NSERC), and particularly express my gratitude to the China Scholarship Council (CSC) for the continuous financial support.

Last but by no means least, my special thanks go to my family: especially my husband and also my best friend Ming Zhu for being with me with great love, ongoing support and understanding;

my dear father for his continuous support and strong spiritual backing. Without their support, it would have been much more difficult to complete a Ph.D. degree.

DEDICATION

This thesis is dedicated to my thoughtful husband and beloved parents for their unconditional love and ongoing support in my life.

TABLE OF CONTENTS

LIST OF TABLES

LIST OF FIGURES

ACRONYMS

BET	Brunauer-Emmett-Teller (BET) Analysis
EDS	Energy-dispersive X-ray Spectrometry
EXAFS	Extended X-ray Absorption Fine Structure
FT-EXAFS	Fourier Transform - Extended X-ray Absorption Fine Structure
NEXAFS	Near Edge X-ray Absorption Fine Structure
SEM	Scanning Electron Microscopy
STXM	Scanning Transmission X-ray Microscopy
TEM	Transmission Electron Microscopy
TGA	Thermogravimetric Analysis (TGA)
XAS	X-ray Absorption Spectroscopy
XANES	X-ray Absorption Near-edge Spectroscopy
XPS	X-ray Photoelectron Spectroscopy
XRD	X-ray Powder Diffraction

CHAPTER 1

INTRODUCTION

Overview of Chapter 1

This introductory chapter briefly outlines the background of the research: the criteria of hydrogen storage, proposed storage materials, and problems to be solved for the storage applications. In addition, the research objectives of this thesis are presented. It also gives a summary of the content of subsequent chapters.

1.1 Overview

Hydrogen as an energy carrier has received considerable attention. The hydrogen-based fuel cells have become commercially available, and these fuel cells could provide a solution to the ongoing depletion of fossil fuel reserves and would contribute to creating a cleaner environment. The fuel cells typically combine hydrogen and oxygen to generate electricity, with heat and water as the byproduct. As the conversion of the hydrogen fuel to energy occurs without combustion, the zero-emission power generation is a highly efficient process[1]. The hydrogen-based fuel cell enables a transition to a safe and renewable energy future[2]. Therefore, the production, storage, and delivery of hydrogen are of great importance to the widespread use of hydrogen. Developing secure, close-packed, dependable, and cost-effective hydrogen storage technologies turns into one of the most technical challenges in the fundamental and applied research for hydrogen economy[2].

The hydrogen used for the fuel cell could be stored as compressed or liquefied gas, a chemical hydride, a metal hydride or in other solid adsorbent materials[1]. Among them, hydrogen storage in solids is the most promising approach to meet the targets, with potential materials of microporous sorbents and metal hydrides being considered[3]. The atomic or molecular hydrogen

bound firmly with other elements in a solid material may enable the storage of hydrogen in larger quantities and smaller volumes at practical conditions[1].

Carbon materials can have diversified forms for the applications. For example, carbon nanotubes (CNTs) are lightweight and have a theoretical surface area of 1315 m^2g^{-1} for single-walled CNTs[4]. However, they contain harmful metallic impurities such as Fe^{56}, Ni, Co, Mo^6, and require a high cost of manufacturing[4]. In comparison, graphene has many favorable features, such as high chemical stability, low manufacturing cost and also can be produced in large quantities[7]. In spite of that, pure graphene cannot secure hydrogen at ambient conditions[8].

To overcome these problems, efforts have been made to combine metals and graphene for hydrogen storage. Such combined system should enable the dispersion of metal and allow functionalization of the graphene and, as a result, should enhance the gravimetric and volumetric storage densities to achieve the similar performance and cost with the gasoline fuel systems. Nevertheless, the relevant critical challenges have not been overcome yet: experimental work on the synthesis of metal/graphene systems has been barely performed; the properties of storage capacity at operational conditions have not been met; the influence of the microstructure of sorbents on the hydrogen storage capacities has not been completely investigated; and the mechanism of hydrogen storage in the sorbents has not been understood.

Among the metals, the Ni particles could stabilize the sorbent structure by altering the geometry of graphene[9,10], catalytically facilitate the hydrogen absorption/desorption performance in nanocomposites[11], and anchor hydrogen as dissociative sites[12,13]. Similarly, Pd particles favorably attract hydrogen at ambient conditions[14–17] and produce a low activation energy barrier to dissociate hydrogen molecules[14,18], thus Pd could greatly improve the hydrogen storage capability[3,19,20]. Therefore, the present work aims at identifying the new materials of Ni/graphene and Pd/graphene nanocomposites with hydrogen storage abilities.

Simple and scalable approaches were developed to synthesize the nanocomposites that allow the industrial productions. As hydrogen sorption is highly correlated with the structure of a sorbent, one can expect to facilitate hydrogen uptake through the adjustment of microstructural

characteristics of the sorbent. By increasing the distributions of metal particles over the graphene surface and strengthening the interaction between the particles and graphene, the microstructures of the sorbents were optimized and stabilized. The local chemistry and electronic structure of the two types of nanocomposites were probed in order to investigate the component interaction within the sorbents. In addition, a custom-made pressure apparatus was designed and constructed for hydrogenation. The impact of pressure on the hydrogen uptake was determined. The conditions of hydrogen uptake and release were thoroughly explored. The properties of the materials were compared to obtain the most favorable candidate for hydrogen storage application, and a mechanism was proposed to explain the hydrogen uptake in these sorbents.

1.2 Research objectives

The main goal of this research was to develop Ni and Pd-decorated graphene systems for hydrogen storage application. The specific research objectives pursued to realize this goal were to:

1. Design, construct and test an apparatus for the evaluation of hydrogen storage.
2. Develop methods to optimize the Ni/graphene and Pd/graphene composite systems for the evaluation of hydrogen uptake capacities in these systems under TGA dehydrogenation conditions.
3. Analyze the composition, morphology, chemical state and electronic structure of the Ni/graphene and Pd/graphene systems.
4. Analyze the Ni/graphene and Pd/graphene systems under TGA dehydrogenation conditions.
5. Determine the mechanism of dehydrogenation in the Ni/graphene and Pd/graphene composites.

1.3 Thesis outline

The relevant work related to the realization of the objectives of this research is described in Chapter 2 to 6. Chapter 2 provides a detailed literature review of the research, including the technological barrier to develop an onboard reversible system for hydrogen storage, the potential storage systems and materials, experimental findings on properties of the storage systems, investigation of the metal-graphene interface, and theory of the hydrogen uptake behavior in sorbents.

Chapter 3 presents the design and construction of a system with controlled operating temperature and pressure for hydrogenation measurements. In addition, the preparation of graphene and metal/graphene composites is discussed. The characterization techniques used in this work are also discussed.

Chapter 4 and 5 discuss the work outlined in the objectives 2 to 5. The synthesis of Ni/graphene composite, the Ni-graphene interaction, and the dehydrogenation characteristics of the prepared composites are discussed.

Chapter 5 describes the chemical state and electronic structure of the Ni/graphene composite that was synthesized by an in-situ chemical method, which was different from that presented in Chapter 4.

Chapter 6 describes the structural characterization, the dehydrogenation characteristics of Pd/graphene composites and a proposed hydrogen uptake mechanism in the composite.

Chapter 7 presents the summary of the results obtained, the conclusions and recommendations for future work.

CHAPTER 2

LITUREATURE REVIEW

Overview of Chapter 2

The evaluation of hydrogen storage is the key factor that determines the success of this research. But, in this process, many important factors need to be considered. This chapter presents a literature review regarding the technologies, and materials used for the determination of hydrogen storage. Graphene as a material used for our composite synthesis is introduced. History of graphene discovery, its preparation methods, various properties and potential applications are discussed. The metal/graphene composite is also discussed, and this involves the property determination, experimental findings, metal-graphene interfaces and hydrogen storage mechanism.

2.1 Hydrogen storage

2.1.1 Technological barriers

Hydrogen carries a high amount of energy per unit mass (142 MJ kg^{-1}). However, this energy carrier has an extremely low density at room temperature and atmospheric pressure[21]. The onboard hydrogen storage is recognized as the main technological subject to automobile applications. The US National Research Council (NRC) and National Academy of Engineering (NAE) identified six technological challenges for the use of hydrogen in the automotive transportation[3,22,23], including hydrogen capture with desirable gravimetric and volumetric densities; commercialization of a cost-effective system. A high cost could result from a complex design, the usage of precious metal, and considerable energy required for the system operation; safety of the system usage; development of an environment-friendly energy-carrier system. Hydrogen is collected as a “fuel” for fuel cell and burned to power vehicles with water as the only end product; development of a high-efficiency energy transition system. It requires a

reversible hydrogen storage unit, and fast release of hydrogen at an operating temperature; and durability for the cycling performance. Some working conditions like the loading cycles, temperatures and impurities may cause system degradation.

2.1.2 Storage technology

Hydrogen can be stored as a compressed gas, cryogenic liquid, non-reversible hydrogen-rich solids and liquids, and by absorption/adsorption in solid state[3,24]. A comparison of types of materials used for storage of hydrogen is shown in Table 2.1[3].

Table 2.1 A comparison of types of materials used for storage of hydrogen[3].

Category / storage method	Material / storage medium	Gravimetric capacity[a] (wt%) (P/MPa)	Volumetric capacity[a] (g L^{-1} or kg m^{-3})	Operating temperature region
Pure H_2	Compressed (70 MPa)	100(70) 4.8, with tank	39.0[b] 23.0, with tank	ambient
	Liquid	100 5.11, with tank	70.8	20 K
Chemical hydrides (hydrocarbons)	Cyclohexane (C_6H_{12})	7.2[c]	28.0	508–623 K[d]
	cis-decalin	7.3[e]	32.7	483 K[f]
	trans-decalin	7.3[e]	31.7	483 K[f]
Chemical hydrides (other)	$NaBH_4$	10.57	113.1	778 K
	$Mg(NH_3)_6Cl_2$	9.2	110	> 400 K
Binary hydrides	AlH_3	10.1	148	< 373 K
Microporous adsorbents	Zeolite-templated carbon	6.9(2.0)	–	77 K
	Na-X zeolite	2.55(4.0)	–	77 K
	MOF-5	5.25(4.85)	31.0	77 K
	MOF-177	7.52(6.85)	32.1	77 K
	trip-PIM	2.7(1.0)	–	77 K
	HCP (BCMBP-based)	3.68(1.5)	–	77 K
	COF-102	7.24(4.0)	29 (excess)[g] 48 (absolute)[g]	77 K
	EOF-2	1.21(0.1)	–	77 K
Interstitial hydrides	TiFe	1.86/*1.5*	100.4/*83.7*	near ambient
	$Ti_{0.98}Zr_{0.02}Cr_{0.05}V_{0.43}Fe_{0.09}Mn_{1.5}$	1.9/*1.3*	*63.6*	near ambient
	$LaNi_5$	1.49/*1.28*	*87.0*	near ambient
	$LaNi_{4.8}Sn_{0.2}$	1.4/*1.24*	*85.4*	near ambient
	$(V_{0.9}Ti_{0.1})_{0.95}Fe_{0.05}$	1.95/*1.8*	*82.0*	near ambient
	Nb_2O_5-doped MgH_2	≈ 7	112.1 [h]	≈ 573 K
Complex hydrides	$NaAlH_4$	7.47/*5.6*	–	373–473 K
	$LiNH_2$.+ 2LiH	10.4/*6.5*	–	≈ 573 K
	$LiBH_4$	18.36/*5–10*[i]/ *13.5*[j]	122.5	453–923 K
	Mg_2NiH_4	3.6/*3.3*	98.8/*87.0*	> 528 K
Clathrates	THF-stabilised H_2 clathrate	≈*1*	–	270–280 K
RTILs	Imidazolium RTIL	–	30	503–573 K
Nanotubes	"Collapsed" BN	4.2(10.0)	–	ambient
	TiO_2	≈ 4(0.6)	–	77 K

Compressed gas. The recently developed system of compressing hydrogen can satisfy the practical storage capacities. For example, the storage of 6 kg of H_2, held in a 260 L vessel at 70 MPa, can be used for the Chevrolet Sequel within a driving range of 160 km. However, this form of storage is unlikely to be commercialized[3]. The considerable weight of the tank is a huge burden to the vehicle, also the tank occupies a large space. Besides, a highly pressurized tank creates an unsafe environment for consumers. Moreover, this form of storage demands a specialized construction material and significant energy to enable the gas compression.

Cryogenic liquid. The liquefaction of hydrogen requires a critical temperature below 20 K-32.9 K (-240.2°C). This form of storage consumes a considerable energy and results in cost-inefficiency[3,24]. Similar to the compressed gas, the cryogenic liquid requires a large-size vessel that is very heavy. Besides, in this method of storage, there are significant hydrogen losses due to the evaporation, which may cause an increased pressure in the container and that leads to safety hazards[3].

Non-reversible hydrogen-rich solids and liquids. Some solid compounds carry a high density of hydrogen. For example, ammonia borane (NH_3BH) contains 19.6 wt.% and 0.145 kg/L of hydrogen. Some hydrogen-rich organic liquids like benzene/cyclohexane (C_6H_6/C_6H_{12}) and toluene/methylcyclohexane (C_7H_8/C_7H_{14}) also have high gravimetric and volumetric densities of hydrogen[23]. However, these non-reversible sorbents require significant energy and efficient catalysts for the hydrogenation and dehydrogenation processes, which are impractical for commercialization.

Absorption/adsorption in solid state. Solid state materials have been proposed as the most promising sorbents for hydrogen storage. This form of storage is defined as the reversible absorption/adsorption of atomic/molecular hydrogen, in which the hydrogen is chemically/physically accumulated with great gravimetric and volumetric densities[25]. Nevertheless, some metal hydrides have low hydrogen capacities, their structures are often degrading, and they require special processing for practical hydrogen storage. The next section will introduce more details on the solid storage materials.

2.1.3 Storage materials

The storage materials are mainly divided into three categories: complex hydrides, interstitial hydrides, and microporous systems. Hydrogen can be stored as bulk metal hydrides. In the case of complex hydrides, atomic hydrogen forms ionic or covalent bonds with the bulk metal, and becomes a part of the host material, such as in alanates ($NaAlH_4$), borohydrides and complex transition metal hydrides (NiH_4 tetrahedra)[23,26]. This system releases hydrogen at temperatures of 100-300°C or sometimes higher[3].

In the interstitial hydrides, molecular hydrogen attaches to the metal surface, and the dissociated hydrogen atoms diffuse into the metal lattice forming a metal hydride[3]. These interstitial metals include some compounds ($LaNi_5H_6$)[27], and binary hydrides (PdH_x[27], MgH_2[28]). Some interstitial hydrides have favorable features for reversible storage, such as low activation energy, low operating temperatures and pressures. However, both types of metal hydrides are rather heavy and that lower the storage densities. Besides, the solid state of metal prevents the penetration of hydrogen. Some hydrides suffer from the high cost of metals.

In the case of microporous materials, hydrogen storage at a temperature as low as the nitrogen boiling point acquires desirable capacities, and this form of storage is known as the physisorption of molecular hydrogen in the porous materials. These materials include some carbon materials (such as activated carbon[29,30], carbon nanotube and graphene[30], templated carbons), zeolites (such as sodalite $Na_8(Al_6Si_6O_{24})C_{l2}$)[31], metal-organic frameworks[32] and organic polymers[3,33]. The materials in this category are light, but impractical because of high temperatures and pressures.

As highlighted in section 1.1, graphene is an attractive host material for hydrogen with favorable features. In particular, it has a low molar mass and high specific surface area. Besides, it shows great chemical stability and is easily functionalized into various forms, which facilitates the development of graphene-based materials for hydrogen storage.

2.2 Graphene

2.2.1 Graphene nanomaterials

Carbon exists as the most captivating element in the periodic table. It serves as the base of all known life on Earth[34]. The carbon atoms can be arranged into diverse allotropes, mainly including the well-known forms of graphite, diamond, fullerene, amorphous carbon, carbon nanotube and graphene (Fig. 2.1)[35]. Among them, graphene has been extensively studied for over one decade. By definition, the term "graphene" was named by Hanns-Peter Boehm in 1962 as a combination of graphite and postfixene[36], and represents a single sheet of graphite[37].

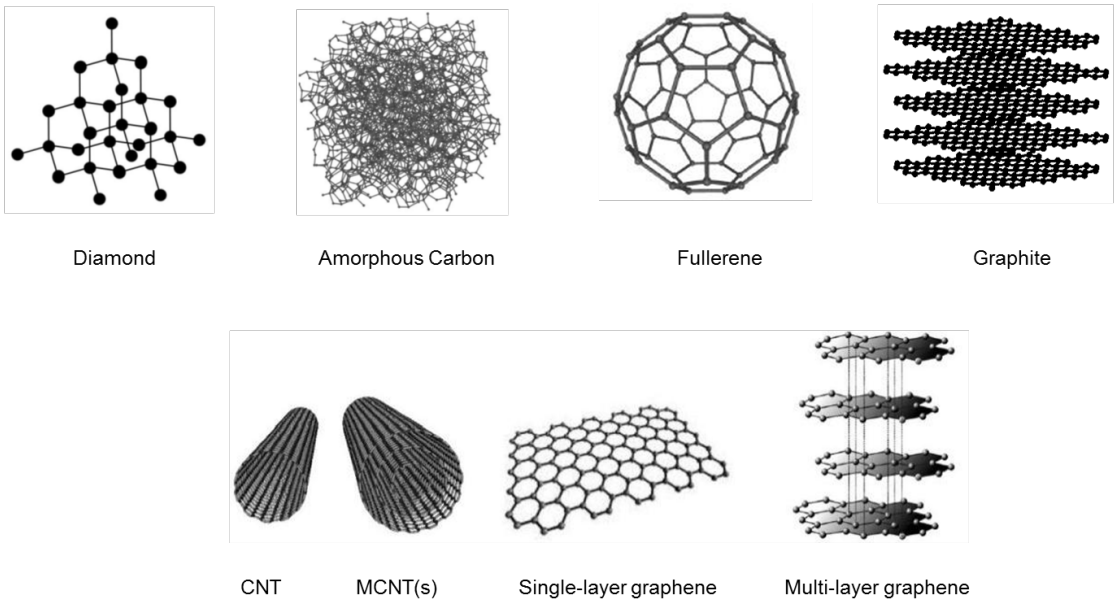

Fig. 2.1 Allotropes of carbon materials[35].

A single sheet of graphene is an atomic layer of sp^2-hybridized carbon densely packed into a honeycomb pattern (hexagonal lattice), in which each atom forms a vertex with a C-C distance of 0.142 nm in a fluctuated plane[3,34,38]. It represents a two-dimensional allotrope of carbon and is recognized as the first two-dimensional crystalline material. This benzene-ring structure is a basic building component for the other dimensional graphitic materials like 0D fullerenes, 1D carbon nanotubes and 3D graphite (Fig. 2.2)[39].

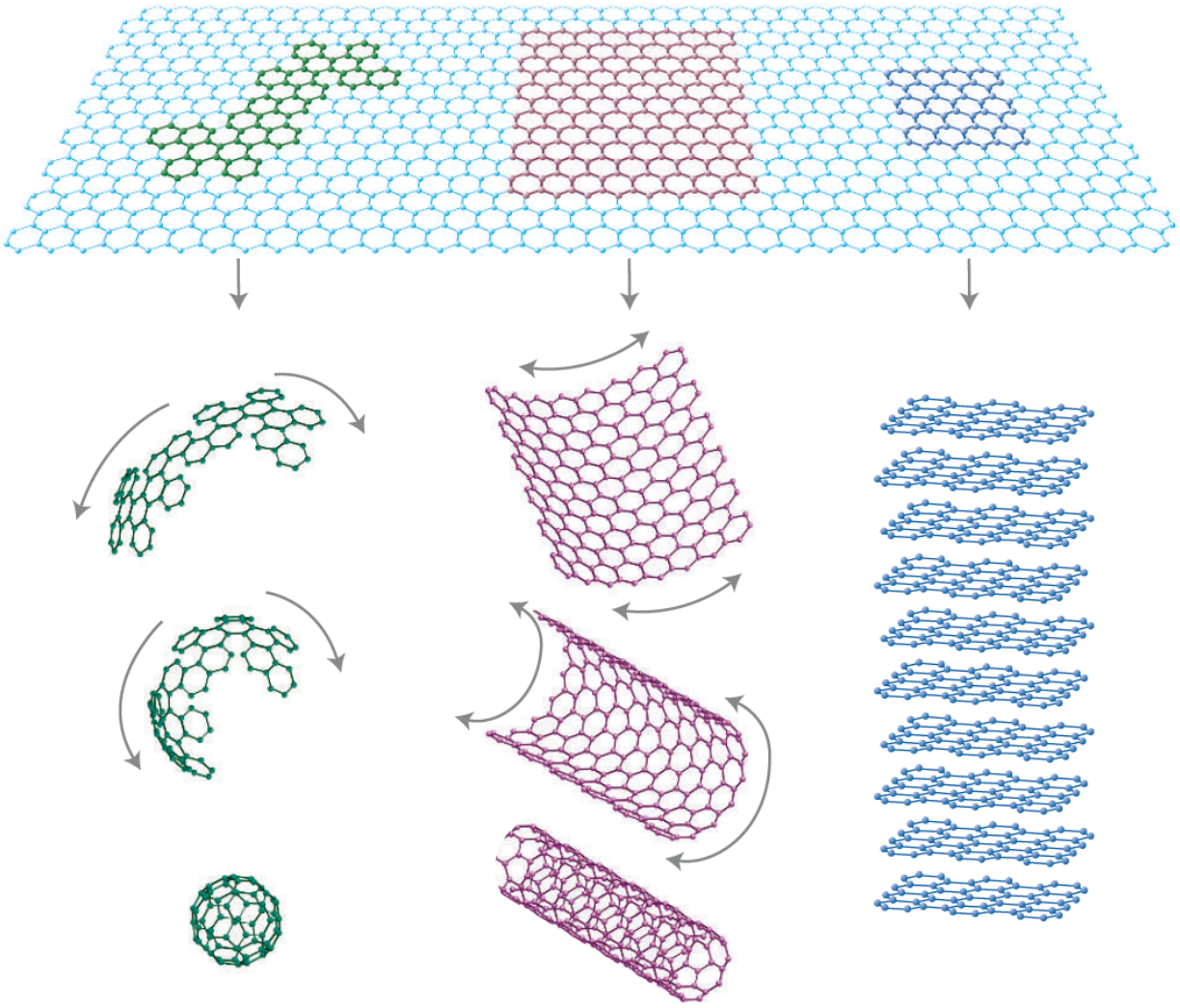

Fig. 2.2 Single layered graphene is the basic component to form the fullerene, carbon nanotubes, and graphite[39].

The research on graphene has been carried out for over one century. It was theoretically explored in 1947[40] and originally observed by using electron microscope in 1961[41]. In 2004 at the University of Manchester, Andre Geim and Kostya Novoselov' team successfully fabricated an isolated mono-layered graphene by simply peeling the thin layers off a graphite crystal with a Scotch tape. This method is called mechanical exfoliation[42]. The high-quality of the two-dimensional material instantly attracted widespread attention. That finding even brought the two discoverers the Nobel Prize in Physics 2010[34]. Up to date, the graphene has been developed into

diverse forms, including monolayer sheets[43], bilayer[44], multilayers[45], nanoribbons[46], oxides[47], ligand/complexes[48], fibers[49], 3D materials[50], reinforced materials[51], aerogels[52], and nano-coils[53].

Due to the variability of state (shape, form, and structure), berthollide characters and insufficient analytical techniques, the chemical structure of this material has been debated for years. To date, the ambiguous modeling still continues[54]. However, the most popular and commonly recognized structural model is the "Lerf-Klinowski model", which was proposed to explain the chemical structure of graphite oxide layer by Heyong He in 1998[55] (Fig. 2.3). Some localized defects could exist in the plane of the graphitic structure caused primarily by the chemical oxidation method[54]. The complex composition makes it extremely challenging to elucidate the detailed reaction mechanism.

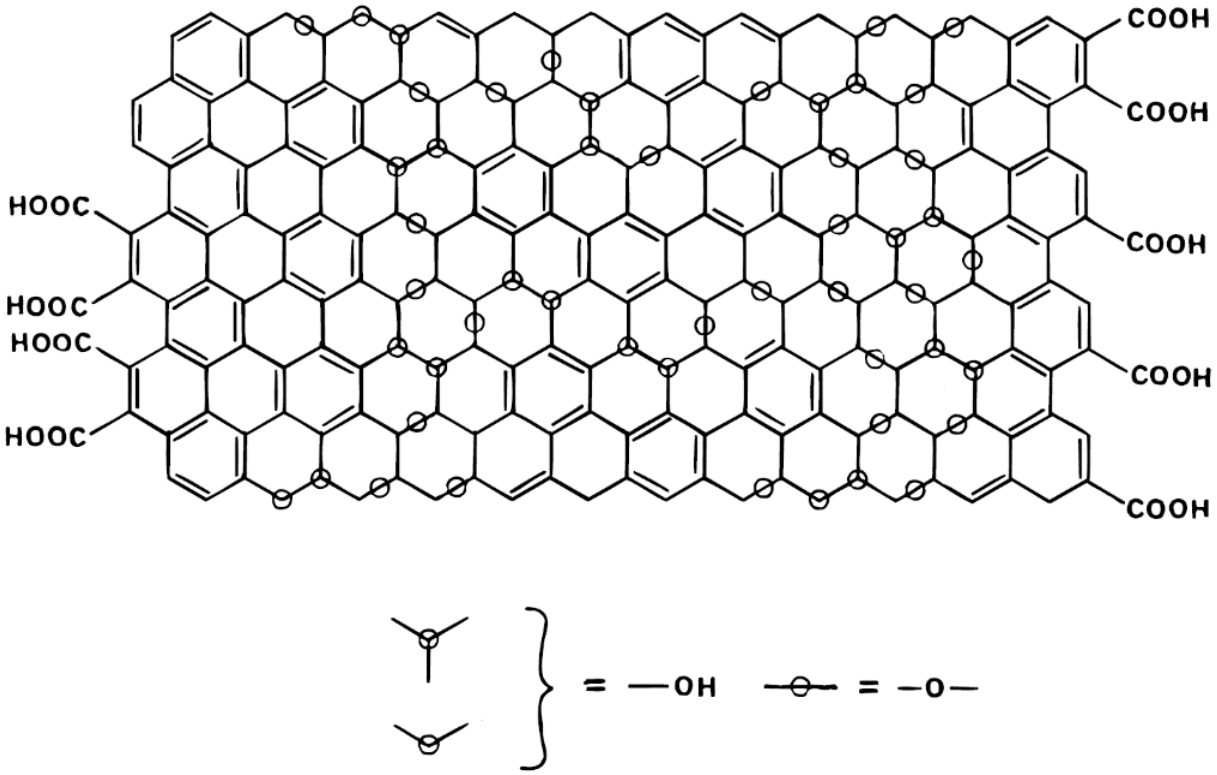

Fig. 2.3 Lerf-Klinowski model of the graphene oxide platelets[55].

2.2.2 Preparation

Various laboratories have been developing preparation methods for graphene manufacturing. The adopted methods include exfoliation[56]. This approach includes adhesive tape split[42], wedge-based exfoliation[57], graphite oxide reduction[58], shearing, molten salts[59] and electrochemical synthesis[60], all these methods could chemically or mechanically split graphite into separate layers. Another method of hydrothermal self-assembly[61], allowing synthesis of graphene by using sugar. The method of chemical vapor deposition (CVD)[62] usually requires a metal catalyst to facilitate the growth of graphene. Other methods like carbon dioxide reduction[63], spin coating[64], supersonic spray[65], microwave-assisted oxidation[66] and ion implementation[67] are less-often used.

Each method has its own advantages and disadvantages. For example, although the "Scotch tape" or peel-off method yields high quality of graphene films[42], it is inefficient for large-scale production. Likewise, the CVD approach requires high temperature and critical gas environment, resulting in cost-inefficiency, and also needs a substrate to grow graphene on it[68].

In this work, a combined approach of the chemical oxidation and mechanical exfoliation was adopted to prepare graphene, which was developed from the modified Hummers' method[69]. It enables the large-scale and cost-efficient synthesis of graphene. Unavoidably, the products contain some irregular shape of sheets and multiple layers of graphene due to the complex processing. Additionally, the oxygen-containing groups are hardly eliminated from the planes of graphene by using the chemical reduction method. Thus in this work, both the reduced graphene oxide and the graphene oxide are considered as "graphene".

2.2.3 Properties and applications

Researchers, especially from the areas of physics, chemistry and materials science, have been exploring many potential properties of graphene. In particular, graphene is a good electrical conductor[42]. The electrical conductivity makes it rather promising for the design of electronic devices. The potential products include the field effect transistors, sensors, transparent conductive films and clean energy devices[70]. Additionally, graphene is harder than diamond.

Especially the defect-free and processed graphene has remarkable fracture strength and tensile strength[70,71]. These mechanical properties may greatly facilitate the fabrication of a new generation of super-strong materials. Further, the optical transitions of graphene are layer-dependent, and can be adjusted via the electrical gating[70,71]. The optical properties may enable its usage on the infrared optics and optoelectronics[72]. Moreover, graphene also shows a super thermal conductivity that is dominated by phonons[73]. The thermal conductivity of single-layer isolated graphene at ambient temperature could reach 3000-5000 W m^{-1} K^{-1} with the value varying based on the size of sheet[74]. This property can be applied to the electronics for thermal management. Besides, graphene can also be utilized to the areas of membranes, biomedical fields, composites and coatings, energy and many other areas. In the field of energy storage, the graphene-based nanomaterials can be fabricated to store hydrogen physically and chemically. For example, the material can electrochemically store energy in rechargeable batteries as supercapacitors[8,38].

2.3 Hydrogen storage in metal/graphene

2.3.1 Methods for hydrogen storage

The measurement techniques can be divided into three categories: gravimetric, volumetric and temperature-programmed (or thermal desorption) approaches[3]. Fig. 2.4 displays the typical schematic diagrams of these techniques[75–77]. The gravimetric systems are mainly assembled with a microbalance that is mounted in a pressure-rated, vacuum-rated and hydrogen-compatible chamber. These gravimetric approaches determine the amount of hydrogen uptake and hydrogen release by monitoring the change of sample weight[75]. The volumetric systems are installed with fixed, known-volume vessels. These methods determine the hydrogen storage capacities by determining the variation of the hydrogen pressure or volumetric flow rate. These two categories of techniques plot the hydrogen sorption isotherm versus hydrogen pressure at fixed temperatures. The temperature-programmed techniques determine the amount of hydrogen release at elevated temperatures, and the hydrogen desorption amount is plotted as a function of temperature. Other techniques, such as thermal analysis and calorimetry, surface area and pore volume determination, powder diffraction, can be used as complementary analysis[3].

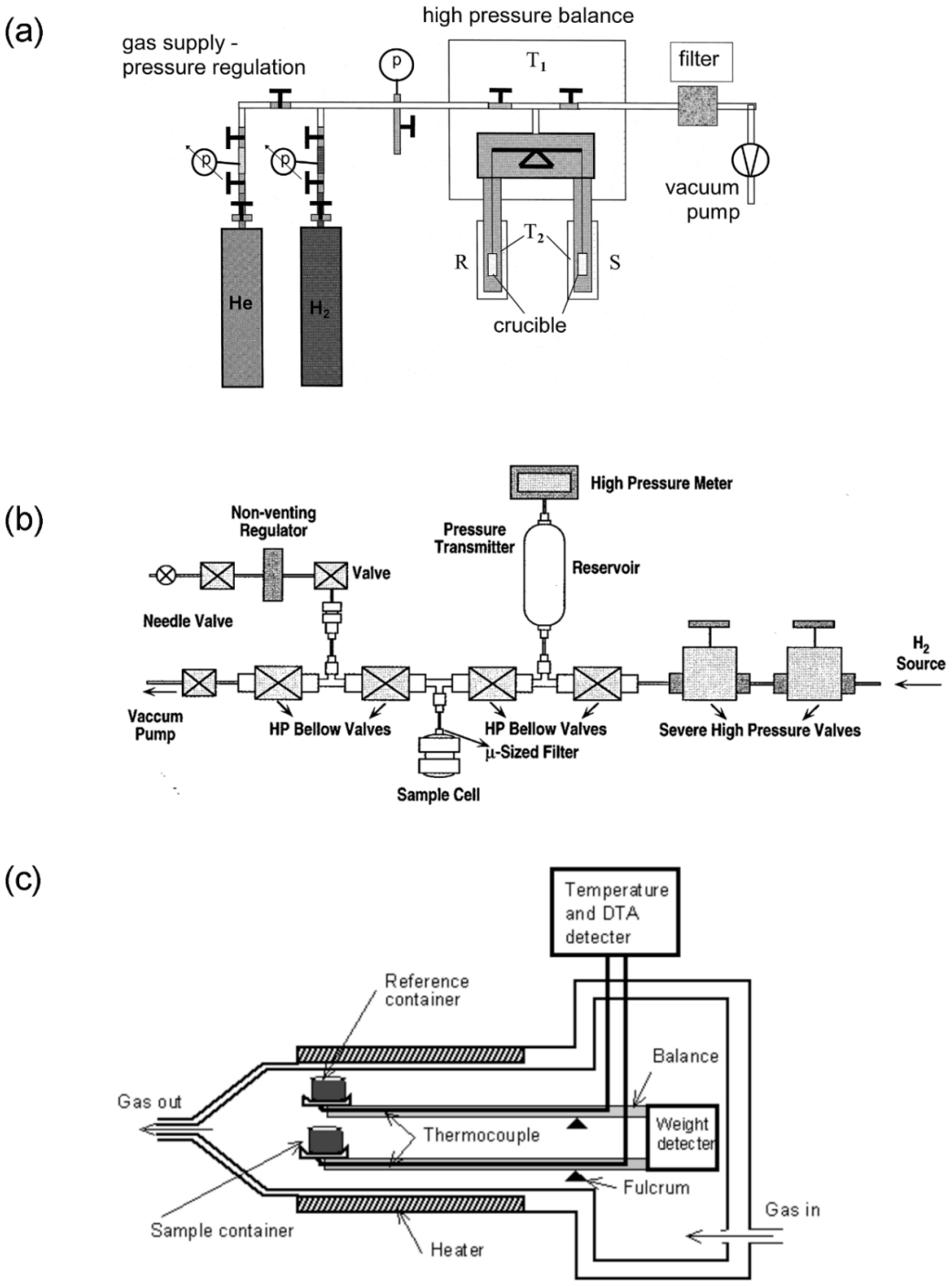

Fig. 2.4 Typical schematic diagrams of the gravimetric[75], volumetric[76] and thermal desorption systems[77].

However, each technique has flaws in design, which may lead to inaccurate calculation[3]. The gravimetric measurements limit the sample mass to milligram scale, and the buoyancy effect and disturbance of balance affect the measured weight. While the volumetric techniques largely rely on the thermal gradients between two cells, the ratio of sample size to cell volume, the dead space of the cell and the accumulative errors at the isotherm multipoint. Likewise, the thermal desorption systems are limited by the sample size, the temperature ramp rate and signal calibration. Besides these experimental considerations, some other objective factors also play roles in the measurement, including the properties of gas-phase hydrogen (purity, compressibility and thermal conductions of hydrogen), material characteristics (volume, mass, density, purity, sensitivity to air and moisture), and general instrumentation issues (vacuum and pressure capability, thermal stability and homogeneity). Efforts still continue to optimize the techniques for the accurate data collection.

2.3.2 Theoretical and experimental findings

Some metals have been used for the decorations of pristine graphene and boron[78,79], nitrogen[80]-doped graphene, mainly including Li[79,81], Al[82,83], Ca[84,85], Ni[78,86–88], Pd[19,80,89,90] and Pt[89]. Both theoretical and experimental work has been done to evaluate hydrogen uptake performance in the metal/graphene. For example, T. Hussain et al., theoretically predicted that the Ca/graphene with a Ca concentration of 11.11% could achieve a hydrogen storage capacity at ambient conditions as high as 6 wt.%[85]. They also reported that Li/graphene with a 25 % doping concentration of Li could reach a theoretical hydrogen capacity as high as 12.12 wt.%[81]. By the density functional theory calculations, Fair et al., predicted that Ca atoms, other than form clusters on graphene plane, could become stabilized on the double carbon vacancies[91]. One Ca atom could bind six hydrogen molecules[91]. The adsorption energies of hydrogen on the composite is below 0.20 eV, the practical level for onboard storage[81,85]. Moreover, Wong et al. applied the simulation of generalized gradient approximation (GGA) functional and VDW-DF2 functional, and selected Ni as the decoration material. The Ni/graphene system has many attractive features, such as low mass, high chemical stability and practical hydrogen binding energies (0.2-0.6 eV)[86]. Moreover, Cristian I. Contescu designed a first principle modeling and proposed that, on the flat graphene, each Pd atom could bind three hydrogen molecules at room temperature and pressure of 20 bar[92].

In comparison, the experimental work obtains less attractive values. For example, by using the volumetric technique, Chen determined that the Pd-decorated graphene/superactivated carbon has a hydrogen uptake capacity of 0.82 wt.% at room temperature and 8 MPa[90]. Wang synthesized a Ni-B nanoalloy/graphene composite (Ni 0.83 wt.% and B 1.09 wt.%) by a chemical reduction method, and measured an hydrogen capacity of 4.4 wt.% at 77 K and 106 kPa by using a pore and surface analyzer[78]. These experimental studies have not achieved the U.S. DOE target yet.

2.3.3 Metal-graphene interface

Researchers have applied the first-principles calculations (density functional theory, DFT) to investigate the metal-graphene interfaces, and predicted that Ni and Pd could chemically bind[93,94] or diffuse[95] to the graphene plane. At the Ni-graphene and Pd-graphene interfaces, the graphene intrinsic π-band electronic structure can be altered: The wave functions overlap between the Ni or Pd d electrons and graphene π-electrons[93]. That is, these interfaces correlate with the hybridization of graphene p states and metal d states, which results in a band gap in graphene and significantly decreases the work function of graphene[94]. Hussain claimed that graphene sheet could stabilize Ca and prevent the aggregation of Ca due to the binding energy higher than the cohesive energy[96]. Pumera experimentally characterized that the noble metal nanoparticles on graphene could facilitate the heterogeneous electron transfer of graphene[97].

Lee et al. explored the metal-graphene interaction by observing the Raman G band splitting, ratio of I_{2D}/I_G and band position, and they suggested that metal could be chemically doped to graphene sheet, specially to single-layer graphene via n-doping (upshift of the G band and the downshift of the 2D band) or p-doping modes (both upshift of the G band and the 2D band)[98]. Wang et al. also confirmed that electrons can transfer between Ni and graphene based on the Raman study, and identified a p-doping of Ni to the graphene structure[99]. The close interaction at the Ni-graphene interface probably results from the strong coupling of Ni open d orbitals and graphene p electrons[100]. The metal atoms bind to graphene plane most likely at the sites of the hollow centers of C hexagon (H1) and C-H hexagon (H2), the bridges of the C-C bond type 1 (B1) and type 2 (B2), the tops of C atom type 1 (T1) and type 2 (T2), as shown in Fig. 2.5[101].

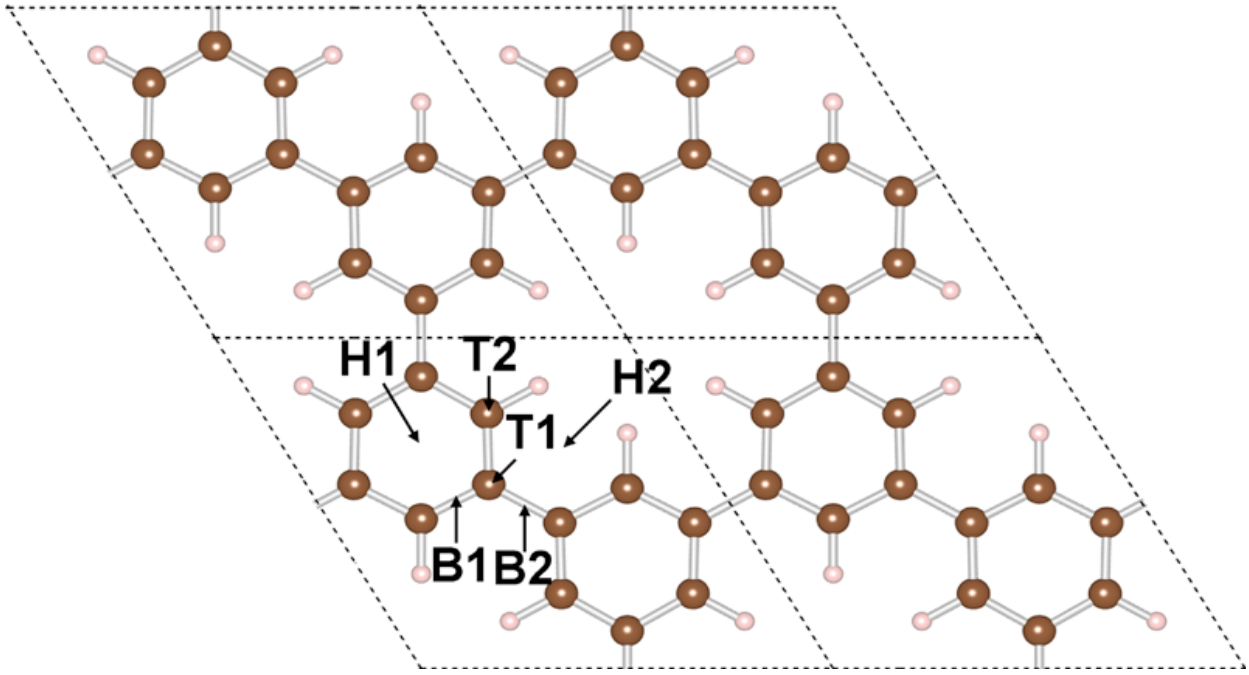

Fig. 2.5 Schematic diagram of atomic geometry of graphene with the sites of decorated metal atoms: C (brown), H (pink)[101].

2.3.4 Mechanism of hydrogen storage

Extensive research has proposed the spillover theory as the hydrogen storage mechanism in metal/carbon nanomaterials[102–108]. The spillover theory is defined as a process during which diatomic molecule primarily attaches and dissociates on an active surface, then migrates to another surface that individually and originally cannot adsorb or absorb the diatomic molecule under the same conditions[109]. Fig. 2.6 illustrates the spillover process in a supported metal catalyst system for hydrogen uptake[104].

Fig. 2.6a depicts a supported metal and an adhered molecular hydrogen. Fig. 2.6b schematically presents the low-capacity receptor of hydrogen that is an adsorbent with the spacious inner area. Fig. 2.6c, d schematically demonstrates the primary and secondary spillover process of hydrogen. The close interaction between the metal particles and supporting material may form a catalytic bridge that facilitates the primary spillover process, as shown in Fig. 2.6e.

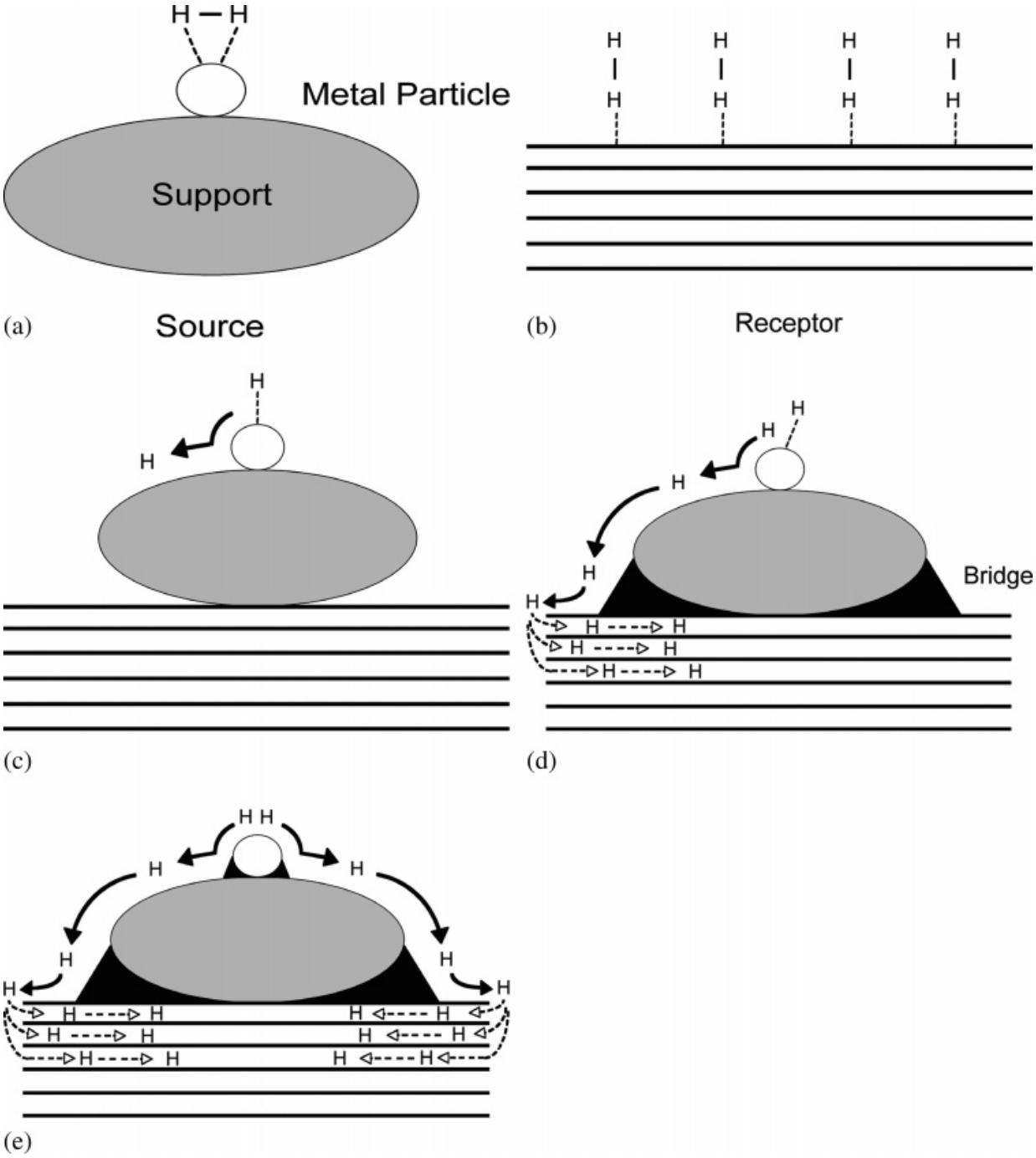

Fig. 2.6 Hydrogen spillover process in a supported metal catalyst system: (a) adsorption of hydrogen on a supported metal particle, (b) low-capacity receptor, (c) primary spillover of hydrogen, (d) secondary spillover via a bridge and (e) enhanced primary and secondary spillover process by the improved metal-support interface[104].

In the case of the metal/graphene system, the active metal particles serve as a catalytic medium that attracts and dissociate molecular hydrogen. The metal-graphene interface acts as a catalytic bridge and diffuses the atomic hydrogen to the graphene receptor. When heated properly, hydrogen tends to diffuse to interlayers rather than escaping from the host materials[104]. Compared to the individual components, the metal/carbon system could greatly enhance the hydrogen storage capacity[3].

2.4 Summary

In this chapter, many technological barriers for hydrogen storage application were described. Four main categories of storage technologies were discussed and compared. Among the potential storage materials, the metal/graphene system is a very promising system for hydrogen storage application. As graphene is the raw material for the synthesis of metal/graphene composites, the chapter introduced the structure, preparation methods, properties, and applications of this material.

Three main techniques have been applied to determining the hydrogen storage capacity. However, all of them have some experimental errors, and the optimization of measurements is still in progress. Besides, although theoretical models and calculations have proposed some attractive systems, the experimental work has not yielded yet desirable results.

Further, both theoretical and experimental works have indicated that the metal could bind to graphene sheets. Composite systems should have substantially enhanced hydrogen storage capacities when compared to the individual components. This chapter also covered a description of spillover mechanism that is currently the most popular theory of hydrogen uptake mechanism in the metal/carbon materials.

CHAPTER 3

METHODOLOGY

Overview of Chapter 3

This chapter introduces the work on the first objective of the project: designing and building a system with operating temperature and pressure for hydrogen storage measurement. The apparatus was originally designed to combine a volumetric technique and a mass spectrometer as described in appendix A. The system enables the in-situ determination of hydrogen charging and discharging performances.

Because of the safety concerns and various limitation of testing facilitates, the actual apparatus was different from the original design. The safety concerns include the potential explosion hazard of hydrogen that might result from the high operating pressure and temperature. Besides, a possible leakage of hydrogen may accumulate rapidly in a room and could be harmful to people. There was very restricted lab space for the installation of a hydrogen cylinder; limited space to locate the whole system; and limited usage of the fume hood for the outlet of hydrogen.

Therefore, we had to abandon the preexisting vacuum system, not use a mass spectrometer and relevant components, but instead assembled an apparatus simply for hydrogen charging process. After hydrogen charging, the specimens were transferred to a TGA apparatus for the determination of hydrogen storage properties, as descrbied in details in Chapter 4. Nevertheless, due to the complexity, accuracy and effectiveness of the original design, and considerable effort that had been devoted to this work, the original design is described in Appendix A. In order to guarantee a safe and reliable operation, detailed descriptions have been provided regarding the system functions, component specifications, operation procedures and safety concerns. Only a simple system is introduced in this chapter.

Besides, in this chapter, the preparation of graphene and synthesis of composites are described, and the characterization techniques applied in this project are introduced.

Contributions

My contributions to the apparatus include collecting information from the experts about the measurement techniques, optimizing the design, selecting component specifications, fitting and purchasing the components, assembling component, setting place for the apparatus, solving potential safety issues, preparing the standard operating procedure (SOP), testing the apparatus conditions for usage, and conducting safety inspection.

Dr. J. A. Szpunar supervised the design and offered advice to the installation and measurement. T. Soh, one of our research group members, participated in the design, selection of components and apparatus assembly.

Acknowledgements

I would like to express my sincere gratitude to Dr. J. Huot for the three hours of face to face discussion on the system design, the potential issues related to measurement, and the list of the component specifications for his custom-made apparatus. Likewise, I am grateful to Dr. D. P. Broom for his help and discussion of the technological barriers of measurement techniques.

We sincerely appreciate Mr. Blair from the Machine Shop for his help with the apparatus assembly and testing from time to time and appreciate Mr. Daniel from the Machine Shop for the usage of tools and his advice on the assembly. We appreciate discussion with Mr. F. Fan and Mr. X. Wang, Mr. G. Lee regarding the details of the design and potential safety issues. We acknowledge Mr. R L. Prokopishyn for the repair of the temperature controller. We thank our research group member Dr. Salman for his advice on the design and thank the U of S Workplace Safety and Environmental Protection (WSEP) representative Mr. Darrell Hart for the safety inspection.

3.1 Apparatus for hydrogen charging

Fig. 3.1 displays the custom-made apparatus for hydrogen charging process. The instrument is mainly equipped with a hydrogen cylinder (HY 5.0UH-T, UHP Grade 99.999%, Praxair), a pressure regulator (KPP1RSH422P2A030, Swagelok), a sample vessel (250 mL, 453HC-316-0719842151, Parr Instrument), a rupture disc (Parr Instrument), a heater (854HC, Parr Instrument), a pressure gauge (PPC5352, Winters Instrument), a temperature controller (room temperature to 1200°C, 210/TIMER-K mode, J-KEM Scientific) with a ceramic insulated thermocouple (870°C, XC-20-K-24, Omega) and a filter (pore size of 2 μm, SS-4FW-VCR-2). All tubes (SS-T2-S-028-20), valves (SS-4UG-V51-VS), connectors and fittings (gasket, 457HC2) were purchased from Swagelok. Due to the high operating pressure and potential corrosion, the components including all reactors, valves, connectors, and fittings are made of 316 stainless steel. All valves are bellows-sealed with a maximum working temperature of 343°C and pressure of 240 bar.

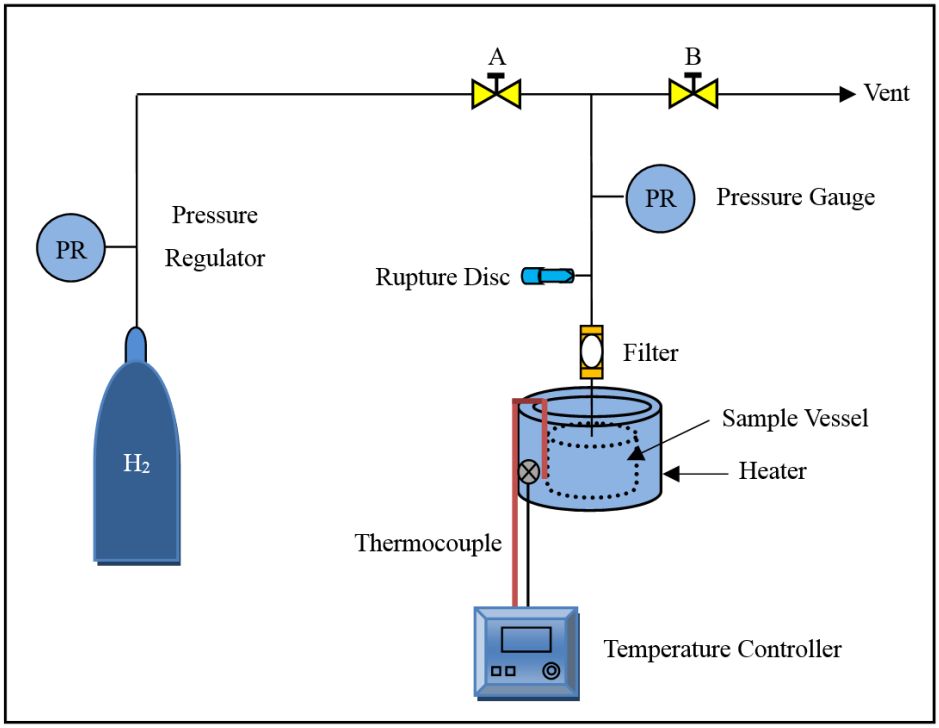

Fig. 3.1 Custom-made instrument for hydrogen charging.

For practical applications, the hydrogen charging tests were conducted at room temperature with pressures ranging from atmospheric pressure to 60 bar. After hydrogen charging process, the specimens were transferred to a TGA apparatus for the determination of hydrogen uptake. The detailed determination procedures will be presented in the experimental sections of Chapter 4 and Chapter 6. Consequently, to avoid repetition, this chapter does not contain the detailed description of the operation process.

3.2 Preparation

3.2.1 Preparation of graphene

Graphite oxide was prepared by using the modified Hummers method[69,110,111] and then exfoliated to graphene oxide[112] in distilled water by mechanical stirring for seven days[113]. Fig. 3.2 shows the scheme of the preparation process of graphene sheets. To prepare a concentration of 5 mg/mL of graphene oxide gel, the graphite (~44 μm, 1 g), potassium permanganate (4 g), concentrate sulfuric acid (98%, 45 mL) and a beaker (80 mL) were placed in a stainless steel vessel and cooled to 0°C. Then the graphite and potassium permanganate were added into the concentrated sulfuric acid in the beaker. Next, the vessel was covered, tightly fastened, and kept at 0°C for 1.5 h, followed by maintaining at 100°C in an oven for 1.5 h. After heating, the resulting dark purple mud was diluted with deionized water (500 mL). With magnetic stirring, a diluted hydrogen peroxide solution (3%, 250 mL) was slowly added to the diluted suspension with stirring till the color turned to be golden yellow, which was then followed by ultrasonic treatment (600 w) for 20min. After that, the mixture was repeatedly washed by using a vacuum filtration with hydrochloric acid (3%, 50 mL) and then washed multiple times with deionized water until the suspension (200 mL distilled water) became neutral. With seven days of vigorous agitation, the graphene oxide gel (5mg/mL) was finally obtained by a complete exfoliation of graphite oxide.

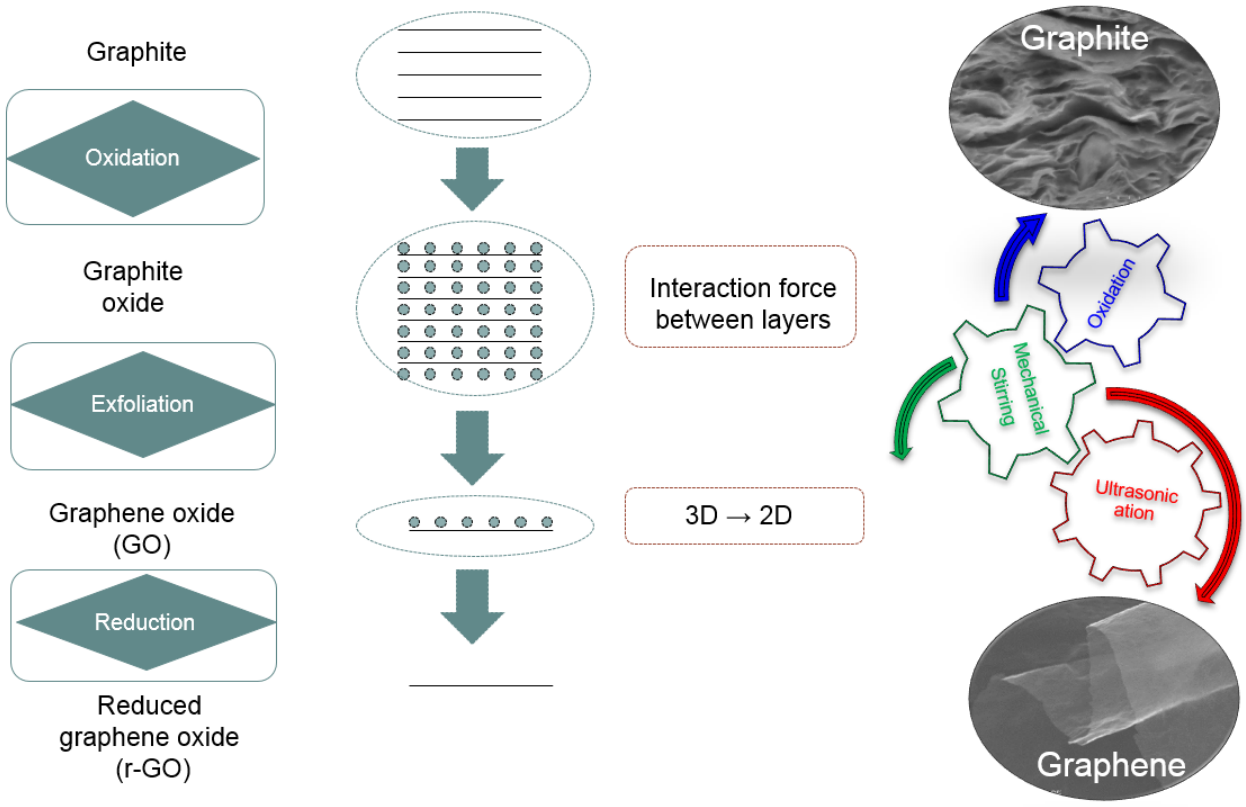

Fig. 3.2 Schematic process of preparation of graphene from graphite.

Fig. 3.3 displays the digital images of the resultant graphene oxide gel, and Fig. 3.4 exhibits the morphology observations of graphene oxide by scanning electron microscopy (SEM) and transmission electron microscope (TEM). The graphene sheet (Fig. 3.4a) could be paper-like (Fig. 3.4b), crumpled (Fig. 3.4b), porous (a diameter of ~6 μ m, Fig. 3.4c), wrinkled (Fig. 3.4d) and folded (Fig. 3.4e).

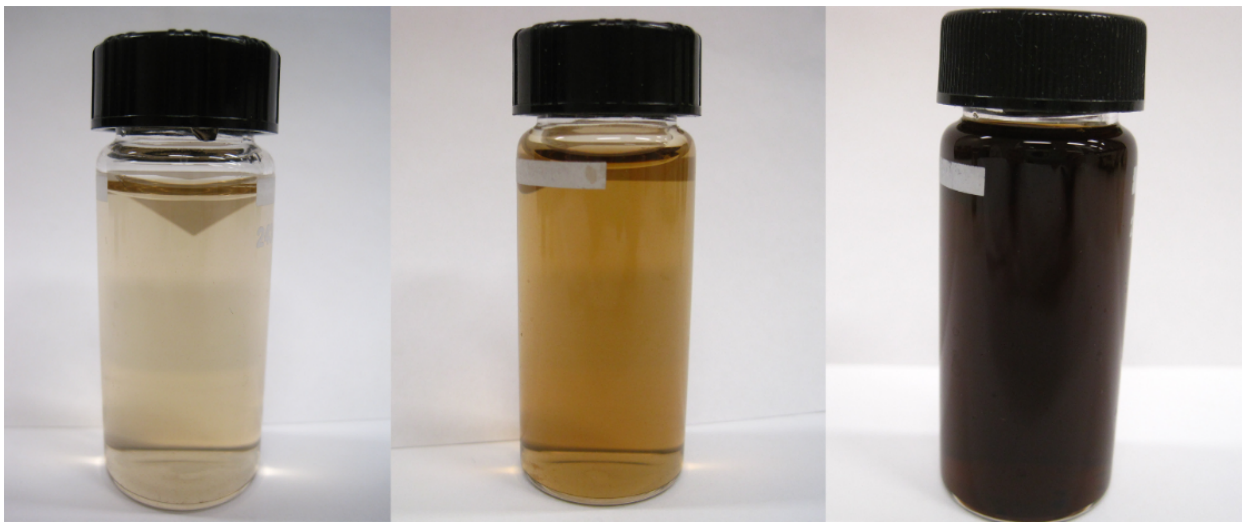

Fig. 3.3 Digital images of the prepared graphene oxide with increasing concentration from left to right.

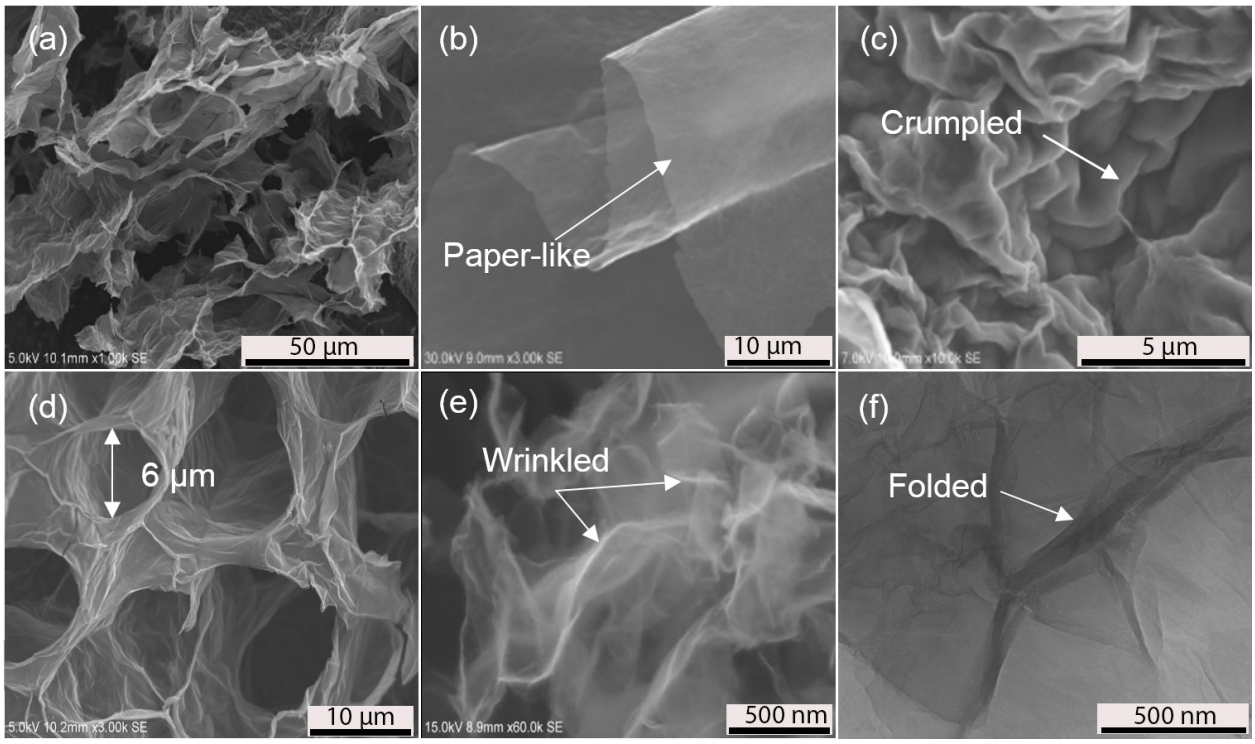

Fig. 3.4 Morphology observations: (a-e) SEM images and (f) TEM image of graphene sheets.

3.2.2 Synthesis of Ni/graphene composite

Fig. 3.5 schematic illustration depicts the in-situ synthesis flow of the Ni/graphene composite by using a simple chemical treatment.

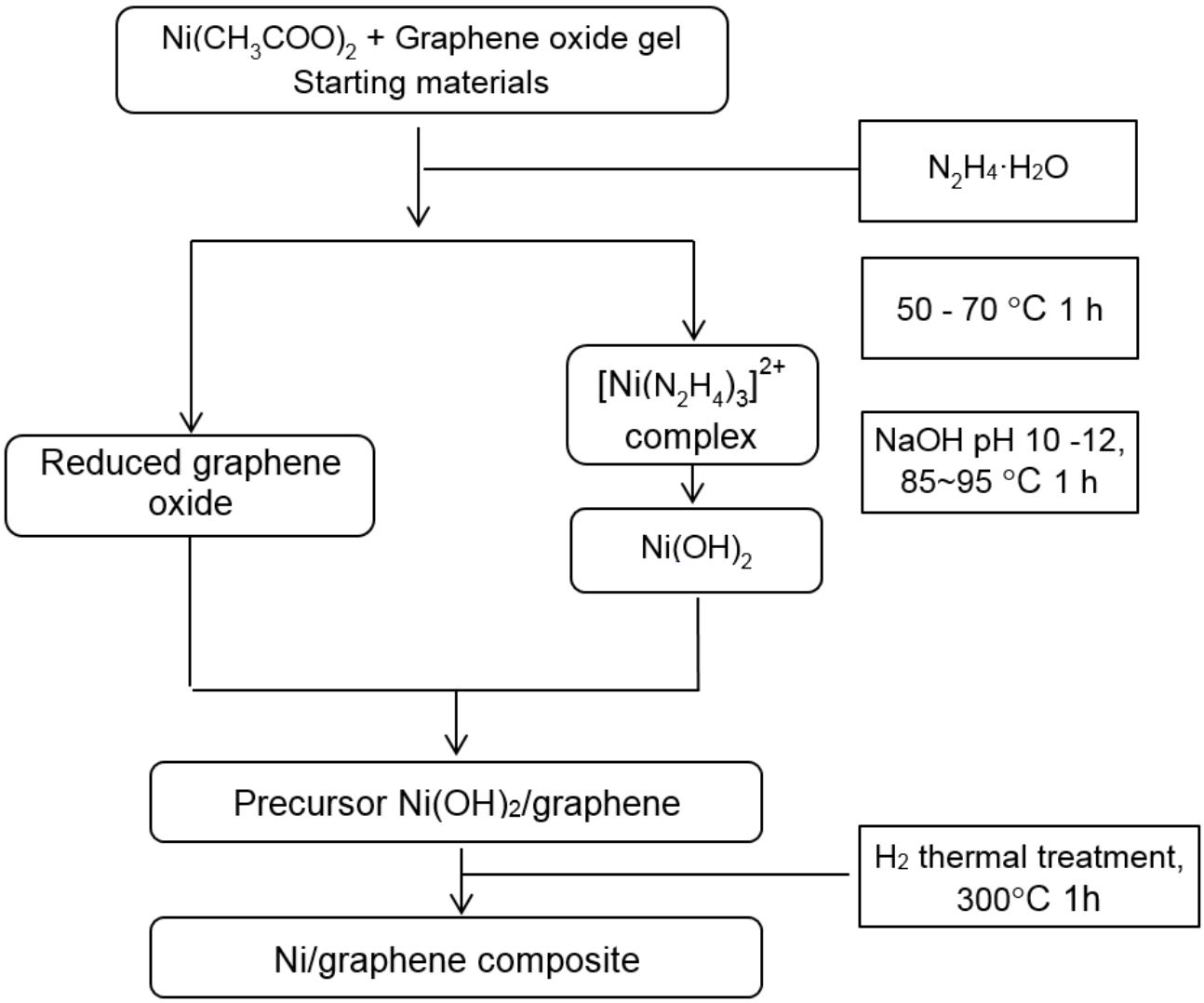

Fig. 3.5 Schematic synthesis flow of Ni/graphene composite.

This graphene oxide gel and nickel acetate [$Ni(OAc)_2$] were used as the starting material to synthesize the Ni/graphene composite, and the process flow of the synthesis is displayed in Fig. 3.6. The atomic ratio of Ni to C was further designed to be 0.053 (5 at.% : 95 at.%) in the composite. Accordingly, the corresponding amounts of the raw materials [$Ni(OAc)_2$ and graphene oxide] were calculated and used for the synthesis.

Basically, 1.86 g $Ni(OAc)_2$ was dissolved in 50 mL deionized water, and then the solution was added into a beaker with 97.20 mL, 20 mg/mL graphene oxide gel. The dark brown mixture was vigorously stirred for 10 min and sonicated for 10 min at room temperature to obtain a uniform dispersion. Then 10 mL of hydrazine hydrate was dropwise added to the blend. After an agitation of 10 min, 1 mol/L NaOH solution was slowly added with the pH value controlled within 10-12. After another agitation for 10 min, the beaker was placed into a pressure vessel, which was then tightly covered, fastened, and heated in an oven at 50-70°C for 1 h. Subsequently, a pressurized multiplex reduction was further carried out at 85-95°C for 1 h. Next, the homogeneous mixture was centrifuged and washed repeatedly with deionized water by centrifugation, in order to remove water and residual impurities in the mixture. Afterward, the precipitate mud was collected and transferred to a freeze dryer, and the final dried powder was denoted as precursor $Ni(OH)_2$/graphene. By applying hydrogen thermal treatment with hydrogen (99.999%, purity), the precursor was finally converted to Ni/graphene composite during heating at 350°C for 3 h.

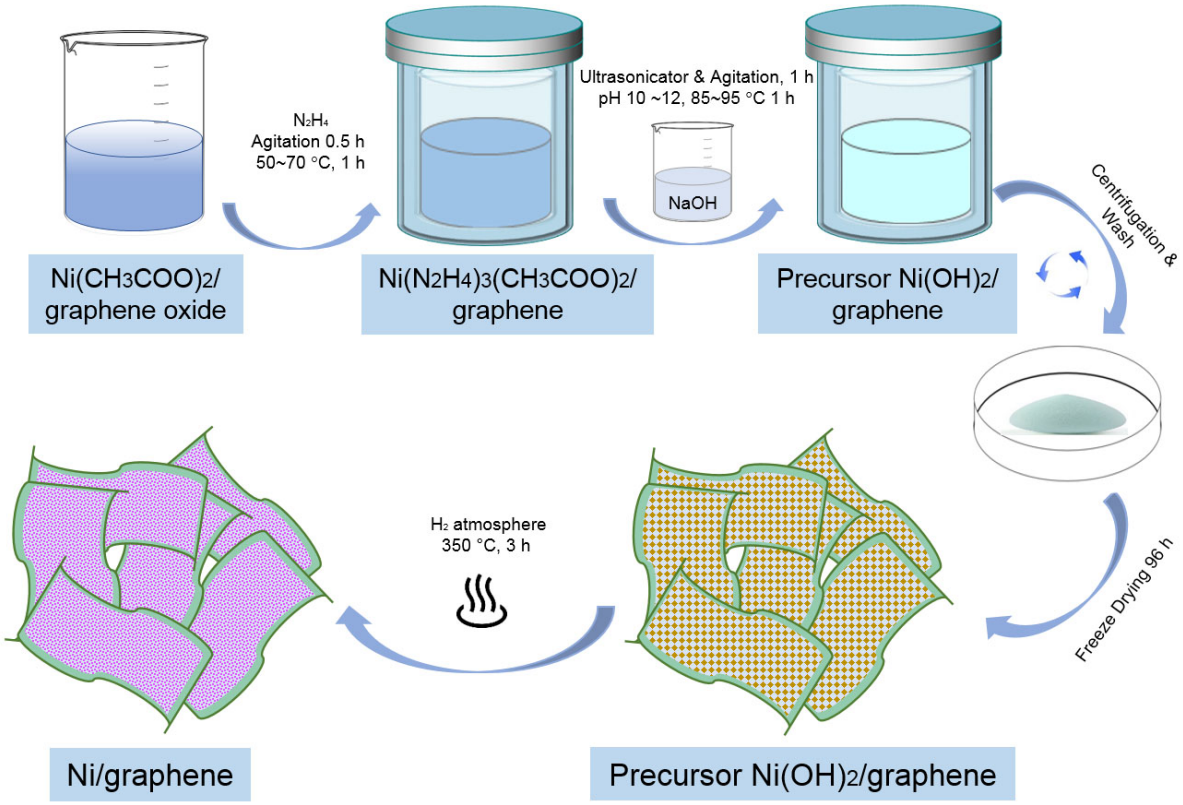

Fig. 3.6 Process flow of synthesis of Ni/graphene composite.

Fig. 3.7 illustrates the stages of formation of the Ni/graphene material. By controlling the reaction conditions (temperature, pH value and aging time), the nano-sized $Ni(OH)_2$ particles were formed by the reduction of Ni-complex that obtained from the reaction of nickel acetate and a hydrazine solution. Simultaneously, graphene oxide was reduced to graphene. During these reaction processes, Ni-based particles were deposited onto the surface of graphene. The precursor $Ni(OH)_2$/graphene was further reduced to Ni/graphene by hydrogen thermal reduction, with the Ni-C and Ni-O-C bonds formed on the Ni-graphene interface.

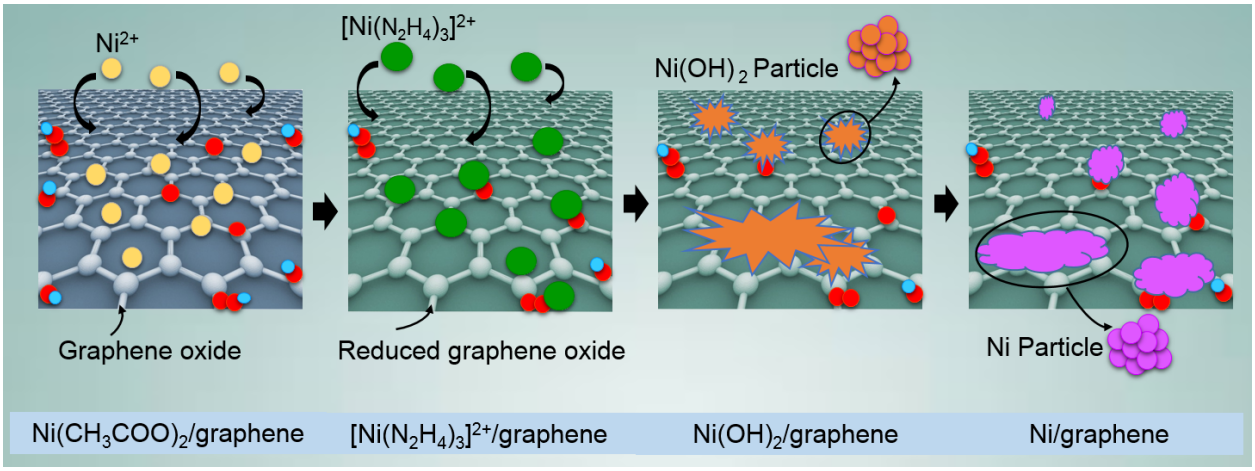

Fig. 3.7 Schematic illustration of the formation of Ni/graphene composite.

3.2.3 Synthesis of Pd/graphene composite

The Pd nanoparticle-decorated graphene nanocomposite was synthesized by a simple and scalable method. A schematic illustration of this process is presented in Fig. 3.8, and the synthesis flow is shown in Fig. 3.9. To synthesize the 5%Pd/graphene, palladium acetate [$Pd(OAc)_2$, 0.6713 g] was dissolved in ethanol (EtOH, 30 mL). The resulting $Pd(OAc)_2$ solution was slowly added into graphene gel (34.2 mL, 20 mg/mL). The dark brown blend was then vigorously agitated for 1 h and sonicated for 0.5 h at room temperature for a uniform mixture. Subsequently, this mixture was centrifuged and extensively washed with deionized water multiple times by centrifugation to eliminate the ethanol and remaining impurities. Afterward, the precipitate was dried to yield an ultrafine powder of $Pd(OAc)_2$/graphene precursor by a freeze dryer. Finally, the precursor was reduced to the Pd/graphene nanocomposite in a hydrogen atmosphere at 300°C for 1 h. The resultant atomic ratio of Pd to C was 5:95 in the final product. For the synthesis of 1%Pd/graphene, the atomic ratio of Pd to C was adjusted to 1:99 by altering the amounts of the palladium acetate and graphene gel, and the same procedures were repeated.

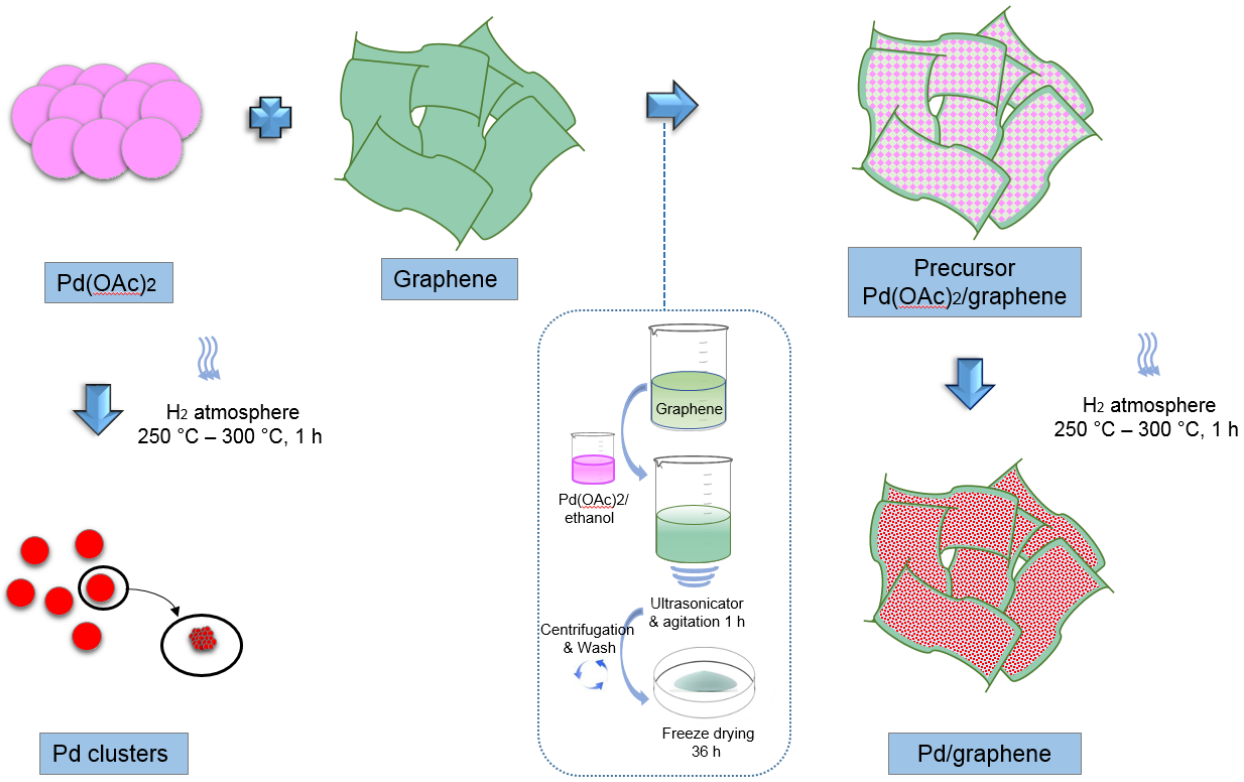

Fig. 3.8 Organization of the synthesis flow of Pd/graphene composite and Pd.

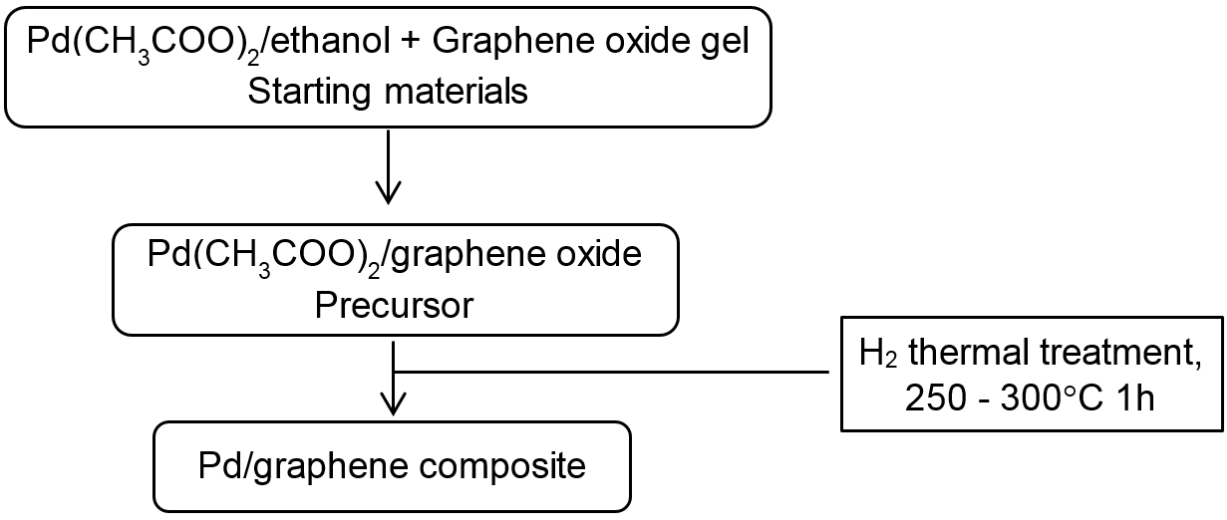

Fig. 3.9 Schematic process of synthesis of Pd/graphene composite.

3.3 Characterization techniques

3.3.1 XRD analysis of crystal structure

X-ray powder diffraction (XRD) is a common analytical technique that can be applied for the phase identification of Ni and Pd crystals (crystal structure and lattice parameters) in the composites. It was used to determine the interplanar spacing d_{hkl} of graphene and calculate the size of Ni, Pd nanocrystals based on the peak broadening. The Bragg's Law ($n\lambda=2d_{hkl}\sin\theta$) involves the wavelength of electromagnetic radiation, diffraction angle and lattice spacing in the crystalline samples. As each crystalline sample has unique d-spacing parameters, the phase composition of metals can be identified by comparing the diffraction peaks to the standard reference patterns.

An X-ray diffractometer (Bruker D8) equipped with a Cr K_α source (λ=0.229 nm) was used for the determinations of graphite, Ni/graphene, and Pd/graphene. A Cu Kα radiation (λ=0.154 nm) was used to measure the graphene oxide and graphene. The ω angles of the normal scan were set at 30, 60, and 90° with a scanning rate of 2°/min.

3.3.2 BET analysis of surface area, pore size and porosity

Brunauer-Emmett-Teller (BET, ASAP 2020 V3.01 H) analysis can be applied to determine the specific surface area and porosity of graphene. BET analysis evaluates the specific surface area by using non-corrosive gas (such as nitrogen, argon, carbon dioxide), determining the multilayer adsorption as a function of relative pressure. Based on the external and internal areas, this technique determined the entire specific surface area in m^2/g and further yielded the porosity of graphene.

3.3.3 Microscopy analysis of morphology

3.3.3.1 SEM

Scanning electron microscopy (SEM) primarily utilizes secondary electrons or backscattered electrons to investigate the morphological structure of a sample. It is a rapid technique to detect

the surface morphologies of graphene and Ni, Pd/graphene composites (shape, size and particle arrangement). The SEM (HITACHI SU6600) observations were carried out at 5 kV-25 kV with approximate working distances of 5-10 mm,

3.3.3.2 TEM

Compared to SEM, the transmission electron microscopy (TEM) has a higher resolution, and can be used to determine the detailed topographies of graphene and metal/graphene composites. To prepare the sample, a tiny amount graphene gel was diluted in ethanol with particles in the suspension invisible to the naked eye, which was then deposited on a copper grid and naturally dried for the TEM (Philips CM10) observations at 100 kV.

3.3.3.3 STXM

Scanning transmission X-ray microscopy (STXM) is an X-ray microscopy technique for the chemical imaging and component identification of Ni/graphene in this study. Besides, a combined technique of the STXM and X-ray absorption spectroscopy (XAS) could provide high spatial resolution images with elemental spectra (C, O, and Ni) that were collected from some interesting small spots on the surface of Ni/graphene.

STXM with a spatial resolution of 30 nm was performed on the soft X-ray spectromicroscopy beamline 10ID-1 at the Canadian Light Source (CLS). XANES at the C, O K-edges, and Ni L-edge were extracted from STXM image stacks scanned over a range of photon energies.

3.3.4 Spectroscopy analysis of chemical and electronic structure

3.3.4.1 EDS

Energy dispersive X-ray spectrometry (EDS) was utilized for a localized chemical analysis of the graphene and composites. It was applied for the qualitative analysis of elements, and quantitative determination of the elemental concentrations and distributions on the sample surfaces. The elemental signals and mapping of the surface of Ni/graphene were collected by using the EDS

(HITACHI SU6600) at a voltage of 20 kV, while a voltage of 30 kV was used to characterize the surface of Pd/graphene.

3.3.4.2 XPS

X-ray photoelectron spectroscopy (XPS) was used to analyze the elemental composition on the surface[114] of the graphene and composites. The peak position and separation can be used for the qualitative analysis of elemental identification and chemical states of the Ni, Pd on graphene, while the peak heights and areas were used for the elemental quantitative analysis on the top few atomic layers of the materials. To examine the chemical state of the Ni, O, and C, an XPS test was conducted by using a Kratos Axis Ultra Al-α (1.4866 keV) spectrometer.

3.3.4.3 XAS

X-ray absorption spectroscopy (XAS) was used to investigate the local chemistry and electronic structure of Ni, Pd/graphene composites. The XAS spectra are sensitive to the oxidation state, coordination chemistry, and the distances, coordination number of the species that surround the selected elements of Ni and Pd. This characterization investigated the interaction between the metals and graphene, and indirectly revealed the hydrogen evolution in the sorbents during the hydrogen charging process.

The Ni K-edge X-ray absorption measurements were performed at an energy range of 8.32-8.38 keV under an ambient atmosphere on the soft X-ray microcharacterization beamline (SXRMB, 06B1-1) at the CLS.

Pd L_3-edge XAS in situ measurements were also performed on the SXRMB (06B1-1) at the CLS. The in situ measurement was conducted using an energy scan range for the Pd L_3-edge of 3,150 to 3,190 eV and 3,140 to 3,200 eV. The hydrogen thermal reaction was conducted with the conditions of a gas mixture of 2 % hydrogen and 98 % nitrogen at a gas flow rate of 100 ml/min, 300°C for 1 h.

3.3.4.4 Raman Spectroscopy

Raman spectroscopy provided the information of vibrational, rotational transitions[115] in the graphene and composites, which identified the type of sp hybridizations of carbon upon the metal decoration of graphene. To characterize the structure and type of bonding, the Raman spectra were collected by using a Renishaw 2000 Raman microscope with the 514 nm wavelength of the laser source and the scattered light dispersed with an 1800 L/mm grating.

3.3.5 TGA test of weight change

Thermogravimetric analysis (TGA) provides the information about the physical phenomena of vaporization, sublimation, and physisorption. It also determines the chemical phenomena involving chemisorption, decomposition and solid-gas reactions (such as oxidation or reduction). In this study, the thermal analysis determined the amount of hydrogen desorption from the composites by measuring the weight changes of composites as a function of temperature at a constant heating rate, or as a function of time with a constant temperature.

In the case of Ni/graphene, a 5-10 mg portion of the hydrogen-charged sample was used for each desorption test. The TGA analyzer (SDT Q600) can be used to release hydrogen from the sorbents upon heating. The tests were carried out under an argon atmosphere at a flow rate of 100 mL/min from ambient temperature to 250°C with a heating rate of 20°C/min. In addition, the stability of the hydrogen storage was assessed by testing the amount of hydrogen that was released from the sorbents at 25°C during 100 min.

In the case of Pd/graphene, the TGA analyzer (SDT Q600) was used to measure hydrogen release from the hydrogen-charged sorbents. A 5-10 mg portion was placed in a crucible at room temperature and stay there under argon flow (100 mL/min) for 15 min for stabilizing the experimental conditions. Then the temperature was started to increase and the hydrogen release was measured. The measurements were carried out under argon flow (100 mL/min) from ambient temperature to 200°C with a heating rate of 20°C/min. In addition, the hydrogenated samples (0 bar and 60 bar) were tested for both 1%Pd/graphene and 5%Pd/graphene

nanocomposites at 25°C for 100 min in order to evaluate the unstable amount of hydrogen uptake.

3.4 Summary

This chapter has introduced the custom-made apparatus for hydrogen charging. Methods were developed to prepare graphene and synthesize the Ni/graphene and Pd/graphene composites by simple and scalable approaches. The characterization techniques have been described for the analysis of crystal structure, surface area and porosity, chemical and electronic structure, and the hydrogen storage determination.

CHAPTER 4

NI/GRAPHENE NANOCOMPOSITE

Overview of Chapter 4

This chapter presents the manuscript titled “Ni/graphene nanocomposite”. The work includes optimization of the synthesis of Ni/graphene composite, investigation of the interaction between the Ni particles and graphene substrate, determination of the storage characteristics and suggestion of a hydrogen uptake mechanism of the composite.

Modifications

The manuscript presented in this chapter is different from the published version in that:

1. The title was changed from “Synthesis of Ni/graphene nanocomposite for hydrogen storage” to “Ni/graphene nanocomposite”.
2. The sentence “This system exhibits attractive features like high gravimetric density, ambient conditions and low activation temperature for hydrogen release” was removed from abstract.
3. The expression “hydrogen storage” was changed to “hydrogen release”.
4. Fig. 3.1 in Chapter 3 shows the custom-made apparatus in the Supporting Information. To avoid repetition, this figure was removed from the Supporting Information of Chapter 4 in Appendix B.
5. The detailed experimental procedures of synthesis were moved to the section 3.2.2 of Chapter 3.
6. The digital images and microstructural observations of graphene were moved from the Supporting Information of Chapter 4 to the Fig. 3.3 and Fig. 3.4 in Chapter 3.
7. The pore volume of graphene was added to the section 4.4.1.

8. An influencing factor of hydrogen storage capacity was added to the section 4.4.3: (6) partial removal of the sorbent material under a constant flow of argon.
9. The section 4.4.5“Violation of the Van’t Hoff Law in TGA” was added.

Manuscript status

The manuscript was published in journal ACS Applied Materials & Interfaces:

C. Zhou, J. A. Szpunar, and X. Cui. Synthesis of Ni/Graphene Nanocomposite for Hydrogen Storage. *ACS Appl. Mater. Interfaces*, 2016, **8**, 15232−15241.

Copyright

The copyright permission to use the manuscript in the thesis was obtained and provided in Appendix B. The references for this chapter along with the references of other chapters are provided at the end of the thesis.

Notes

The authors declare no competing financial interest.

Author Contributions

C. Zhou designed and performed the experiments. C. Zhou, Dr. X. Cui and Dr. J.A. Szpunar analyzed the data. C.Z wrote the manuscript. Dr. J.A. Szpuanr planned and supervised the project. All the authors contributed to the manuscript.

Acknowledgements

This work is supported by the Canada Research Chair program and the National Engineering Research Council of Canada.

C. Zhou gratefully acknowledges the continuous financial support of the China Scholarship Council (CSC). We sincerely appreciate Dr. H. Wang for the discussions and his help with data analysis. We acknowledge Dr. Y. Hu and Dr. Q. Xiao for the help and support of the XAS tests and data analysis at the Canadian Light Source (CLS). We appreciate Mr. F. Fan and Mr. X. Wang for their help in the data collection and discussion.

Supporting Information

SEM morphology observation of bare metallic Ni prepared from hydrogen thermal treatment; SEM observations of Ni/graphene composites before and after hydrogen charging; and the Scherrer analysis of the crystallite size of Ni in the composite.

Ni/graphene nanocomposite

Chunyu Zhou[*,†], Jerzy A. Szpunar[†] and Xiaoyu Cui[‡]

[†]Department of Mechanical Engineering, University of Saskatchewan, Saskatoon, SK, S7N 5A9, Canada.

[‡]Canadian Light Source Inc., Saskatoon, SK, S7N 2V3, Canada.

4.1 Abstract

A Ni-graphene composite was designed with Ni nanoparticles of ~ 10 nm in size, uniformly dispersed over a graphene substrate. When charged at room temperature and an atmospheric hydrogen pressure of 1 bar, it could yield a hydrogen capacity of 0.14 wt.%. When hydrogen pressure increased to 60 bar, the sorbent released 1.18 wt.%. The hydrogen release could occur at an operating temperature below 150°C and complete at 250°C.

KEYWORDS: hydrogen storage, Ni/graphene, interface, composite, gravimetric density

4.2 Introduction

Hydrogen-based fuel is a promising solution for the steady depletion of traditional energy resources because of its environmental cleanliness and remarkable energy efficiency[116,117]. However, it is technically challenging to store hydrogen effectively and safely in a compact way for practical applications. Recently, nanostructured graphene has attracted much attention as a promising hydrogen storage media. This graphene network has excellent features of lightweight, high specific surface area, significantly chemical stability, and great onboard reversibility[14,118].

Aside from graphene, some metal catalysts can actively trap hydrogen[3,15,119]. In spite of that, some issues could arise when storing hydrogen in bare graphene or in metal[120]. Hydrogen molecules attach weakly to carbon via van der Waals forces[7,121], which restricts the hydrogen uptake. In addition, due to a high cohesive energy[101], the easy aggregation of metal particles

could limit the number of anchoring sites for hydrogen. Further, slow kinetics of metal-hydrogen interaction and its poor reversibility lead to an inactive system for hydrogen loading[20].

Lately, researchers have suggested that the decoration of the surface of graphene by metal could greatly facilitate the hydrogen uptake[3]. Among the metals, the existence of Ni particles stabilizes the sorbent structure by tailoring the geometry of graphene[9,10]. They could catalytically facilitate the hydrogen absorption/desorption performance in nanocomposites[11], and also anchor hydrogen as dissociative sites[12,13]. Besides, NiO/Ni/graphene[122] and reduced graphene oxide (r-GO)/Ni foam composites[123] show remarkable cycling performance.

The combination of graphene and Ni system should greatly enhance the hydrogen storage capacity when compared to the capacity in the independent components of bare graphene and metal[14,124]: that composite may achieve high gravimetric and volumetric densities of hydrogen storage. In this work, a Ni/graphene composite was synthesized. The system allows a hydrogen capture at ambient conditions and, with a low temperature below 150°C, could activate the hydrogen discharging process. The amount of hydrogen uptake is roughly proportional to the pressure of hydrogen; specifically, with a hydrogen charging pressure of 60 bar, the composite system reaches a hydrogen storage capacity of 1.18 wt.%.

4.3 Experimental procedures

4.3.1 Synthesis of Ni/graphene nanocomposite

The detailed experimental procedures were described in the section 3.2.2 of Chapter 3.

4.3.2 Characterization techniques

To determine the crystal structure and phase composition of the samples, an X-ray diffractometer (XRD, Bruker D8) equipped with a Cr Kα source (λ=0.229 nm) was used for graphite, and a Cu Kα radiation (λ=0.154 nm) for graphene oxide and graphene, and the ω angles of normal scan were set at 30, 60, and 90° with a scanning rate of 2°/min. The specific surface areas and pore size of graphene were measured by using the Brunauer-Emmett-Teller (BET, ASAP 2020 V3.01 H) equipment. The elemental signals and mapping of the sample surface were collected by using

the energy-dispersive spectroscopy (EDS) at a voltage of 20.0 kV. To acquire electron micrographs, Scanning electron microscopy (SEM, HITACHI SU6600) observations were carried out at 25 kV with approximate working distances of 9.8 and 5.9 mm, and transmission electron microscope (TEM, Philips CM10) observations at 100 kV with the magnifications of 92 and 125 k. To characterize the structure and type of bonding, the Raman spectra were collected by a Renishaw 2000 Raman microscope with the 514 nm wavelength of the laser source and the scattered light dispersed with an 1800 L/mm grating. To examine the chemical state of the Ni, O, and C, an X-ray photoelectron spectroscopy (XPS) test was conducted by using a Kratos Axis Ultra Al-α (1.4866 keV) spectrometer. In order to investigate the local chemistry and electronic structure of the system, the Ni K-edge X-ray absorption measurements were performed under an ambient atmosphere on the Soft X-ray Microcharacterization Beamline (SXRMB, 06B1-1) at the Canadian Light Source (CLS), operating at an energy range of 8.32-8.38 keV, and processed the data using the Athena software (0.9.25)[125].

4.3.3 Hydrogen charging and discharging

To test the hydrogen charging, a custom-made apparatus was designed as described in Fig. 3.1 and used to charge samples at different hydrogen pressures. After hydrogen charging, the amount of hydrogen uptake in the sorbents was measured using thermogravimetric analysis equipment (TGA, SDT Q600). Before the sorption experiment, the tightness of the custom-made apparatus was tested with hydrogen at room temperature and 100 bar for 12 h. Prior to hydrogen charging, a degassing treatment was performed to remove remaining gases and moisture impurities from the composite. The dry and fine composite powder was placed in the sample vessel, heated to 300°C and maintained at that temperature for 1 h. The sample was then placed in a glass container and preserved in a vacuum desiccator.

For each hydrogen sorption test, ~100 mg of the degassed sample was used as a sorbent. This sorbent was placed in the vessel. Hydrogen (99.999%, purity) was then introduced into the vessel at 10 bar and immediately released. This gas exchange was repeated five times to further remove the moisture and air from both the sample and the vessel. Afterward, hydrogen was purged into the vessel again at pressure values (0.5, 1, 10, 20, 30, 40, 50 and 60 bar). Then the hydrogen

sorption process began, and the sample was charged for 30 min. After hydrogen sorption, the sample was placed in a glass container that was then firmly sealed and transferred to the TGA instrument within 5 min for the desorption test.

A 5-10 mg portion of the hydrogen-charged sample was used for each desorption test. The TGA analyzer can be used to release hydrogen from the sorbents upon heating. The changes in the weight of samples were recorded as a function of temperature along with the amount of hydrogen release. The tests were carried out under an argon atmosphere at a flow rate of 100 mL/min from ambient temperature to 250°C with a heating rate of 20°C/min. Nine samples were measured in total: One sample was not charged with hydrogen (Ni/graphene_0 bar) and one sample was hydrogen-charged at 0.5 bar (Ni/graphene_0.5 bar), and they served as references. The other seven samples were charged at different pressures (Ni/graphene from 1, 10, 20, 30, 40, 50 and 60 bar). In addition, the stability of the hydrogen storage was assessed by testing the amount of hydrogen that was released from the sorbents at 25°C during 100 min.

4.4 Results and discussion

4.4.1 Phase composition and morphology

The X-ray diffractometer (XRD) pattern characterizes the crystal structures and phase composition of the samples. Fig. 4.1a displays the XRD patterns of graphite, as-prepared graphene oxide, and graphene. The diffraction peak at $2\theta = 39.92°$ represents the presence of graphite (green line). After oxidation, the graphite peak completely disappears from the spectra and only graphene oxide (blue line) and graphene (red line) are observed. When zoomed in, two spectra show weak broad peaks that are located at $2\theta = 17.81°$ and 23.54° (inset spectra): these two peaks are characteristics for the graphene oxide[126] and graphene[127]. The interlayer distance of the graphene (23.54°, d-spacing ~0.38 nm) becomes smaller compare to that of graphene oxide (17.81°, d-spacing ~0.99 nm).

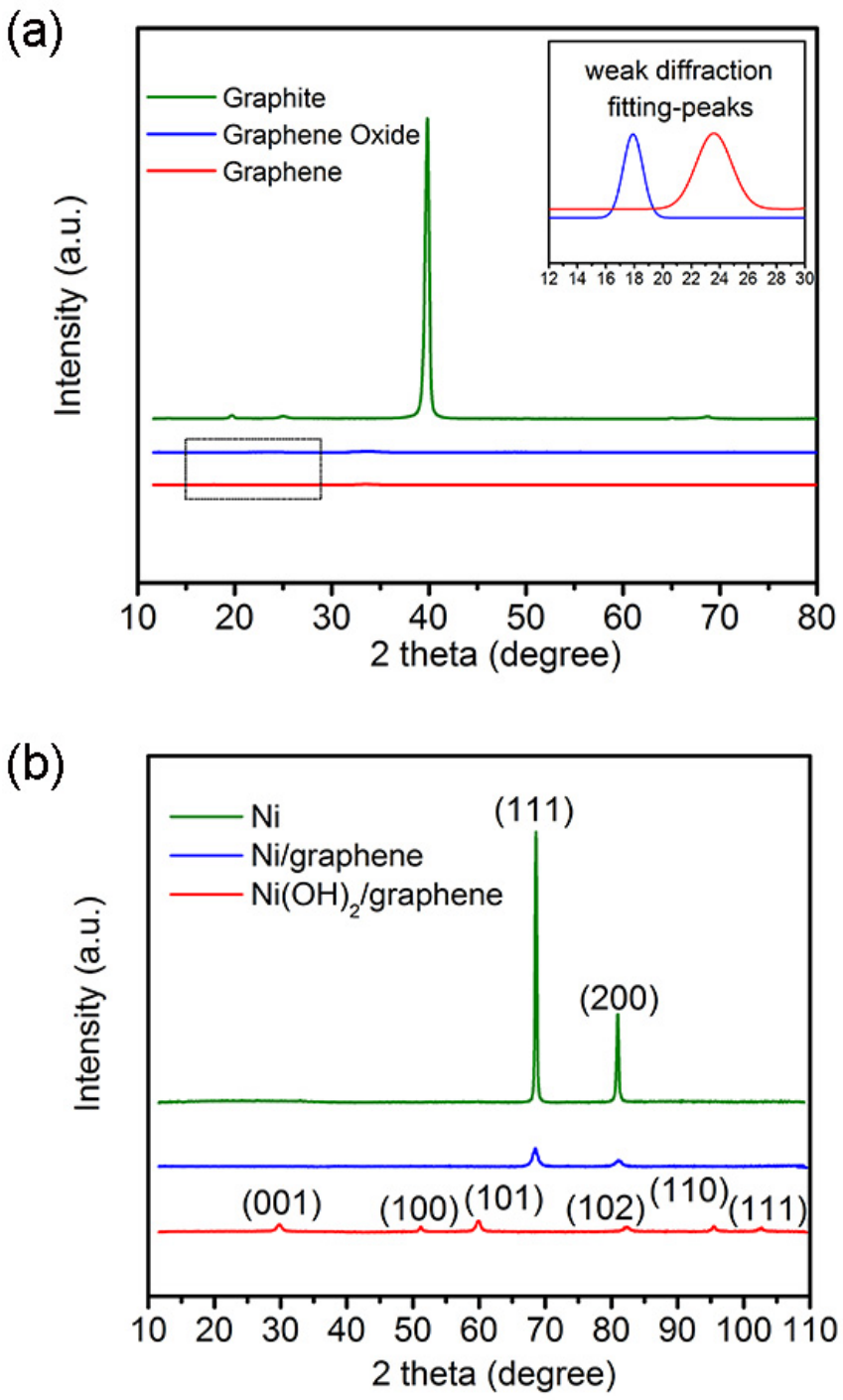

Fig. 4.1 XRD patterns: (a) graphite (green line), graphene oxide (blue line), and graphene (red line) and (b) metallic Ni (green line), Ni/graphene composite with Ni 5 at.% (blue line), and precursor $Ni(OH)_2$/graphene (red line).

Fig. 4.1b depicts the XRD pattern of Ni/graphene composite. For comparison, the XRD patterns of $Ni(OH)_2$/graphene and metallic Ni were also collected. After reduction, the complete absence of the $Ni(OH)_2$ pattern in the Ni/graphene (blue line) suggests that it was converted to Ni in the graphene matrix. Two characteristic peaks appear in the diffraction spectrum of Ni/graphene (blue line) at $2\theta = 68.61°$ (111) and 80.92° (200), which coincided well with those positions in the diffraction pattern of Ni. This result further confirms the successful transformation of $Ni(OH)_2$ to Ni in the graphene matrix. In addition, the broadening of the peaks in the composite as compared to peaks in the metallic Ni indicates a decrease of crystallite size, and the average crystal size of Ni in graphene surrounding medium was calculated to be 7-9 nm by using the Scherrer equation (details are described in Supporting Discussion)[128].

The SEM observation in Fig. 4.2a displays a relatively fluffy structure formed by a 3D interconnected graphene network with pores having a size of 5-20 μm. Nitrogen isothermal adsorption-desorption analysis further measured the Brunauer-Emmett-Teller (BET) specific surface areas of the loose graphene to be 751.9 m^2/g with the average pore width of 3.3 nm and the pore volume of 0.6 cm^3/g. A corresponding energy dispersive spectroscopy (EDS) spectrum (Fig. 4.2b) of the area squared in Fig. 4.2a reveals the presence of C and O on the graphene surface with a C/O atomic ratio of 5.85 (86 at.% : 14 at.%), and the EDS elemental mapping exhibits a homogeneous distribution of these elements on the graphene surface (Fig. 4.2c). Moreover, SEM observation of Ni/graphene illustrates the fluffy structure of the composite (Fig. 4.2d), and the EDS spectrum (Fig. 4.2e) of the area squared in Fig. 4.2d shows C, O and Ni with a C/O/Ni atomic ratio of composition to be 83.8 at.% : 11 at.% : 5.3 at.%, which is in good agreement with the component ratio used for the synthesis (Ni : C = 0.053; 5 at.% : 95 at.%).

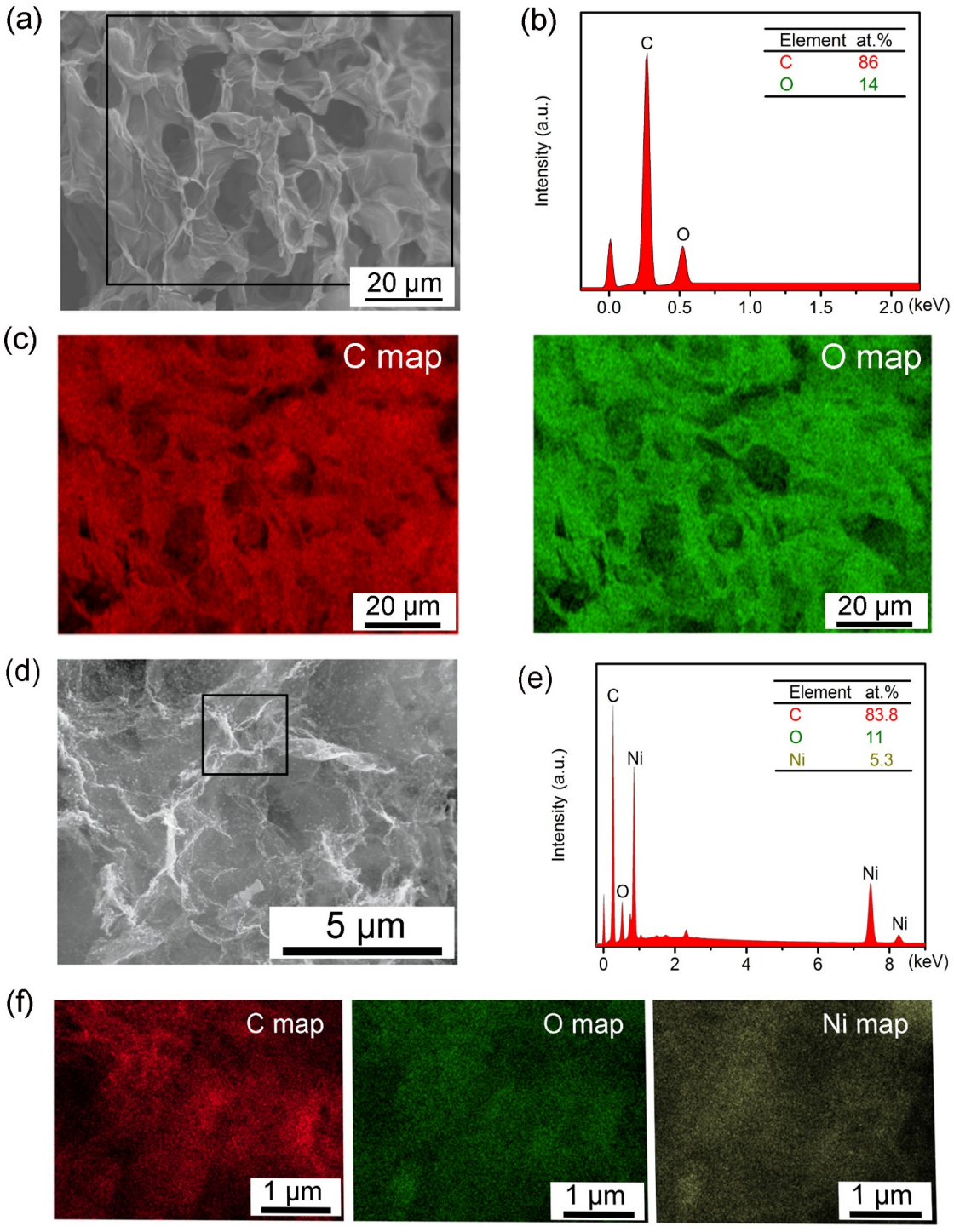

Fig. 4.2 Morphology and surface composition analysis: (a) SEM image of graphene oxide, the corresponding (b) EDS spectrum and (c) elemental mapping (squared area in (a)), (d) SEM image of Ni/graphene, the corresponding (e) EDS spectrum, and (f) elemental mapping (squared area in (d)).

It should be noted that some residual oxygen still exists in the composite after reduction, which could be typical for the redox produced graphene[112]. The EDS elemental maps in Fig. 4.2f further confirm the uniform distribution of C, O, and Ni in the composite. This uniform distribution of Ni particles could be attributed to defects[20], vacancy sites[129], and oxygen-containing functional groups on the graphene surface[130], which facilitates the attachment of Ni atoms on the surface of graphene network. This close interaction between Ni particles and graphene substrate may have prevented the Ni nanoparticles from aggregation.

The improved dispersion state of Ni particles in the graphene substrate correlates with higher hydrogen storage in the Ni/graphene composite. Fig. 4.3a (SEM) and Fig. 4.3c (TEM) display the morphologies of the precursor $Ni(OH)_2$/graphene as a reference, while Fig. 4.3b (SEM) and Fig. 4.3d (TEM) illustrate the surface morphologies of the Ni/graphene. The $Ni(OH)_2$ particles deposited on the graphene surface have particle sizes in the range of 20-65 nm (Fig. 4.3e). After hydrogen thermal treatment, graphene sheets remains fuzzy and have crinkled structure (Fig. 4.3b, d). Compared to the pure Ni particles after hydrogen thermal reduction of $Ni(OAc)_2$ (~250 nm, Fig. B.1, Supporting Information); the Ni particles in the Ni/graphene composite are uniformly spread over the graphene substrate (Fig. 4.3b, d) and have a grain size of ~10 nm (Fig. 4.3f), this size is similar to that determined from the XRD measurements (Fig. 4.1b, average crystal size of Ni as 7-9 nm). This considerable diminishing of Ni particle size can be attributed to the improved distribution of Ni particles in the graphene matrix, which is consistent with the EDS results (Fig. 4.2).

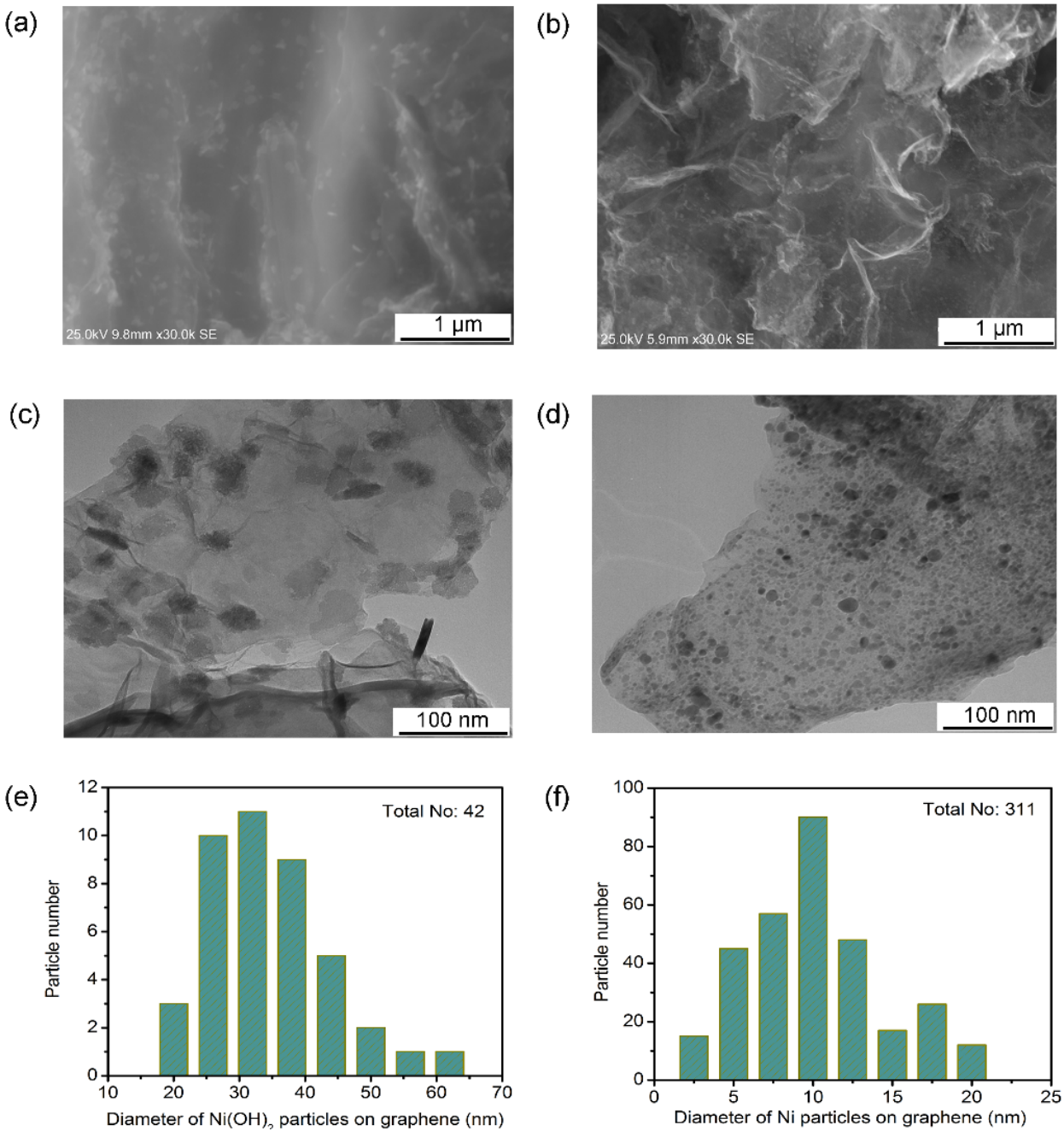

Fig. 4.3 Electron images: SEM images of (a) $Ni(OH)_2$/graphene and (b) Ni/graphene, TEM images of (c) $Ni(OH)_2$/graphene and (d) Ni/graphene, and particle size distributions of (e) $Ni(OH)_2$ particles in $Ni(OH)_2$/graphene and (f) Ni particles in Ni/graphene.

4.4.2 Electronic structure

Raman spectra detect the vibrations of structure and interatomic bonding that arise from the structural change from pure graphene to Ni/graphene (Fig. 4.4a). The D and G bands are the predominant features of the spectrum of the graphene structure: particularly the D band represents sp^3-bonded carbon as the disordered or defected band, and the G band involves sp^2 hybridized carbon being in-plane vibrational mode[131]. They are located respectively at the positions of 1356.15 and 1593.84 cm^{-1}. The Raman spectrum of Ni/graphene shows no shift in peak position; however, a significant increase in the D/G intensity ratio is observed, reflecting a weakened sp^2 hybridization and a comparatively strengthened sp^3-bonded carbon[131], probably due to hybridization of Ni d orbitals with carbon π orbitals on the graphene surface.

The X-ray photoelectron spectroscopy (XPS) spectrum reveals the chemical state of the elements on the composite surface and determines the possible bonds at the Ni-graphene interface. In Fig. 4.4b, the survey spectra detect the presence of O and C in graphene, and Ni, O, and C in the composite. The corresponding Ni 2p spectrum of Ni/graphene (Fig. 4.4c) displays the Ni $2p_{3/2}$ and Ni $2p_{1/2}$ core levels[132]: the peaks at 852.8 eV (Ni $2p_{3/2}$) and 870.46 eV (Ni $2p_{1/2}$) are typically featured as Ni(0), while the peaks at 855.84 eV (Ni $2p_{3/2}$) and 874 eV (Ni $2p_{1/2}$) represent Ni-O-C bond in the composite, and the Ni-C peaks are observed at 860.83 eV (Ni $2p_{3/2}$) and 879.5 eV (Ni $2p_{1/2}$).

The split peaks of C 1s spectrum in graphene, located at ~283.62 eV, ~285.52 eV, ~287.92 eV and ~291.39 eV, are mainly attributed to the carbon-containing groups, including the carbon ring C-C/C=C, C-O, C=O, and O-C=O bonds, respectively[133,134] (Fig. 4.4d). In comparison, a peak appears at 286.52-286.57 eV in the Ni/graphene C 1s spectrum, indicating an interaction between Ni and graphene probably via Ni-C bond[135] (Fig. 4.4d). Similarly, the split peaks of the O 1s spectrum in graphene can be assigned to the C-O (~532.58 eV), C=O (~534.98 eV) and O-C=O (~538.03 eV) bonds[133,134], while a peak at ~531.01 eV in Ni/graphene suggests a possible Ni-O-C bond at the Ni-graphene interface[135] (Fig. 4.4e).

After the loading of Ni, the peaks of these functional groups become more intense and narrower, implying that the presence of Ni could help in preserving oxygen in the composite, probably through the formation of Ni-O-C bond formed during the synthesis process. The existence of these bonds (Ni-O-C and Ni-C) are assumed to improve the affinity of the Ni to graphene substrate. This attachment may further enhance the structural stability of the composite and its efficiency for hydrogen storage.

To further probe the local coordination environment and electronic structure of the system, Ni K-edge X-ray absorption spectroscopy (XAS) spectra were collected (Fig. 4.4f), and conducted blank tests on the precursor $Ni(OH)_2$/graphene and used a standard Ni foil as a reference. The standard spectrum of metallic Ni was used to evaluate the extent of reduction of Ni (II) in the composite. The peak area and edge position reflect the specific oxidation state of Ni[136], and the peak area is related to the density of unoccupied states[137]. Fig. 4.4g illustrates that the peak area significantly decreased after the reduction (from green line to blue line). This weaker absorption implies a reduction of Ni (II). In addition, the derivative of the spectrum signifies the absorption position. The weak pre-edge structure prior to K-edge results from the 1s→3d bound state transition[138]. In the Fig. 4.4g on the inset spectrum, the pre-edge absorption of Ni/graphene and Ni foil are located at the same position (8.3321 keV) and this suggests that Ni is reduced in the Ni/graphene, as the 3d orbitals become partially unoccupied after reduction, and this enables the excitation of 1s core electron to the d state.

Moreover, the strong Ni K-edge absorption correlates with the excitation of 1s → 3d-4p mixing states that hybridized with O 2p orbitals. At the bottom of Fig. 4.4g, the derivative of spectra illustrates that the white line is downshifted from the energy of the Ni (II) precursor (green line) toward the final reduced Ni (blue line) in Ni/graphene, implying a reduction of hybridization of the Ni 3d-4p and O 2p states[139]: as the empty state with Ni 3d-4p character is occupied, a smaller energy band emerges between the 1s and 3d-4p states; thus a lower energy is required to excite 1s electrons to another unfilled d, p state. Hence, this absorption edge is shifted towards lower energies and this further verifies the reduction of Ni (II).

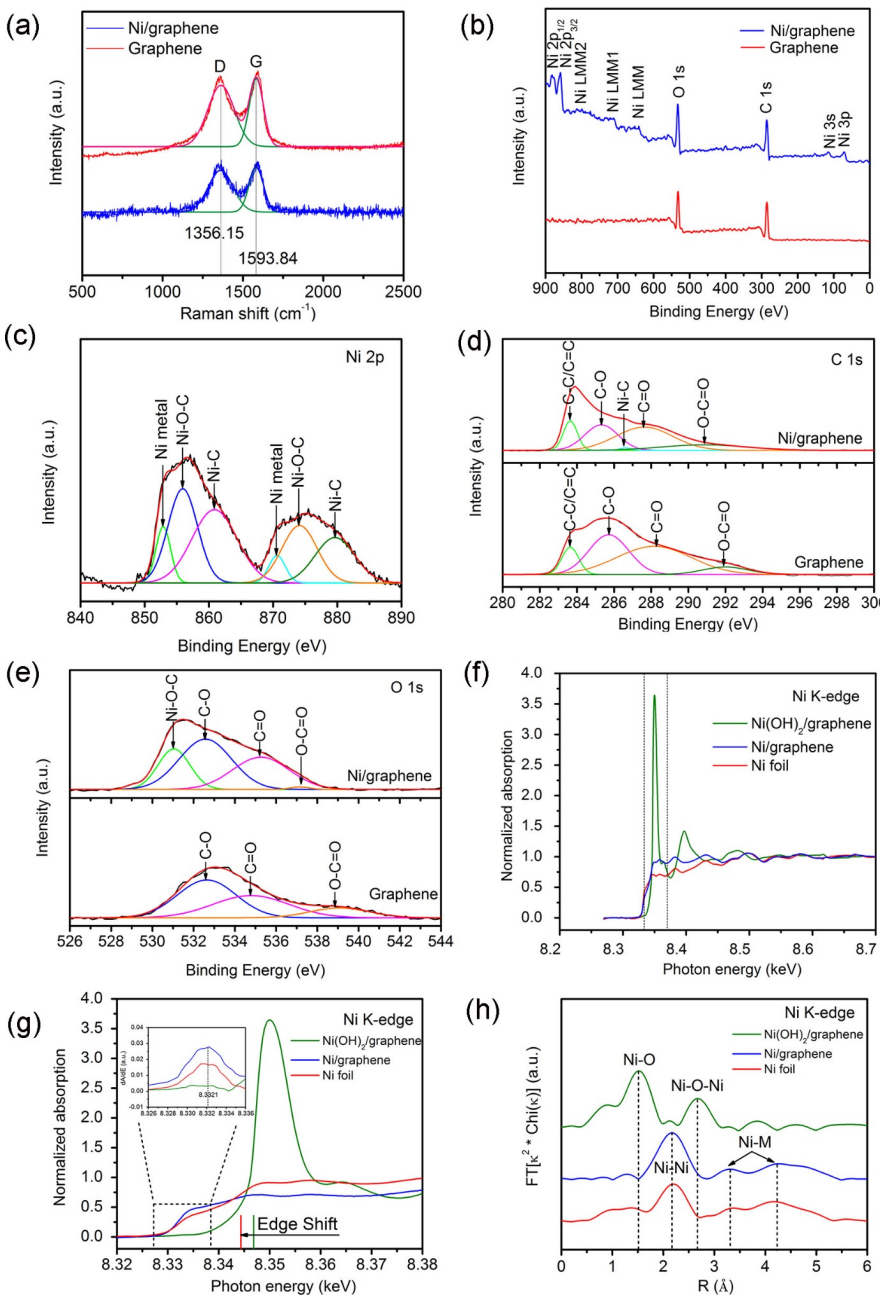

Fig. 4.4 Electronic structure analysis: (a) Raman spectra and (b) XPS survey spectra of graphene and Ni/graphene, and the corresponding XPS spectra of (c) Ni 2p, (d) C 1s, and (e) O 1s. (f) Ni K-edge XAS spectra of Ni foil, precursor $Ni(OH)_2$/graphene and Ni/graphene, and (g) the corresponding magnified energy ranging from 8.32-8.38 keV with a derivative of the pre-edge spectra (inset) and the shifts in respective absorption edges at the bottom of the spectra. (h) Ni K-edge FT-EXAFS spectra of the Ni nanoparticles.

Nevertheless, one still can see that the absorption energy of the Ni K-edge in the Ni/graphene is slightly different from that of the metallic Ni foil. This spectral difference is presumably due to a difference in electronic structure between the Ni and graphene in the Ni/graphene composite; electron density was probably dragged towards defects in the graphene[136].

A similar finding was obtained from the k-weight Fourier transform of Ni K-edge extended X-ray absorption fine structure (EXAFS) spectra as shown in Fig. 4.4h. The intense peaks centered at 1.52 Å and 2.66 Å in the precursor $Ni(OH)_2$/graphene FT-EXAFS spectrum typically represent Ni-O shell and Ni-O-Ni higher coordination shell, respectively[140,141]. In the Ni/graphene FT-EXAFS spectrum, the main peak at 2.16 Å corresponds to Ni-Ni bond, while two weak peaks that present at the same positions (3.29 Å and 4.28 Å) but are slightly more intense compared to those in the Ni foil FT-EXAFS spectrum, are presumably related to the Ni-M bond which is a mixture of Ni-Ni higher shell and Ni-O-C/Ni-C shells at the interface of Ni-graphene. In addition, the absence of Ni-O shells in Ni/graphene spectrum further verifies that Ni (II) was indeed converted to the metallic Ni (0) during the hydrogen thermal treatment. All these results demonstrate the interaction of Ni-graphene via Ni-O-C and Ni-C bonding. The presence of these bonds can prevent Ni diffusion and aggregation in the graphene network, as depicted by the morphology and distribution of nanoparticles (Fig. 4.2f and Fig. 4.3d).

4.4.3 Hydrogen release measurement

TGA was applied to determine the hydrogen release from the Ni/graphene upon the conditions of flowing argon at a heating rate of 20°C/min, and Fig. 4.5 shows the experimental results. Blank tests were performed on the non-charged composite (Ni/graphene_0 bar) and hydrogen-charged composite at 0.5 bar (Ni/graphene_0.5 bar) as references to determine the hydrogen uptake and the storage capacity in the hydrogen-charged sorbents.

The Ni/graphene_0 bar sample had a mild mass loss (Fig. 4.5a). As graphene structure remains chemically inert at the ambient environment[39], it is hardly oxidized in air at room temperature[142]. The possibility of the formation of chemical products in graphene during the transfer process may be precluded. Thus, the slight weight loss in the Ni/graphene_0 bar presumably arises from

the elimination of adsorbed moisture and gas impurities[143,144]. The hydrogen-charged samples had a continuously declining weight for sorbents that at hydrogen charging pressures from 1 to 60 bar (Fig. 4.5a), revealing an increasing amount of hydrogen uptake in the specimens. Notably, the Ni/graphene_1 bar had a larger weight loss than the non-hydrogen charged sample. This indicates that the sorbent can anchor hydrogen at atmospheric pressure.

Five factors are assumed to contribute to the weight changes of hydrogen-charged samples by using TGA: (1) hydrogen release; (2) removal of the adsorbed water and gas impurities during the transfer process[3]; (3) hydrogen reduction of NiO_x. The XRD measurements indicate metallic Ni in the composite (Fig. 4.1b), which is in agreement with the experimental results reported by Yang et. al[123]. The XRD results detected no pattern of the oxidized Ni, however, the oxidation might occur during the transfer process in air which could be reduced by thermal hydrogen reaction in TGA; (4) an elimination of water that generated from a possible oxidation of hydrogen at the presence of Ni during the transfer process[145]; (5) an irreversible interaction between hydrogen and composite upon heating; (6) partial removal of the sorbent material under a constant flow of argon. To accurately calculate the hydrogen storage capacity in the composites, the weight changes that resulted from the factor (2), (3), (4), (5) and (6) are needed to be precluded by using the weight loss of the Ni/graphene_0.5 bar as a reference. Therefore the amount of hydrogen release is calculated by deducting the mass loss of the Ni/graphene_0.5 bar from the weight loss of each hydrogen-charged specimen at a higher pressure from 1 bar to 60 bar.

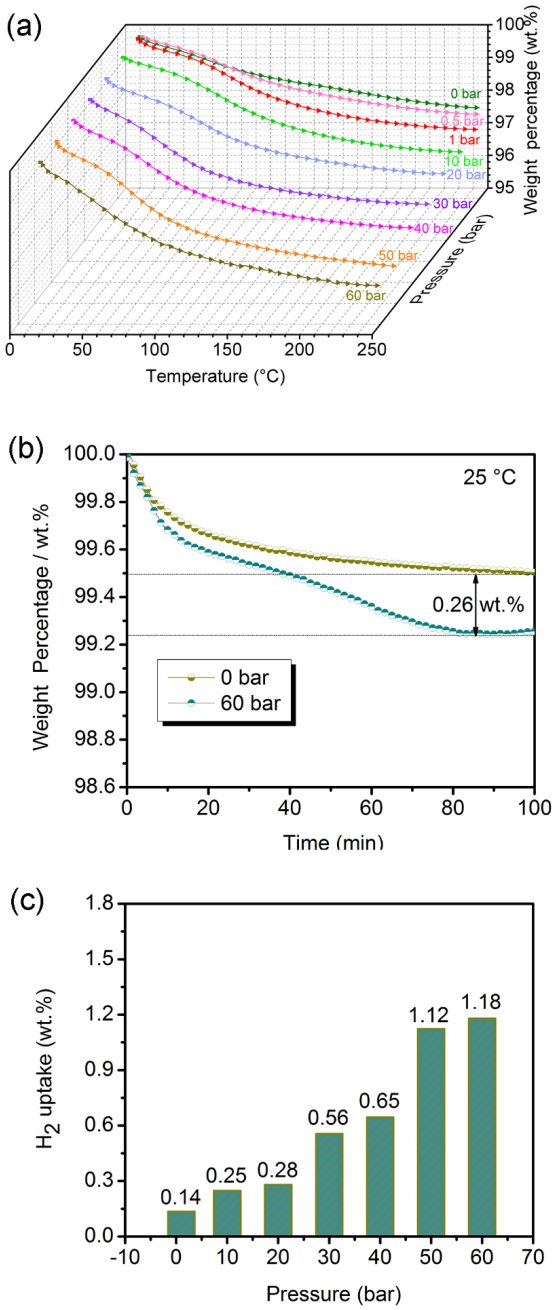

Fig. 4.5 Thermogravimetric analysis: (a) hydrogen storage capacities in the Ni/graphene composites with a loading amount of Ni 5 at.% that charged at hydrogen charging pressures from 0.5 to 60 bar, (b) mass changes of non-hydrogen charged sorbents and 60 bar hydrogen-charged sorbents at 25°C in 100 min, (c) hydrogen capacity that is stably stored in the sorbents after hydrogen charging at pressures from 1 to 60 bar.

To investigate the stability of the hydrogen storage in the composite, the weights of the hydrogen-charged samples (0 and 60 bar) were measured at 25°C for 100 min as shown in Fig. 4.5b. The specimen weights tended to stabilize after 80 min with a slight release of hydrogen (0.26 wt.%). The hydrogen uptake capacities were then calculated with different pressures by deducting the weight loss of the Ni/graphene_0.5 bar (Fig. 4.5a) and the quantity of unstable hydrogen uptake of 0.26 wt.% at ambient conditions (Fig. 4.5b) from the weight loss of each hydrogen-charged specimen (Fig. 4.5a). Subsequently, the final hydrogen uptake capacity was plotted as a function of the hydrogen charging pressures in Fig. 4.5c. Remarkably, the composite traps hydrogen with a capacity of 0.14 wt.% at room temperature and an atmospheric pressure of hydrogen. When the hydrogen charging pressure rose to 60 bar, the gravimetric uptake of hydrogen reached 1.18 wt.% in the composite.

Further, the hydrogen-charged samples tended to lose weight quickly from room temperature to 150°C, whereas, there was a slow hydrogen release from 150 to 250°C. The fast hydrogen discharge implies that a quick desorption process could occur at a temperature below 150°C. It has been reported that the hydrogen desorption from some bare metal hydride like MgH_2 and CaH_2 requires high heat (> 300°C)[146,147], while hydrogen charging of carbon material demands a super low temperature (77 K)[148]. It is highly advantageous that the hydrogen storage in the present Ni/graphene sorbent discharges hydrogen below 150°C, suggesting that a physisorption or weak chemisorption could dominate the hydrogen uptake in our composites.

It has been reported that Chen et al. determined that Pd-decorated graphene/carbon had a hydrogen storage capacity of 0.82 wt.% at room temperature and 8 MPa[90] by using a volumetric technique. Wang et al. synthesized a Ni-B nanoalloy/graphene composite (Ni 0.83 wt.% and B 1.09 wt.%) by a chemical reduction method. They applied a pore and surface analyzer and determined that the composite could achieve a hydrogen uptake capacity as high as 4.4 wt.% at 77 K and 106 kPa[78]. These two materials either require an extremely high charging pressure or need a superlow temperature for the storage. The most recent work on the graphene/Mg that was reported by Cho et al. in 2016[149] shows an attractive gravimetric density of hydrogen storage of 6.5 wt.% with the hydrogen charging conditions of 250°C and 15 bar and a discharging temperature of 300°C. Despite that, the material demands high temperatures for the hydrogen

charging/discharging processes. In comparison, the Ni/graphene nanomaterial in this work exhibits many attractive features. The Ni/graphene composite can trap hydrogen with a capacity of 0.14 wt.% at room temperature and an atmospheric pressure of hydrogen. The gravimetric density of hydrogen reached 1.18 wt.% at room temperature and a hydrogen charging pressure of 60 bar. Additionally, the composite released hydrogen below 150°C and completed the desorption at 250°C.

4.4.4 Hydrogen release mechanism

After hydrogen uptake, the composite well retains the fluffy morphologies (Fig. B.2, see Supporting Information). The XRD patterns exhibit newly formed peaks at 66.21°and 78.65° of the Ni/graphene_60 bar, which involves a formation of a new crystalline phase in the composite (Fig. 4.6a). Raman spectroscopy investigates the structural evolution of graphene in the composite upon hydrogen charging (Fig. 4.6b). When comparing the Ni/graphene to the Ni/graphene_H_2, the D band shifts from 1356.15 to 1349.34 cm^{-1}. This downshift implies a relatively weaker vibration of the sp^3-bonded carbon in the hydrogen-charged sample, suggesting that the uptake hydrogen could interact with the defects in graphene. In addition, no observable variation of the I(D)/I(G) ratios was detected before and after hydrogen charging (Ni/graphene of 1.01 and Ni/graphene_H_2 of 1.07). It suggests that the defects in the graphene structure are well maintained and possibly contribute to the hydrogen transport during the charging process[149].

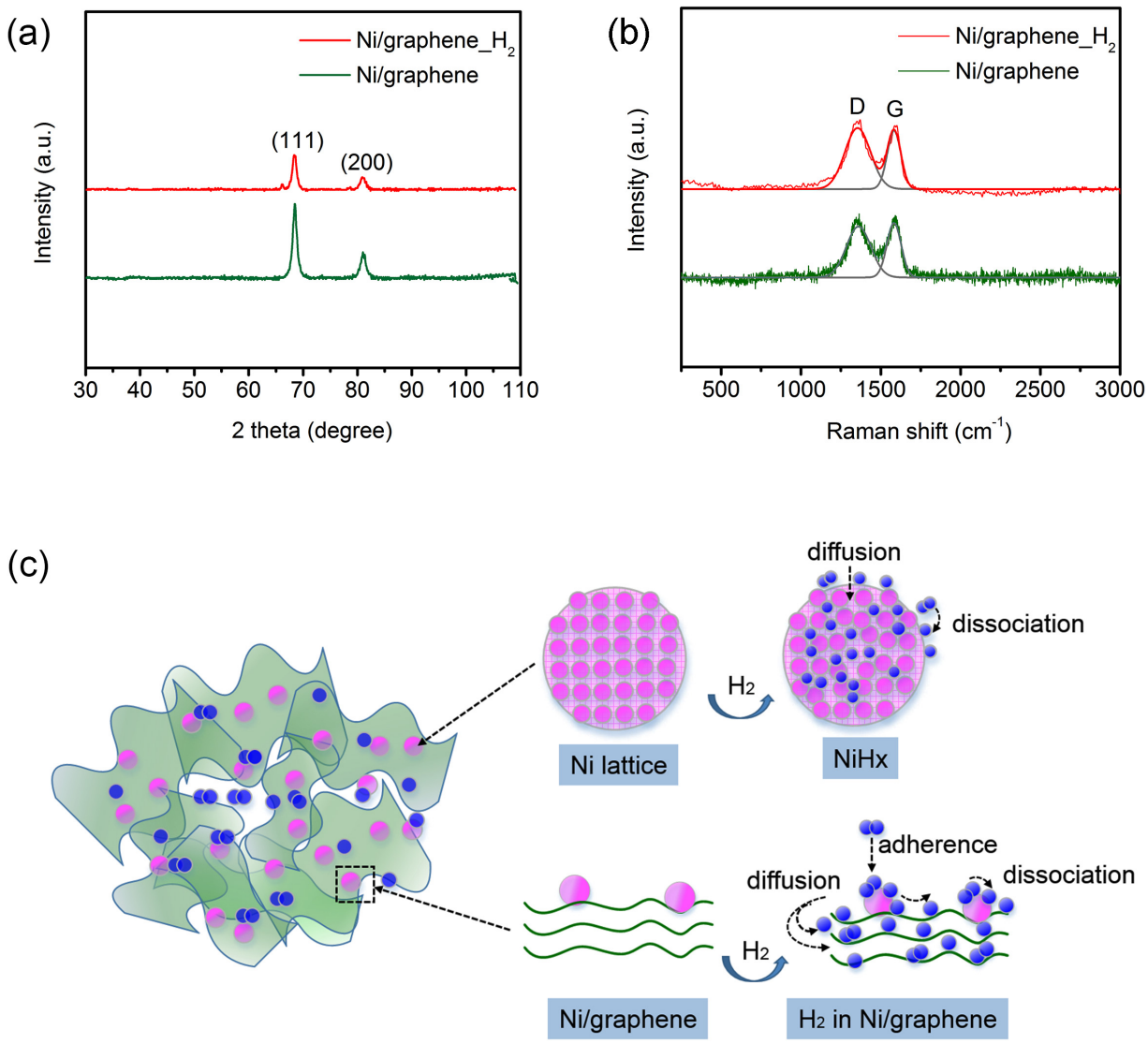

Fig. 4.6. Hydrogen uptake performance in the Ni/graphene sorbent: (a) XRD patterns, (b) Raman spectra of the Ni/graphene_0 bar and Ni/graphene_60 bar (right), (c) hypothesis of the hydrogen storage mechanism in the composite. Green: 3D graphene sheet, blue: H, pink: Ni.

On the basis of the hydrogen storage properties and the structural characterization of the hydrogen-charged composite, four categories of hydrogen uptake behaviors are hypothesized that occur during the catalytic storage at high pressure, as the schematic illustrates in Fig. 4.6c: (1) Adherence of molecular hydrogen onto the surface of Ni nanoparticles[150]: The Ni nanoparticles could adhere multiple hydrogen molecules on the surface, and some of these

anchored hydrogen molecules dissociate into atomic hydrogen at the presence of Ni[102,151]. (2) Storage in Ni lattice. A part of the dissociated hydrogen atoms penetrates into Ni lattices that is stored in Ni[147]; (3) Hydrogenation of graphene. Some dissociated hydrogen atoms migrate into graphene support via the Ni-graphene interface which serves as a linker (Ni-O-C/Ni-C) and facilitates the hydrogen spillover process[102]. These hydrogen atoms could trap at the unsaturated sites in the graphene matrix[151,152]. (4) Adsorption of hydrogen in the 3D porous graphene matrix[92]: As Fig. 4.5 shows, an increasing hydrogen charging pressure contributes to a continuously raised amount of hydrogen uptake, thus, the elevated pressure is presumed to help compress the molecular hydrogen and squeeze them into graphene. These hydrogen molecules should have been trapped in the inner layers, and delocalized through the graphene planes[8,19,150]. These proposed hydrogen uptake behaviors allow the reversible hydrogen charging and easy hydrogen discharging at a comparatively low temperature.

4.4.5 Violation of the Van't Hoff Law in TGA

The usage of TGA is not a typical methodology for the determination of hydrogen storage capacities. The experiment was carried out at a constant flow of argon from room temperature to 250°C, which could violate the Van't Hoff Law[3,153] in four aspects: (1) the measurement is not performed in a continuous pressure of hydrogen. Hence, it cannot be used for an in situ analysis of hydrogen sorption process; (2) the argon atmosphere might eliminate the thermodynamic barriers that should have existed at a desorption pressure no less than one atmospheric hydrogen for a desorption process; (3) the argon flow may cause a partial loss of sample, which could result in an inaccurate determination of hydrogen storage capacities in the sorbent; and (4) the increasing temperature cannot be used for the evaluation of isothermal hydrogen sorption process. Furthermore, the limitation of the hydrogen storage measurements in this work and the typical methodology for the hydrogen storage determination are described in details in sections 7.4 and 7.5, Chapter 7, respectively.

4.5 Conclusions

The Ni/graphene composite system was developed with the goal of stable and efficient hydrogen storage. The Ni nanoparticles of 10 nm size are well dispersed within the graphene matrix, and they presumably are attached to graphene via Ni-O-C and Ni-C bonding. As the composites were charged with hydrogen, they yielded a hydrogen capacity of 0.14 wt.% at room temperature and an atmospheric hydrogen charging pressure of 1 bar. The amount of hydrogen uptake is proportional to the hydrogen charging pressure. When charged with 60 bar of hydrogen, the sorbent had a hydrogen gravimetric density of 1.18 wt.%. Furthermore, hydrogen release occurred at an operating temperature below 150°C and completed at 250°C.

CHAPTER 5

X-RAY CHEMICAL IMAGING AND ELECTRONIC STRUCTURE OF A SINGLE NANOPLATELET NI/GRAPHENE COMPOSITE

Overview of Chapter 5

This chapter presents the manuscript titled "X-ray Chemical Imaging and Electronic Structure of a Single Nanoplatelet Ni/graphene Composite". It introduces the work on the synthesis of Ni/graphene composite and the investigation of the interaction between the Ni particles and graphene substrate.

Modifications

The manuscript presented in this chapter is different from the published version in two parts:

1. The experimental section is added with the content of synthesis and characterization techniques that moved from the introduction section.
2. Fig. B.4 is added, which shows the whole STXM image and selected spot; and Fig. B.5 is added, which is the STXM XANES C 1s, O 1s and Ni 2p spectra of the single Ni/graphene nanoplatelet.

Manuscript status

The manuscript was published in RSC Chemical Communications:

C. Zhou, J. Wang, and J. A. Szpunar, "X-ray chemical imaging and the electronic structure of a single nanoplatelet Ni/graphene composite.," *Chem. Commun. (Camb).*, vol. 50, no. 18, pp. 2282-5, 2014.

The copyright permission to use the manuscript in the thesis was obtained and provided in Appendix B. The references for this chapter along with the references of other chapters are provided at the end of the thesis.

Author Contributions

C. Zhou designed and performed the preparation of Ni/graphene composites, conducted the SEM and XRD tests, collected the STXM and XANES data and analyzed the data, and wrote the manuscript. Dr. J. Wang is the CLS beamline scientist of the SM beamline who acquired and analyzed the synchrotron data and cooperated with the manuscript writing. Dr. J.A. Szpunar planned and supervised the project. All the authors contributed to the manuscript.

Acknowledgements

This work was supported by the Canada Research Chair program and the National Engineering Research Council of Canada. C. Zhou is grateful to the China Scholarship Council (CSC) for continuous financial support. We sincerely appreciate the use of thermal treatment system in Dr. H. Wang's research lab. We also appreciate the data collection in the Canadian Light Source (CLS). The CLS is supported by the Natural Sciences and Engineering Research Council of Canada, the National Research Council Canada, the Canadian Institutes of Health Research, the Province of Saskatchewan, Western Economic Diversification Canada, and the University of Saskatchewan.

Supporting Information

Digital image and schematic diagram of the reactor part for the thermal treatment; STXM chemical imaging of the Ni/graphene sample; STXM XANES C 1s,O 1s and Ni 2p spectra of the single Ni/graphene nanoplatelet; XRD patterns of samples before and after thermal processing: as-purchased $Ni(OAc)_2$ and Ni, and Ni/graphene precursor and Ni/graphene from thermal processing (RT to 800°C in Ar, 500°C in H_2 for 1 h); SEM images of graphene oxide, Ni and Ni/graphene composite.

X-ray chemical imaging and electronic structure of a Single nanoplatelet Ni/Graphene composite

Chunyu Zhou[a], Jian Wang[b]*, and Jerzy A. Szpunar[a]*

[a] Department of Mechanical Engineering, University of Saskatchewan, Saskatoon, SK, S7N 5A9, Canada.

[b] Canadian Light Source Inc., Saskatoon, SK, S7N 2V3, Canada.

5.1 Abstract

Chemical imaging and quantitative analysis of a single graphene nanoplatelet grown with Ni nanoparticles (Ni/graphene) have been performed by scanning transmission X-ray microscopy (STXM). Local electronic and chemical structure of Ni/graphene has been investigated by spatially resolved C, O K-edges and Ni L-edge X-ray absorption using near edge structure (XANES) spectroscopy, revealing the covalent anchoring of Ni(0) on graphene. This study facilitates understanding of the structure modification of host material for hydrogen storage and offers a better understanding of the interaction between Ni particles and graphene.

5.2 Introduction

Growing demands for sustainable and clean energy are a huge challenge for the world economy as conventional energy sources are being steadily depleted[154,155]. Among various energy sources, hydrogen is becoming attractive due to its lightweight, and environmentally friendly features[116,117,154]. The development of this alternative energy source for future economy requires not only inexpensive production of hydrogen, but also the safety and efficiency of storage and delivery for practical applications. Hydrogen storage has been commonly studied in the forms of compressed gas[156], liquid hydrogen[157], condensed state[158]. However, if one has concerned with the weight, safety, environmental protection, durability and cost efficiency, the optimum choice

would be some solid state materials in a compact form. Various nanostructured materials have been considered for this application.

Graphene recently emerges as a promising hydrogen storage medium with attractive features, such as low weight, high chemical stability and extremely high specific surface area (up to 2600 cm^2/g)[39,118]. Nevertheless, as a non-polar molecule, hydrogen is very weakly bonded to pristine graphene via van der Waals's forces[8,159], which result in a low hydrogen sorption. Although metal catalyst or metallic compounds are active materials and have strong interactions with hydrogen via chemical bonds[147], the bare metal particles easily aggregate to clusters[160] providing insufficient "anchoring sites", leading to a chemically inert system for gaseous hydrogen uptake. To overcome these drawbacks, doping metal particles, especially transition metal (TM) on graphene should significantly strengthen the interaction among hydrogen, metal and graphene[3,101,159–161], i.e. TM particles, if uniformly dispersed on the surface of graphene, can serve as spacers of layered graphene structure and are hydrogen receptors, thus, they further promote a dissociative chemisorption via hydrogen spillover process[162].

This surface modification of graphene by TM nanoparticles should greatly enhance hydrogen capacity for storage and discharge because of both physisorption in pristine graphene and chemisorption in metal. Among the TMs, the presence of Ni not only alters the geometry of graphene network, resulting in enhanced structure stability[9,10,163,164] of the hydrogen host material, but also actively serves as dissociative sites for hydrogen chemisorption[78,165,166].

So far detailed analysis of the mechanism of TM/graphene interaction is still missing. A combination of X-ray absorption near edge structure (XANES) spectroscopy and scanning transmission X-ray microscopy (STXM) has been widely applied to investigate the chemical interaction and speciation in pristine graphene[167] and various graphene-based hybrid nanostructures. Problems like layered structure in r-GO[167], dopant distribution in N-CNT[168], the state of charge (SOC) in $LiMn_xFe_{1-x}PO4$/graphene[169] as well as interaction within nanostructures consisting of graphene and metallic compounds or alloy hybrids[168–170] have already been investigated.

This work reports STXM characterization of Ni/graphene as a potential hydrogen storage medium. Specifically, chemical imaging and component identification were performed on a single Ni/graphene nanoplatelet. Furthermore, spatially resolved XANES spectroscopy was obtained at the C, O K-edges and Ni L-edge to investigate the local chemistry and electronic structure, particularly Ni valence state and chemical interactions involved in Ni/graphene. TM/graphene has been synthesized through thermal reduction[171–174], CVD approach[163,164,171,175] and so forth, yet the scalability and cost efficiency of synthesis still remain challenging.

5.3 Experimental section

The Ni/graphene was produced in a simple and scalable way by pressurized multiplex solvothermal reduction[58] and followed by thermal processing. The preparation details and laboratory-based characterizations are briefly described in the supplementary information and the thermal treatment system is schematically presented in Fig. B.3, Supporting Information. STXM with a spatial resolution of 30 nm was performed on the soft X-ray spectromicroscopy beamline 10ID-1 at the Canadian Light Source (CLS). XANES at the C, O K-edges, and Ni L-edge were extracted from STXM image stacks scanned over a range of photon energies. For more details of STXM experimental and data analysis, refer to other publications by the author[168–171].

5.4 Results and discussion

5.4.1 Ni-graphene interface analysis

5.4.1.1 STXM observations

A high resolution STXM transmission (absorption) image at the Ni L_3-edge (853.3 eV) of a randomly selected Ni/graphene nanoplatelet is shown in Fig. 5.1a (See the Supporting Information, the whole STXM image and the selected spot in Fig. B.4; the STXM XANES C 1s,O 1s and Ni 2p spectra of the single Ni/graphene nanoplatelet in Fig. B.5). Ni particles can be clearly seen on the graphene nanoplatelet as dark spots and patches, which is consistent with the XRD results (Fig. B.6, Supporting Information) and SEM observations (Fig. B.7, Supporting Information), confirming the growth of Ni on graphene substrate in the nanostructured composite.

Even with some degree of Ni aggregation, Fig. 5.1a still shows the majority of Ni particles on the graphene nanoplatelet are nanoscaled/sub-micron scaled size, and they are more widely and evenly distributed than the localized aggregation. Then medium resolution STXM image stacks were acquired on the same nanoplatelet at C, O K-edges and Ni L-edge in order to derive quantitative chemical maps of the components.

Fig. 5.1b and Fig. 5.1c present the thickness map of graphene and Ni respectively, derived by fitting the C 1s and Ni 2p STXM stacks with the quantitatively scaled reference spectra of pure graphene and Ni. Fig. 5.1d displays the colour composite map of the Ni/graphene nanoplatelet. The graphene thickness map shows the lateral size and thickness of the layered graphene from thermal reduction as ~10 μm and ~25 nm, respectively.

In addition, the thickness variation of Ni particles (up to 75 nm due to partially aggregation) displayed in Fig. 5.1c suggests that a high loading of Ni on graphene was successfully achieved. Interestingly, few aggregated Ni particles attached to the edge of the graphene nanoplatelet without support were also observed, probably due to particle migration during high temperature thermal processing or coordination of Ni particles to the dangling bonds within the edge structure[9,44,51].

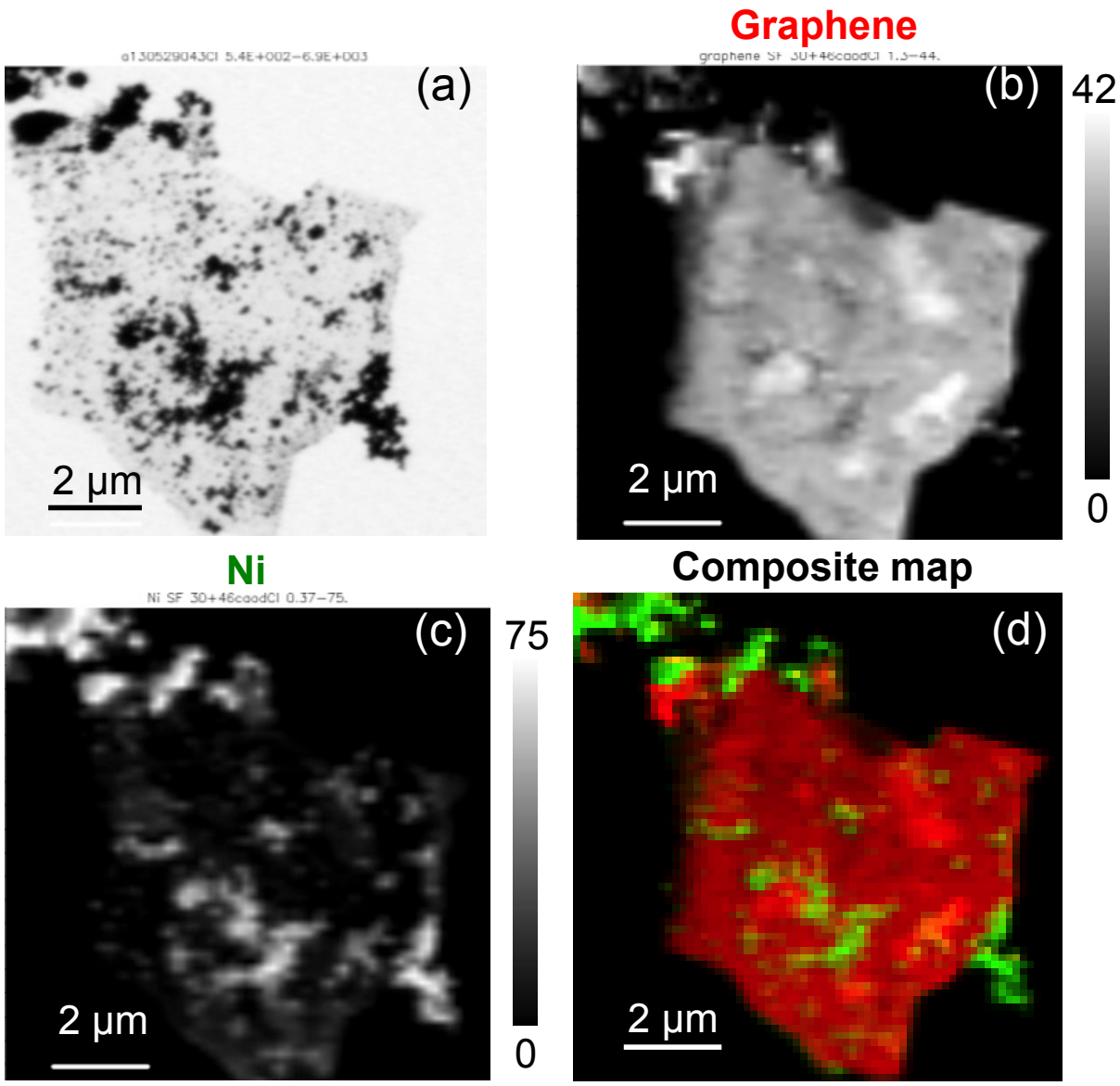

Fig. 5.1 STXM chemical imaging of a single Ni/graphene nanoplatelet: (a) high resolution STXM transmission (absorption) image at the Ni L_3-edge (853.3 eV), in which the morphology of the metallic Ni particles and the substrate graphene nanoplatelet are clearly resolved, (b) Graphene and (c) Ni thickness maps derived by medium resolution STXM image stack scans, all vertical grey scales represent the materials thickness in nm, (d) colour composite map, red: graphene, green: Ni.

5.4.1.2 XANES analysis

To further investigate the local chemistry and electronic structure of the composite, selected regions on the sample were used to extract XANES absolute absorbance (i.e. optical density) spectra from STXM stacks at the C, O K-edges and Ni L-edge in Fig. 5.2. These carefully selected regions as displayed in Fig. 5.2a include almost pure graphene (red regions), pure Ni particles off the nanoplatelet (green regions), and Ni/graphene (blue regions). The extracted C K-edge XANES spectra from the selected regions in Fig. 5.2b confirm that the green spectrum is barely featured with carbon, i.e. unsupported Ni appears along or off the edge of graphene nanoplatelet, which is in good agreement with the chemical imaging in Fig. 5.1. However, the main peaks of Ni/graphene (blue spectrum) are located at the same positions as those of almost pure graphene (red spectrum).

To make a more quantitative analysis, a linear combination of the pure Ni and graphene spectra (i.e. 0.45*Ni + 1.0*Graphene, orange lines in Fig. 5.2) matching the pre- and post-edges of Ni/graphene is included for comparison. This linear combination fit removes the sample thickness and other experimental effects and serves as a reference spectrum to quantitatively compare Ni/graphene and pure Ni + Graphene. Since XANES spectrum probes the projected unoccupied density of states (UDOS) near each elemental edge, the spectral difference between Ni/graphene and pure Ni + Graphene clearly shows the electronic structure change and subtle chemical composition difference between them.

In general, XANES peak position is sensitive to the chemical environment of the X-ray absorbing atoms, such as functional group, oxidation state/valence, bonding type etc., while XANES peak intensity is proportional to the amount of the absorbing atoms and related to the bonding orientation or chemical interactions between the absorbing atoms and the surrounding atoms, such as charge transfer, π-π interaction etc. It is commonly known that the spectral features at ~285 eV and ~292 eV are corresponding to the transitions from C 1s to graphitic states of π* and σ* respectively[167,169]. These features confirm the preservation of graphitic framework in Ni/graphene.

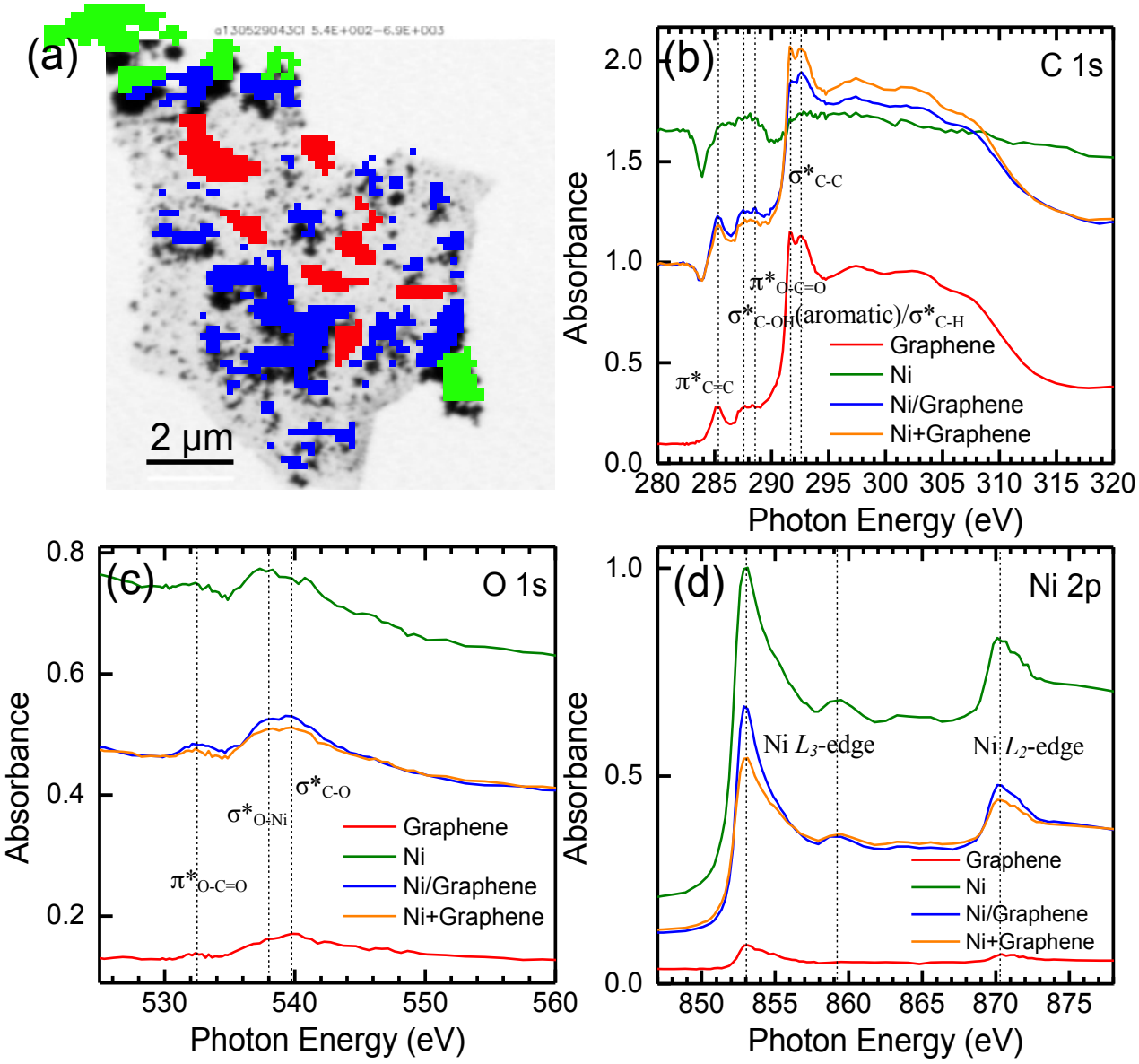

Fig. 5.2 STXM XANES spectra of a single Ni/graphene nanoplatelet: (a) selected regions on the sample to exact XANES spectra by STXM stacks, red regions: almost pure graphene, green regions: almost pure metallic Ni particles off the nanoplatelet, and blue regions: Ni/graphene; (b) C 1s, (c) O 1s, and (d) Ni 2p XANES spectra of the selected color coded regions in (a), a linear combination of the pure Ni and graphene spectra (i.e. 0.45*Ni + 1.0*Graphene, orange lines) is included to compare with Ni/graphene. All vertical dashed lines in the spectra indicate the spectral regions of interest and are labeled with electronic structure assignments.

The much stronger and broader π* peak (285.3 eV) in Ni/graphene than in almost pure graphene suggests a higher degree of wrinkling and folding within the graphene nanoplatelet after Ni nanoparticle deposition[170], suggesting a strong interaction between them, presumably that the Ni nanoparticles are favorably adsorbed on the hollow of the graphene hexagons, bridge of C-C bonds and are placed on top of C atoms[176], resulting in deformation of the graphene nanoplatelet. The less intense peak at 287.5 eV is due to σ^*_{C-H} or aromatic hydroxyl σ^*_{C-OH} or epoxyl σ^*_{C-O-C} band, while the peak at 288.5 eV is dominated by carboxyl groups $\pi^*_{O-C=O}$. The most sharpest and intense peaks at 291.7 and 292.7 eV are featured as a resolved double-peak via σ^*_{C-C} resonance[164].

Among these localized features, when compared to those of graphene, the Ni/graphene spectrum exhibits enhanced intensity between 287-290 eV due to additional carbon-oxygen functional groups (most likely the interface oxygen bridge between Ni and Graphene), and reduced intensity in the intensity-flipped double-peak σ* (291.7 and 292.7 eV) probably because of a significant charge transfer effect (more details to follow at the Ni 2p edge) and a weak polarization effect associated with a slightly higher degree of wrinkling and folding for the graphene substrate. These spectroscopic changes suggest that the graphene framework was strongly interacted/functionalized with Ni nanoparticles via Ni-C and Ni-O-C (including nickel carbonate Ni-O-C=O) covalent bonding structures.

At the O 1s in Fig. 5.2c, compared to almost pure graphene (red line) and Ni (green line) and their linear combination, O 1s spectrum of Ni/graphene (blue line) displays an overall enhanced π* and σ* intensity, strongly suggesting additional bonding/carbon-oxygen functional groups in Ni/graphene via Ni-O-C bonding structure to anchor Ni nanoparticles onto the graphene substrate, which is consistent with the C K-edge result. The correlated peaks at 532.3 and 539.9 eV are the characteristics of carboxyl groups ($\pi^*_{O-C=O}$) and σ^*_{C-O} band[164], respectively. Another pronounced peak in both Ni/graphene and Ni at ~538 eV is attributed to the σ^*_{O-Ni} band and it is absent in the almost pure graphene region.

Fig. 5.2d presents the Ni 2p XANES spectra from the three regions. Two main peaks at ~853.0 eV and 870.1 eV are located at the same energies of the elemental Ni $2p_{3/2}$ (L_3-edge) and Ni $2p_{1/2}$

(L_2-edge) levels[177], respectively. In addition, there is no evident peak splitting in the Ni 2p peaks for both Ni and Ni/graphene, indicating that the oxidation state for both is Ni(0). The Ni 2p edge jump of the Ni spectrum is about double of that of Ni/graphene, suggesting the Ni thickness in the former is about twice of the latter, which is in good agreement with the spectrum fitting coefficients in Fig. 5.2. This also implies that Ni nanoparticles off the graphene nanoplatelet tend to aggregate significantly. Compared to Ni+Graphene (orange line), the Ni 2p spectrum of Ni/graphene (blue line) shows significantly enhanced L_3 and L_2 edges (i.e. unoccupied states), suggesting a significant net charge transfer from Ni to graphene since the Ni(0) oxidation state was essentially reserved. This is considered as a result of covalent bonding of Ni-C and Ni-O-C, and the other striking observation of the charge transfer is that in the C 1s edge the $\sigma^*_{C\text{-}C}$ intensities (291.7 and 292.7 eV sharp features and other broad features from 295 to 310 eV) of graphene were significantly reduced, confirming the charge transferred to the graphene framework as XANES probes the UDOS at the carbon sites.

5.4.2 Schematic configuration of Ni-graphene interface

The schematic configuration of Ni attachment upon graphene framework in Ni/graphene is displayed in Fig. 5.3, showing the Ni adsorbed, functionalized sites, as well as the charge transfer from Ni to graphene. Although trace amount of oxygen was detected at both regions, it was most likely due to surface oxidation of the Ni(0) nanoparticles. Based on above information, the covalent interactions between Ni and graphene significantly help stabilize the nanostructure, which is expected to substantially extend the lifecycle of the host material for hydrogen uptake. Further hydrogen storage test of this material is underway.

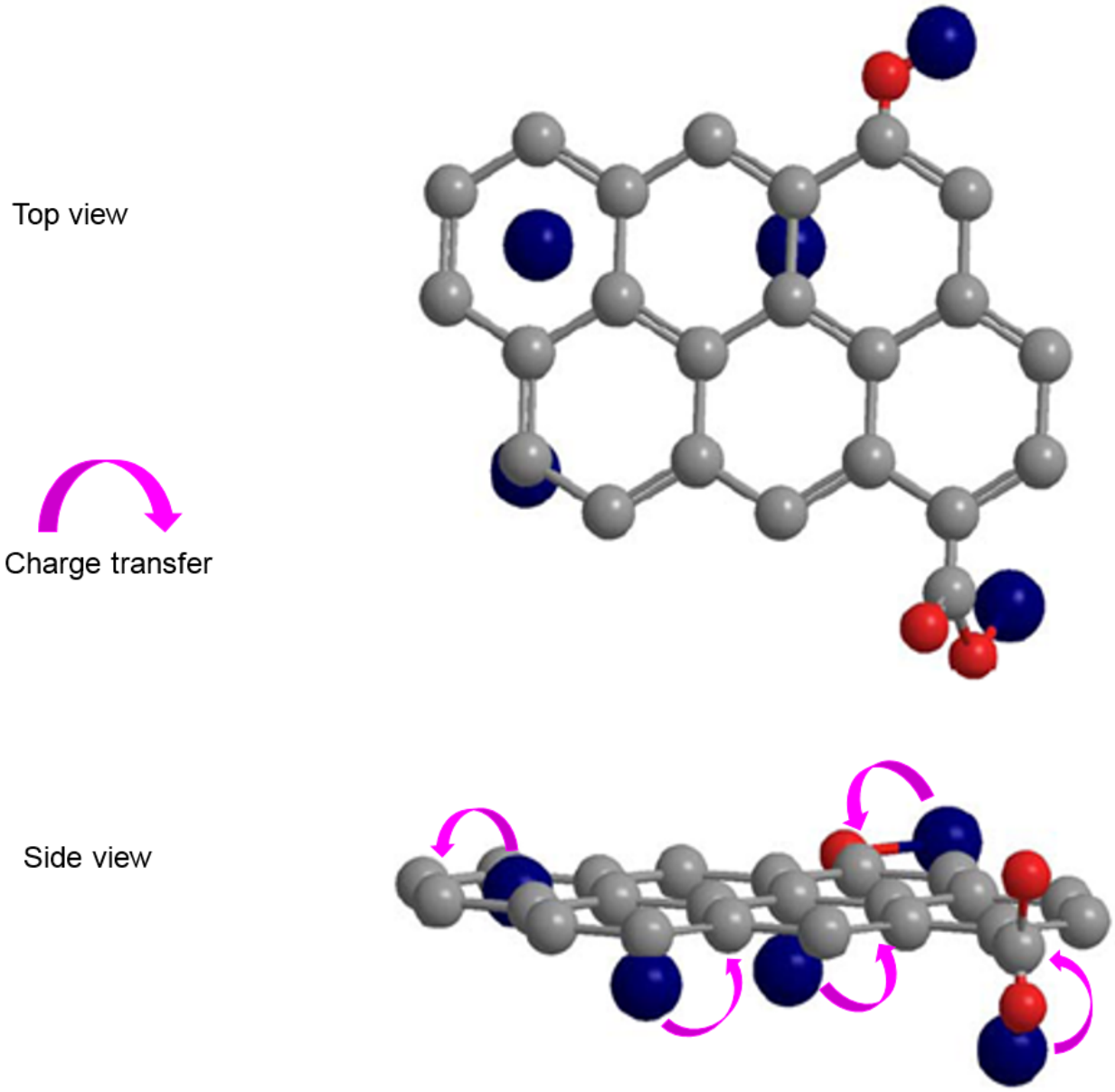

Fig. 5.3 Schematic configuration of Ni attachment upon graphene framework in Ni/graphene: Ni atoms adsorb on the hollow of the graphene hexagons, bridge of C-C bonds, top of C atoms, and Ni attached to oxygen functional groups via Ni-O-C covalent bonding. The gray, red and blue balls represent C, O and Ni atoms, respectively. The purple curved arrows indicate charge transfer from Ni to graphene.

5.5 Conclusions

STXM was performed to obtain chemical mapping and XANES of Ni/graphene nanocomposite. It was found that Ni nanoparticles prepared from the thermal reduction of nickel acetate deposit mainly on the graphene substrate with a small portion of the aggregated Ni particles attached to the edge of graphene nanoplatelet or depleted completely. The spatially resolved XANES at multiple elemental edges allowed for the determination the Ni (0) state, and the local chemistry and electronic structure, revealing the anchoring of Ni(0) nanoparticles onto the graphene substrate via Ni-C and Ni-O-C covalent bonding. These results have advanced our understanding of the electronic and chemical structure of Ni/graphene, and other similar TM/Graphene systems, and will help to optimize the tailoring of TM/Graphene host materials for hydrogen storage.

CHAPTER 6

PD/GRAPHENE NANOCOMPOSITES

Overview of Chapter 6

This chapter presents the manuscript titled "Pd/Graphene Nanocomposites". It describes the work on the synthesis of the composites and characterization of structures. The properties of hydrogenation/dehydrogenation are discussed and a mechanism for determining hydrogen uptake behaviors is suggested.

Modifications

The manuscript presented in this chapter is different from the submitted version in the following parts:

1. The title was changed from "Hydrogen Storage Performance in Pd/Graphene Nanocomposites" to "Pd/Graphene Nanocomposites".
2. The description "This new hydrogen storage system has favorable features like desirable hydrogen storage capacity, ambient conditions of hydrogen uptake, and low temperature of hydrogen release." was removed from the abstract.
3. The description "This system allows storage of hydrogen in amounts that exceed the capacity of the gravimetric target announced by the U.S. Department of Energy (DOE)." was removed from the abstract.
4. The description "Hydrogen is an attractive fuel because of the important features of energy efficiency and environmental cleanliness[116,117]; nevertheless, it is crucial to store hydrogen in an efficient and safe way for various practical applications. The U.S. Department of Energy (DOE) has announced the goals of volume energy density and gravimetric capacity of an on-board hydrogen storage system at the levels of 0.04 $kg \cdot L^{-1}$

and 5.5 wt.%[3]. Up to now, these goals have not been reached." was removed from the introduction.

5. The expression "hydrogen storage" was changed to "hydrogen release".
6. The expression "hydrogen-charged samples" was changed to "hydrogenated samples".
7. Fig. 3.1 in Chapter 3 shows the custom-made apparatus in the Supporting Information. To avoid repetition, the relevant figure is removed from the Supporting Information in Appendix B.
8. The detailed process flow of the preparation of graphene was moved from this manuscript to the section 3.2.1 of Chapter 3.
9. The detailed experimental procedures of synthesis of Pd/graphene nanocomposites were described in the section 3.2.3 of Chapter 3. The original Fig. B.8 (Process flow of the preparation of graphene) was moved from the Supporting Information of Chapter 6 to the section 3.2.1 of Chapter 3.
10. The Fig. B.10 (Morphology observations of $Pd(OAc)_2$/graphene), Fig. B.12 (EDS mapping of graphene and 5%Pd/graphene), Fig. B.15 (XAS instrument) were added to the Supporting Information.
11. The pore volume of graphene was added to the section 6.4.2.
12. The SEM and TEM micrographs of 5%Pd/graphene nanocomposite were added to Fig. 6.2, and the corresponding morphologies were analyzed.
13. An influencing factor of hydrogen storage capacity was added to the section 6.4.3: (4) exclude the amount of sorbent material that is carried away by a constant flow of argon.
14. The reason of "The 1%Pd/graphene nanocomposites have a higher gravimetric density of hydrogen compared to that in the 5%Pd/graphene nanocomposites at each pressure value." was given in the section 6.4.3: It is probably due to a revolution of thermodynamics properties of the sorbents as the particle sizes decrease. Alternatively, a smaller particle sizes could facilitate the spillover of hydrogen, which increases the hydrogen uptake amount in the sorbents.

Manuscript status

The manuscript was published in journal ACS Applied Materials & Interfaces:

C. Zhou, J. A. Szpunar. Hydrogen storage performances in Pd/graphene nanocomposites. *ACS Appl. Mater. Interfaces*, 2016, DOI: 10.1021/acsami.6b07122.

Copyright

The copyright permission to use the manuscript in the thesis was obtained and provided in Appendix B. The references for this chapter along with the references of other chapters are provided at the end of the thesis.

Author Contributions

C. Zhou designed and performed the experiment, analyzed the data, and wrote the manuscript. Dr. J.A. Szpunar supervised the project. Both authors contributed to the manuscript.

Notes

The authors declare no competing financial interest.

Acknowledgements

This work is supported by the Canada Research Chair program and the National Engineering Research Council of Canada. C. Zhou is grateful to the China Scholarship Council (CSC) for continuous financial support. We acknowledge Dr. Y. Hu and Dr. Q. Xiao for the help and support of XANES tests and data analysis at the Canadian Light Source (CLS). We sincerely appreciate the discussions with Dr. H. Wang and his help with data analysis. We are grateful to Mr. X. Wang and Mr. F. Fan for their help with the data collection.

Supporting Information

SEM observations of the as-prepared graphene; Particle size distribution of Pd nanoparticles on graphene sheets by SEM observation; SEM images of as-prepared graphene, $Pd(OAc)_2$,

precursor $Pd(OAc)_2$/graphene, Pd/graphene nanocomposite, and TEM image of Pd/graphene nanocomposite. EDS mapping of the 1%Pd/graphene and 5%Pd/graphene nanocomposites; Raman spectroscopy of the graphene and Pd/graphene nanocomposites (Gaussian function fitting); XRD (Cr Kα radiation, λ=0.229 nm) patterns of metallic Pd, the precursor $Pd(OAc)_2$/graphene and the as-prepared Pd/graphene nanocomposite; Hydrogen storage capacities of the Pd/graphene nanocomposites with loading amounts of Pd 1 at.% and Pd 5 at.% that charged with hydrogen at pressures from 10 to 60 bar; In-situ hydrogen reduction and XAS characterization of Pd/graphene on SXRMB 06B1-1 beamline at the CLS.

Pd/graphene nanocomposites

Chunyu Zhou* and Jerzy A. Szpunar

Department of Mechanical Engineering, University of Saskatchewan, Saskatoon, SK, S7N 5A9, Canada.

6.1 Abstract

A Pd-graphene nanocomposite was developed for hydrogen storage. The spherically shaped Pd nanoparticles of 5-45 nm in size are homogeneously distributed over the graphene matrix. After hydrogen charging at a pressure of 50 bar, the material released 6.7 wt.% H_2 from the 1%Pd/graphene nanocomposite in TGA. As the applied pressure increased to 60 bar, the released hydrogen in TGA reached 8.67 wt.% in the 1%Pd/graphene nanocomposite and 7.16 wt.% in the 5%Pd/graphene nanocomposite.

6.2 Introduction

Among the potential candidates for high density of hydrogen storage media is nanostructured graphene because it is lightweight and has a high specific surface area, rather porous frameworks, great chemical stability, on-board reversibility[14,118,178]. It is also possible to use some metal catalysts to actively anchor hydrogen[3,15]. However, hydrogen storage in the pure graphene or in metal hydrides has severe drawbacks[120]: the nonpolar hydrogen molecule is weakly bonded to carbon through van der Waals forces[7,121], and this limits the amount of hydrogen uptake; also the metal particles could easily aggregate to form clusters because of high cohesive energy [101], which leads to deficient binding sites and results in a chemically inert system for hydrogen sorption.

Researchers have recently proposed that the deposition of metal on the graphene surface could offer many attractive characteristics[122,179,180], like stable Pd clusters, or interconnected Pd nanodendrite should significantly improve the hydrogen storage capability[3,19,20]. Research

literature already documents that Pd particles favorably anchor H_2 at ambient conditions[14–17]. The particles produce a low activation energy barrier to dissociate hydrogen molecules[14,18]. If homogeneously distributed over the graphene surface, the Pd particles could perform as efficient hydrogen receptors[8]. Besides, these particles can be incorporated into the substrate and change the local ionic structure of the substrate[181]. This system will further facilitate a dissociation and diffusion of hydrogen and storage in graphene via a spillover process[102,103]. The hydrogen storage capacity in such a combined metal-graphene system could be significantly increased compared to what is possible in the individual constituents (graphene and bare metal)[14,124], and this makes Pd/graphene a possible candidate to reach the desirable volumetric and gravimetric densities.

In this work, a simple method was reported to produce the Pd/graphene nanocomposites with Pd loading amounts of 1 at.% (1%Pd/graphene) and 5 at.% (5%Pd/graphene). The synthesized Pd/graphene nanocomposites enable a hydrogen uptake at ambient conditions and a hydrogen release at low temperature. In particular, when charged at a hydrogen pressure of 60 bar, the 1%Pd/graphene nanocomposite system captures 8.67 wt.% of hydrogen.

6.3 Experimental section

6.3.1 Preparation of graphene gel

The detailed procedures of preparation were described in the section 3.2.1 of Chapter 3. Fig. B.8 shows the various morphologies of the as-prepared graphene sample.

6.3.2 Synthesis of Pd/graphene composite

The detailed experimental procedures of the synthesis of Pd/graphene nanocomposites were described in the section 3.2.3 of Chapter 3.

6.3.3 Material characterization

To evaluate the crystal structure and determine the phase composition of the metallic Pd and Pd/graphene nanocomposite, an X-ray diffractometer (XRD, Bruker D8) installed with a Cr Kα

source (λ = 0.229 nm) was used, and the ω angles were set to at 30, 60, and 90° for normal scans with a scanning rate of 2°/min. The pore size distribution and specific surface areas of graphene were determined by applying a nitrogen isothermal adsorption-desorption of Brunauer−Emmett−Teller (BET, ASAP 2020 V3.01 H) technique. Energy-dispersive spectroscopy (EDS) equipment was used to collect the mapping of the Pd/graphene surface at a voltage of 30 kV. The morphologies of graphene and nanocomposite system were analyzed by using a scanning electron microscope (SEM, FEI XL30) at 5 and 20 kV with a working distance of approximately 10 mm and a transmission electron microscope (TEM, Philips CM10) at an acceleration voltage of 100 kV with magnifications of 92 k and 125 k. The Raman spectra were collected by using a Renishaw 2000 Raman microscope, and a laser with an excitation λ of 514 nm was used with the scattered light dispersed by an 1800 L/mm grating. The Pd L_3-edge X-ray absorption near-edge spectroscopy (XANES, SXRMB, 06B1-1 at the Canadian Light Source) measurements were performed to analyze the local chemistry and electronic structure with Pd L_3-edge energy scan ranging from 3140 eV to 3200 eV.

6.3.4 Hydrogen release measurement

The hydrogen release capacities of the Pd/graphene system were tested by using a custom-made instrument (Fig. 3.1) and thermogravimetric analysis (TGA, SDT Q600). The samples were charged with hydrogen at room temperature with different pressures by using the custom-made apparatus. The temperature of the hydrogen charging process was monitored by using a thermocouple-connected temperature controller, and the temperature was displayed with a constant temperature of 23-25°C. Each sample was charged with hydrogen for 30 min and then taken out and immediately within 5 min transferred to the TGA equipment at ambient conditions. The TGA analyzer was used to measure hydrogen release from the hydrogen charged sorbents. Then the sample was placed in a crucible at room temperature with an argon flow of 100 mL/min for 15 min in order to stabilize the experimental conditions. Then the temperature started to increase and the hydrogen release was measured. The sample weight was recorded as a function of temperature for the calculation of hydrogen storage capacities in the sorbents. The measurements were performed under an argon flow of 100 mL/min from ambient temperature to 200°C at a heating rate of 20°C/min. The Pd/graphene specimens that were not charged with

hydrogen and the specimens that were charged at 1 bar of hydrogen were further tested. The measurement results were used as references to subtract any possible water adsorption, impurities, and oxidation products that might have been attached to the sorbents during the transfer process. In addition, the hydrogenated samples (0 and 60 bar) for both 1%Pd/graphene and 5%Pd/graphene nanocomposites were tested at 25°C for 100 min in order to evaluate the unstable amount of hydrogen uptake. These corrections were applied to calculate the hydrogen storage capacities in the sorbents.

6.4 Results and discussion

6.4.1 Decoration of graphene

Fig. 6.1 displays the schematic flow of the synthesis process. The precursor $Pd(OAc)_2$/graphene [$Pd(CH_3COO)_2$/r-GO] was prepared from the homogeneous mixing of palladium acetate solution with graphene oxide gel [$Pd(CH_3COO)_2$/GO], while the graphene oxide was reduced to reduced graphene oxide. Then the precursor was converted to the Pd/graphene nanocomposite with the Pd particle bonded to graphene at the interface.

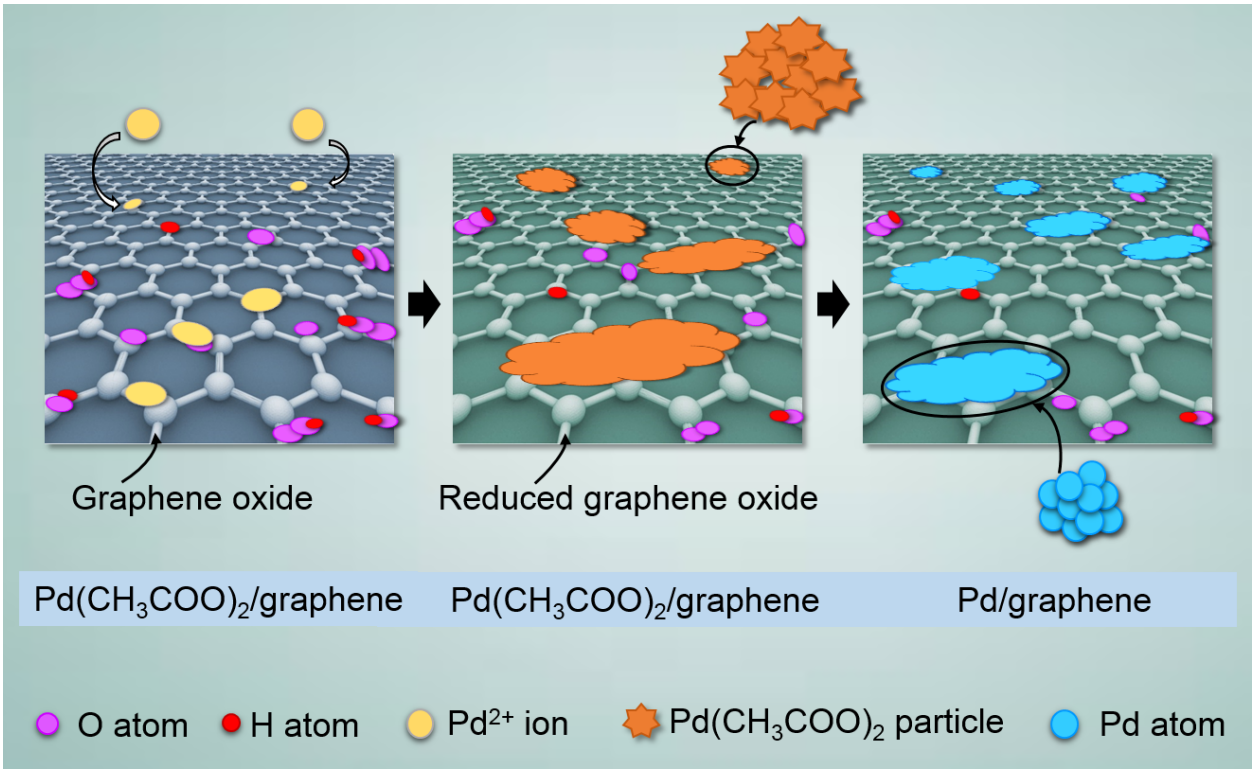

Fig. 6.1 Schematic illustration of synthesis process of Pd/graphene nanocomposite.

6.4.2 Morphology and structure

The quality of dispersion of Pd particles in the graphene matrix significantly influences the hydrogen storage in the nanocomposite. The distribution of particles was optimized, and Fig. 6.2 exhibits the morphologies of the Pd/graphene nanocomposites. For reference, Fig. 6.2 displays the morphology of an as-prepared pure graphene sheet and also shows the bare metallic Pd particles prepared by hydrogen thermal reduction. The pure graphene (Fig. 6.2a) has a wrinkled, crumpled and folded structure with a microscale lateral dimension (Fig. 6.2a, inset). The BET analysis previously had been carried out and determined the specific surface areas and average pore width of graphene to be 751.9 m^2/g and 3.3 nm, respectively[179], and the pore volume were tested to be 0.6 cm^3/g. The Pd particles have a spherical shape with a mean diameter of ~300 nm (Fig. 6.2b).

In comparison, after the reduction of $Pd(OAc)_2$/graphene (SEM images of $Pd(OAc)_2$/graphene are shown in Supporting Information, Fig. B.10), the SEM observation shows that the Pd particles in the 1%Pd/graphene and 5%Pd/graphene nanocomposites appear to have been uniformly dispersed throughout the graphene matrix (Fig. 6.2c) with a mean particle size of ~45 nm (Supporting Information, Fig. B.9). Besides, the TEM observations reveal a uniform distribution of the Pd nanoparticles in the graphene substrate. The particle nanoparticles in 5%Pd/graphene have a slightly larger size than those in 1%Pd/graphene with a mean particle size of ~5 nm in 1%Pd/graphene (Fig. 6.2d, right top) and 5-10 nm in 5%Pd/graphene (Fig. 6.2d, right bottom). In comparison, a larger average particle size by the SEM observation could be attributed to a slight aggregation of Pd during the freeze-drying process. Overall, the sizes of Pd nanoparticles in these two nanaocomposites were assumed in a range of 5-45 nm.

The significant decrease of the Pd particle size in the nanocomposite could be related to an enhanced dispersion and lower mobility of Pd particles in the graphene substrate (see the EDS mappings of the 1%Pd/graphene and 5%Pd/graphene in Supporting Information, Fig. B.11 and Fig. B.12). The particles could have bonded to the edges, defects, and functional groups on the surface of graphene[182,183]. This interaction may have further stabilized the Pd nanoparticles and effectively prevented the particle aggregation on the graphene surface[178].

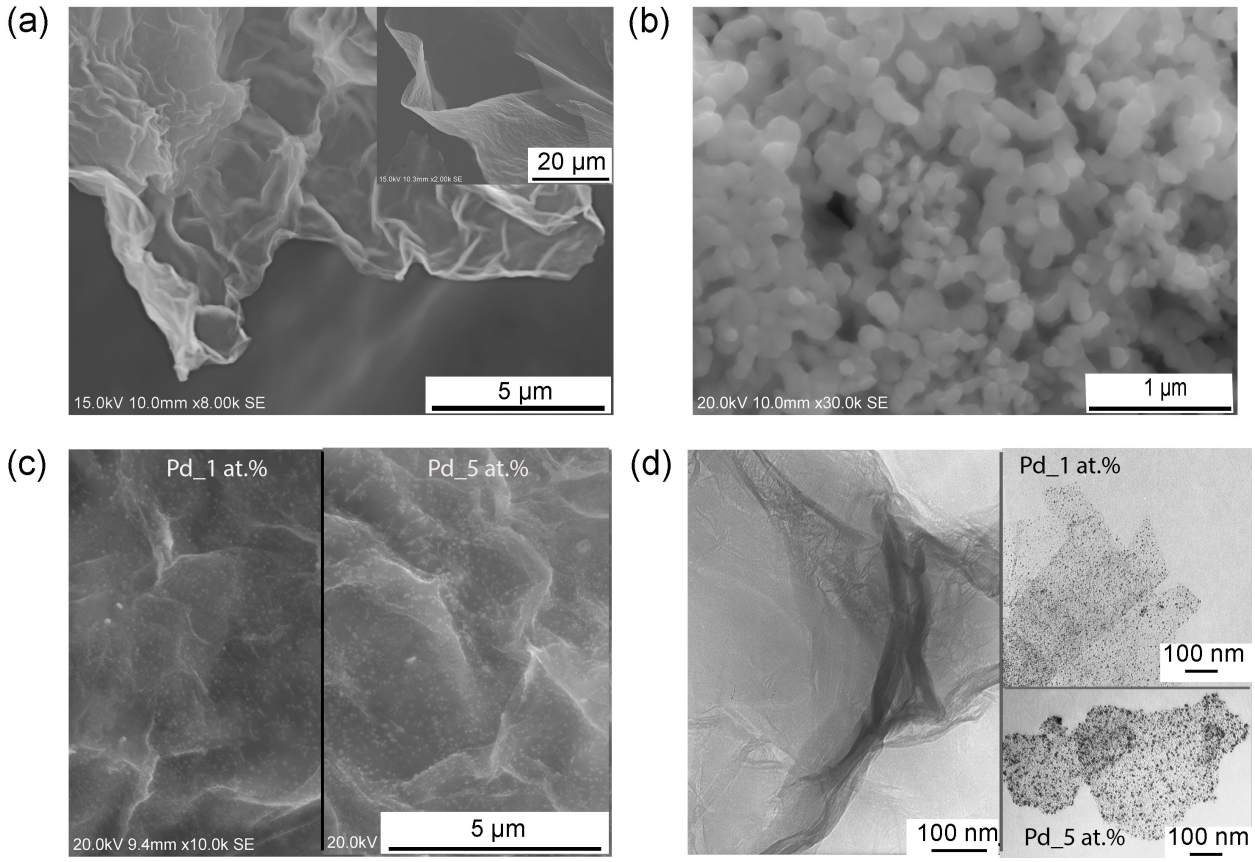

Fig. 6.2 SEM micrographs of (a) as-prepared graphene sheet (inset, low magnification image), (b) as-prepared Pd particles, (c) Pd/graphene nanocomposites of 1%Pd (left) and 1%Pd (right), (d) TEM observations of graphene sheet (left); Pd/graphene nanocomposites of 1%Pd (right top) and 5%Pd (right bottom).

Raman spectroscopy detects the vibrations that result from the changes in geometric structure and chemical bonding of molecules[131]. In Fig. 6.3, the D and G bands predominate the spectral features of graphene structure: especially the D band at ~1355.38 cm^{-1} is a disorder/defect band involving the ring breathing sp^3 carbon, while the G band at ~1588.46 cm^{-1} corresponds to a sp^2-hybridized graphitic structure[131]. The Raman spectra show no prominent shift in peak position from the graphene (red line) to the Pd/graphene nanocomposites (green and blue lines, see Supporting Information, Table B.1). The intensity ratio of D/G bands determines the defects existing in the graphene structure. Compared to that of graphene (I_D/I_G=0.89), the D/G intensity ratio in the spectrum of the Pd/graphene nanocomposite significantly increases in the

1%Pd/graphene (I_D/I_G=1.17) and slightly increases in the 5%Pd/graphene (I_D/I_G=0.91), suggesting a strengthened sp^3-bonded structure and a softened sp^2-hybridized carbon in the composites. This structural change may arise from the charge transfer[184] between the Pd and graphene structure, probably resulting in a formation of Pd-C and Pd-O-C bonds[178]. Further, the difference in the D/G intensity ratio of these two composites reflects that the 1%Pd/graphene has more defects than the 5%Pd/graphene[173]. This indicates that the loading amount of 1 at.% Pd could alter the structure of graphene with a higher quantity of structural defects. That is, a certain amount of Pd may result in a small size of particles, which could expose more nanoparticles to the hexagonal network of carbon atoms and modify the graphene substrate more efficiently.

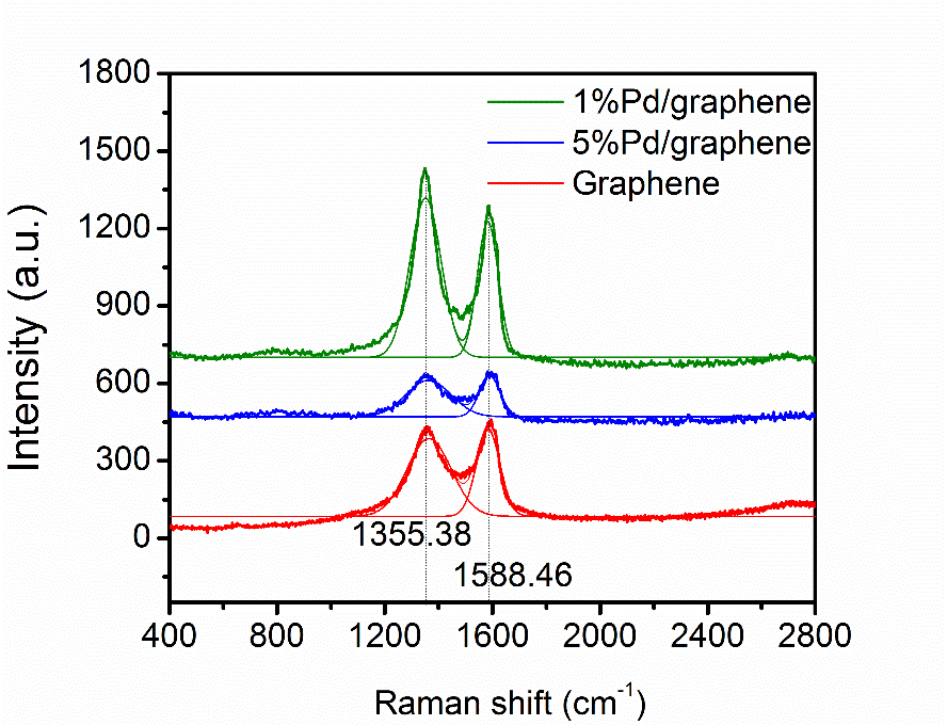

Fig. 6.3 Raman spectra of graphene and Pd/graphene nanocomposites with the Pd amounts of 1 at.% and 5 at.%.

6.4.3 Hydrogen release

The hydrogen release in the 1%Pd/graphene and 5%Pd/graphene were investigated by using TGA in an inert atmosphere of argon with a heating rate of 20°C/min. Fig. 6.4 presents the

results of experiments. The reference measurements were conducted on the non-hydrogenated nanocomposites (Pd/graphene_0 bar, Fig. 6.4a and Fig. 6.4b) and hydrogen-charged nanocomposite at 1 bar (Pd/graphene_1 bar, Fig. 6.4c) to determine the hydrogen storage capacity in the hydrogenated samples. The non-hydrogenated nanocomposites (Pd/graphene_0 bar) slightly lost weight in both 1%Pd/graphene (Fig. 6.4a) and 5%Pd/graphene (Fig. 6.4b) nanocomposites. Since graphene is chemically stable at ambient environment[39], it cannot be oxidized/reduced in air at room temperature and atmospheric pressure[142]. Thus, the probability of the structure variation of graphene during the transfer process in air may be ruled out. Therefore, the weight variation of the Pd/graphene_0 bar sample is probably caused by a removal of adsorbed water.

In addition, as shown in the Supporting Information Fig. B.13, XRD measurements show that the Pd remains metallic, which is in agreement with the experimental results that were collected by Y Li et. al[142]. However, there might be a slight oxidation of Pd when exposed to air[185] that was hardly detected by XRD, and this influencing factor needs to be precluded for the calculation of hydrogen uptake.

Compared to that in the Pd/graphene_0 bar (Fig. 6.4a and Fig. 6.4b), an extra weight loss occurred in the Pd/graphene_1 bar, suggesting a hydrogen uptake in the nanocomposite at ambient conditions (Fig. 6.4c), which has been documented in the literature[186]. Besides the desorption of adsorbed water and any other residual impurities[3], this extra weight loss in the nanocomposite is very likely due to a hydrogen release and a possible removal of water that results from the atmospheric oxidation of the hydrogen in Pd during the transfer process in air[145].

Furthermore, the hydrogenated samples gradually decrease the mass for specimens charged at pressures from 10 to 60 bar (Fig. 6.4a and Fig. 6.4b), indicating the hydrogen release from the sorbents. As increasing hydrogen uptake on Pd results in a decrease of hydrogen oxidation rate in air[145], during the transfer process, the impact of hydrogen charging pressure on the amount of hydrogen oxidation on Pd may be neglected. In the 1%Pd/graphene nanocomposites (Fig. 6.4a), the hydrogen-charged samples had a rapid loss of weight between 60 and 100°C, and a slight weight loss between 100 and 200°C. In the 5%Pd/graphene nanocomposites (Fig. 6.4b), a fast

release of hydrogen occurred at a temperature lower than 80°C with a slow release of hydrogen from 80 to 200°C (See Supporting Information, Fig. B.14). In either case, the probability of an elimination of any oxygen-containing groups from the graphene structure within 200°C may be excluded[143]. The fast desorption at a temperature no higher than 100°C in both 1%Pd/graphene and 5%Pd/graphene samples indicates a dominant physisorption or a weak chemisorption of hydrogen in the sorbents. In addition, the lower discharging temperature in the 5%Pd/graphene nanocomposites was presumably due to an increased number of Pd particles that led to an increased Pd-H_2 interaction, which then allowed a fast hydrogen desorption at lower temperatures[186].

To evaluate the stability of hydrogen storage in the sorbents, the hydrogen-charged samples were tested at 0 and 60 bar for both 1%Pd/graphene and 5%Pd/graphene nanocomposites at 25°C, 100 min. Fig. 6.4d shows that the sample masses gradually stabilized after 80 min with a mild hydrogen release of 1.34 wt.% in the 1%Pd/graphene and 0.18 wt.% in the 5%Pd/graphene nanocomposites. The remaining hydrogen was stored without any additional release at ambient conditions.

In short, when calculating the storage of hydrogen in the Pd-graphene system, four corrections were introduced to the measured data using additional experimental tests: (1) correct for the adsorbed water and gas impurities; (2) exclude the influence of the Pd oxidation; (3) eliminate possible production of water from oxidation of hydrogen gas; (4) exclude the amount of sorbent material that is carried away by a constant flow of argon; and (5) remove an unstable hydrogen uptake from the calculated amount of hydrogen storage.

In 1%Pd/graphene, the trapped hydrogen uptake under various pressures was calculated by subtracting the weight loss of 6.38 wt.% [corrections of (1), (2), (3), and (4) in Fig. 6.4c] and the amount of easily released hydrogen of 1.34 wt.% at ambient conditions [correction of (5) in Fig. 6.4d] from the total weight loss of each hydrogen charged sorbents (Fig. 6.4a). While in 5%Pd/graphene, the trapped hydrogen uptake under various pressures was calculated by subtracting the weight loss of 3.8 wt.% [corrections of (1), (2), (3), and (4) in Fig. 6.4c] and the amount of easily released hydrogen uptake of 0.18 wt.% [correction of (5) in Fig. 6.4d] from the

total weight loss of each hydrogen-charged sample (Fig. 6.4b). These corrections were implemented for the weight losses of the hydrogen-charged samples (Fig. 6.4a and Fig. 6.4b). Then the hydrogen storage capacities were plotted as a function of the applied hydrogen charging pressures from 10 to 60 bar in Fig. 6.4e.

From 10 to 60 bar of hydrogen charge, the 1%Pd/graphene nanocomposites have a higher gravimetric density of hydrogen compared to that in the 5%Pd/graphene nanocomposites at each pressure value. It is probably due to a revolution of thermodynamics properties of the sorbents as the particle sizes decrease (Fig. 6.2)[187]. Alternatively, a smaller particle sizes could facilitate the spillover of hydrogen, which increases the hydrogen uptake amount in the sorbents[188]. Notably, the nanocomposites were displayed with a hydrogen capacity of 6.7 wt.% in the 1%Pd/graphene nanocomposite with hydrogen charging pressure of 50 bar. When the pressure increased to 60 bar, the hydrogen storage capacities were as high as 8.67 wt.% in the 1%Pd/graphene nanocomposite and 7.16 wt.% in the 5%Pd/graphene nanocomposite. The measurement results identified that the hydrogen storage capacity increases under elevated pressures of hydrogen charging, indicating that the hydrogen uptake is pressure sensitive.

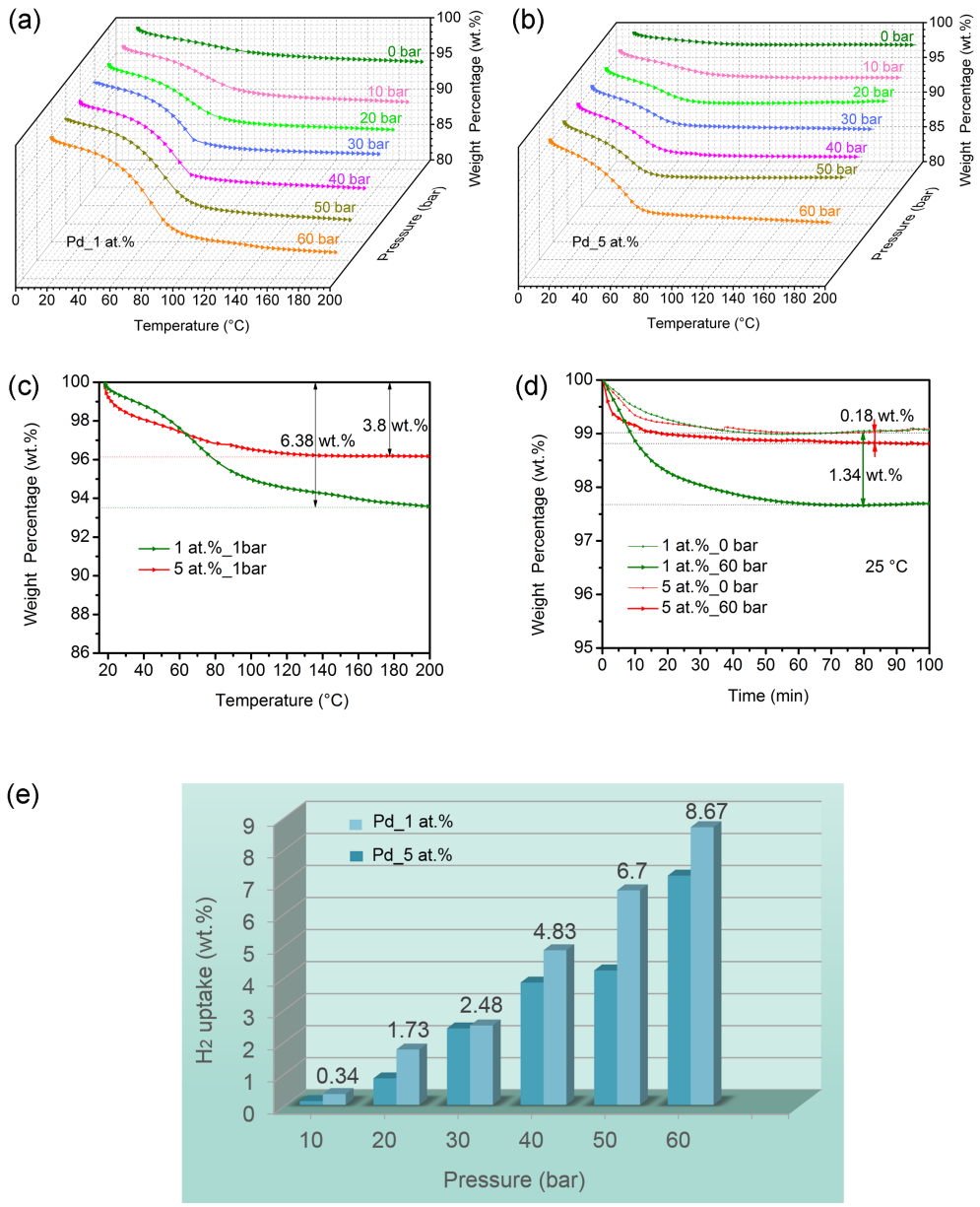

Fig. 6.4 Thermogravimetric analysis of the hydrogen storage capacities in the Pd/graphene nanocomposites with a loading amount of (a) Pd 1 at.% and (b) Pd 5 at.% that charged with hydrogen at pressures from 10 to 60 bar. (c) Weight changes of the hydrogen-charged samples (1%Pd/graphene and 5%Pd/graphene) at atmospheric pressure of hydrogen. (d) Weight changes of the Pd/graphene_0 bar and Pd/graphene_60 bar at room temperature within 100 min. (e) Stable hydrogen storage capacities as a function of the applied hydrogen charging pressures from 10 to 60 bar.

Li et al. reported that the Pd nanocrystals/MOF has a double hydrogen uptake capacity compared to that in the bare Pd nanocrystals[124]. They suggested that the MOF coated with Pd has greatly facilitated the surface/bulk reactivity between the Pd nanocrystals and hydrogen at 303 K and an atmospheric hydrogen charging pressure[124]**.** This material could be a promising hydrogen storage medium for practical applications. Wang et al. determined that a Ni (0.83 wt.%)-B (1.09 wt.%) nanoalloy/graphene system could achieve a hydrogen uptake amount of 4.4 wt.% at 77 K and a hydrogen charging pressure of 106 kPa[78]. Despite that, the material requires an extremely low temperature for the hydrogen uptake. Besides, a Ni (5 at.%)/graphene system was previously synthesized, which achieves a hydrogen storage capacity of 1.18 wt.% at 25°C and 60 bar[179]. Eun Seon Cho et al. synthesized a graphene/Mg composite that reached an attractive gravimetric density of 6.5 wt.% at a hydrogen pressure of 15 bar[149]. However, this system requires impractical temperatures for the hydrogen charging process (250°C) and the discharging process (300°C)[149].

By contrast, the Pd/graphene nanomaterials in this project show multiple desirable characteristics. The 1%Pd/graphene composites can store hydrogen up to 6.7 wt.% at room temperature and 50 bar. Further, at room temperature and 60 bar, the hydrogen storage capacities could reach 8.67 wt.% in the 1%Pd/graphene nanocomposite and 7.16 wt.% in the 5%Pd/graphene nanocomposite. In addition, the composites could favorably discharge hydrogen below 100°C and the process completes within 200°C.

6.4.4 Electronic structure analysis

To further investigate the mechanism of hydrogen storage performance in the 1%Pd/graphene nanocomposite system, Pd L_3-edge XANES spectra were collected on the specimens charged with hydrogen at 0, 20, 40, and 60 bar to characterize the local chemistry and electronic structure as shown in Fig. 6.5. The instrument diagram is described in the Supporting Information, Fig. B.15. The XANES analysis was also performed on the precursor $Pd(OAc)_2$/graphene and a standard Pd foil as blank tests, and the standard Pd spectrum was used to examine the reduction extent of Pd (II) in the nanocomposite. The oxidation state of Pd corresponded to the edge position and peak area[136]. Since the Pd L-edge is mainly correlated with the excitation of the 2p

core electrons to the unfilled Pd 4d states, the peak area directly reflects the density of unoccupied states[137,189,190].

From the green line to blue line in Fig. 6.5a, the peak area was severely reduced after the reduction. The corresponding weaker absorption then indicates the reduction of Pd (II). The derivative of the spectrum can directly reflect the absorption position, and the bottom of Fig. 6.5a displays the absorption edges of spectra. The edge shifted from the energy of the Pd (II) precursor (green line) to lower energies for the final reduced Pd (blue line) and the metal foil (red dashed line). Once the unfilled d states become occupied, it results in a smaller energy bandgap of the 2p-4d states; thus the energy needed to excite 2p electrons to another unfilled d state decreases[190]. Consequently, the absorption edge's shift toward lower energies and this confirms that the Pd (II) became reduced. Additionally, the similar spectral features of the Pd/graphene with the Pd foil are also an indication of Pd reduction, which is consistent with the XRD data (see Supporting Information, Fig. B.13).

The Pd/graphene has a slightly higher absorption energy than the metallic Pd foil. It can be attributed to the variation of the electronic structure of Pd and graphene in the nanocomposite; that is, electron density could be presumably pulled to the defects in the graphene[136] since there is an interaction between Pd and graphene[191]. This interaction can stabilize the Pd nanoparticles against diffusion and aggregation in the graphene matrix, represented by the nanoparticle size distribution and morphology (Fig. 6.2c and Fig. 6.2d). In comparison, if the Pd/graphene nanocomposites were charged at different hydrogen pressures, they exhibited no detectable edge shift (Fig. 6.5a). When zoomed in (Fig. 6.5b), the spectra showed a slight decrease in the peak area after the hydrogen charging, and the peak area tended to decline gradually with increasing hydrogen charging pressure. It indicates a slight reduction of Pd in the nanocomposites, which could result from an increased amount of PdH_x due to an increased hydrogen uptake in the sorbents[92].

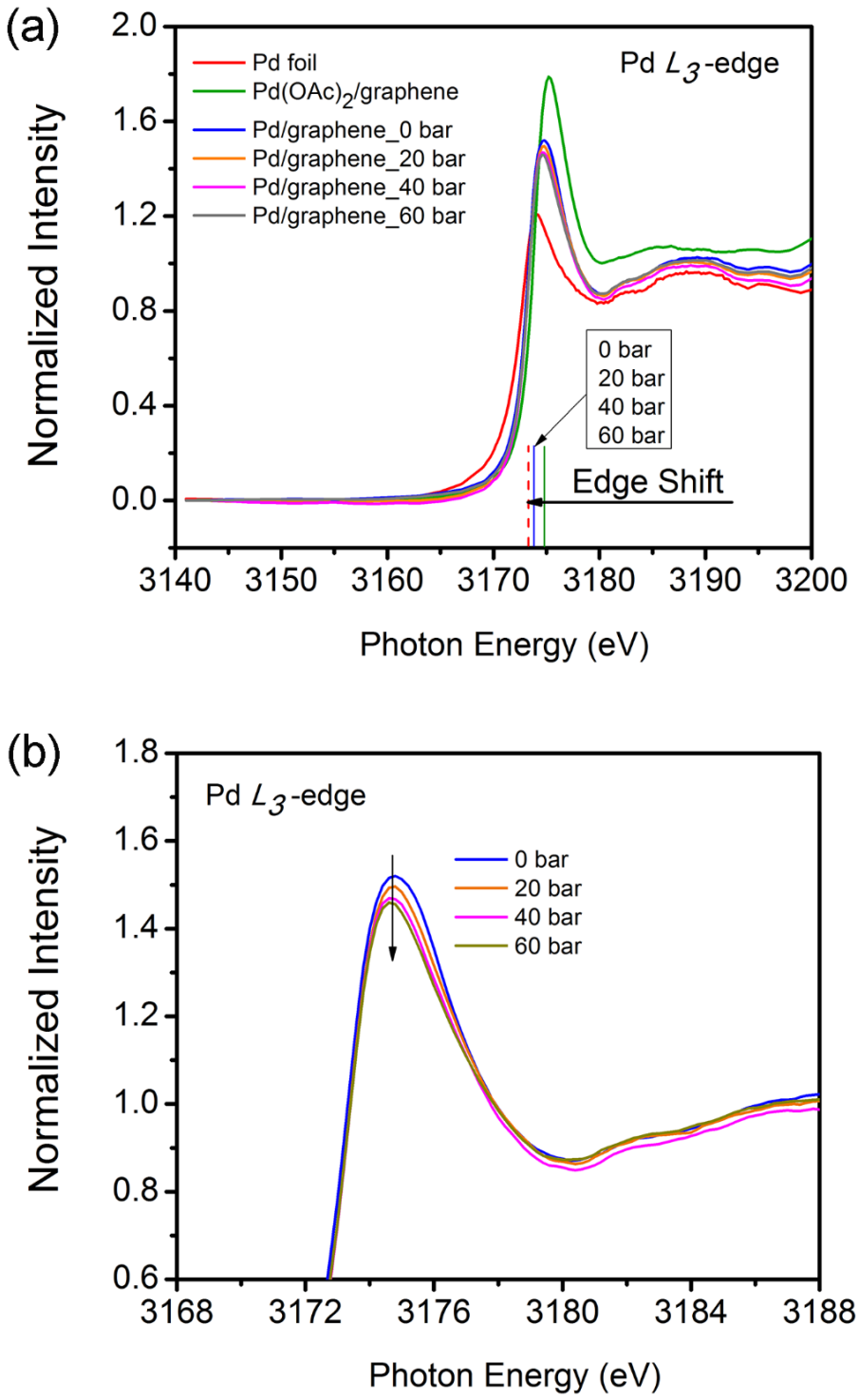

Fig. 6.5 Pd L_3-edge XANES spectra: (a) $Pd(OAc)_2$/graphene, Pd foil reference, 1%Pd/graphene nanocomposites before and after hydrogen charging at pressures of 0, 20, 40, and 60 bar, and (b) 1%Pd/graphene at pressures of 0, 20, 40, and 60 bar at the photon energy ranging from 3168 to 3188 eV.

6.4.5 Hydrogen release mechanism

On the basis of the structural characterization and hydrogen storage properties, four types of hydrogen performances in the Pd/graphene sorbents are hypothesized during the high pressure of catalytic reaction: (1) binding of hydrogen molecules to the Pd atoms[92]; (2) hydrogen atom attached to Pd nanoparticles as PdHx[147]; (3) atomic hydrogen at the unsaturated sites of graphene (hydrogenation of graphene)[151,152]; and (4) molecular hydrogen trapped in the porous graphene support[92,192]. To illustrate the hydrogen uptake performance in the Pd/graphene nanocomposite, a schematic diagram of the storage system is proposed as depicted in Fig. 6.6.

On one hand, the well-dispersed Pd nanoparticles attract multiple hydrogen molecules in an activated state[150]. The presence of Pd could increase the binding energy and facilitate the adsorption of H_2 because of the polarization of the molecular H_2 probably through a hybridization of H_2 σ/σ^* orbitals with the Pd d orbitals[150]. On the other hand, due to a slow hydrogenation kinetics of Pd and a low energy barrier, some of the adsorbed molecular hydrogen may dissociate into atomic hydrogen on the surface of Pd catalyst[102,151]. One part of these hydrogen atoms diffuses into Pd lattices and contributes to the formation of hydride[147]. The rest of the dissociated hydrogen atoms could be ejected from the metal nanoparticles to the gas-phase[151]. Because of the dissociation of H–H bond, the ejected H atoms obtain some kinetic energy and then migrate to the Pd-graphene interfacial zone from the Pd catalytic sites via surface diffusion[151,193], spread further to the layered graphene edges and other uncapped end, and subsequently have access to the layered space and porous nanostructures by surface diffusion[151,152]. These atoms likely interact with graphene through covalent C-H bonds[151,152] at unsaturated sites in the graphene matrix. Due to the polarization of hydrogen, the presence of Pd catalytically facilitates the mobility of hydrogen while providing a desired binding energy of hydrogen with graphene due to the polarization of hydrogen. This catalytic gas-phase hydrogenation of graphene would enable the reversible storage at moderate temperature[150,194]. This hypothesis of hydrogen storage in the Pd/graphene system is mainly consistent with the spillover theory, which has been reported frequently[102,151,193].

Furthermore, as the nanocomposites have gradually enhanced hydrogen storage capacities with increasing charging pressures from 10 to 60 bar, the molecular hydrogen is assumed to be compressed, squeezed into graphene, secured in the interlayer space, and probably delocalized on the graphene planes at an elevated pressure as was demonstrated earlier[8,19,150]. When the high pressure is released, the adsorbed hydrogen could remain partially trapped in the graphene structure at ambient conditions. Consequently, a combination of these various mechanisms of hydrogen uptake contributes to the high capacity of hydrogen storage in the Pd/graphene sorbents.

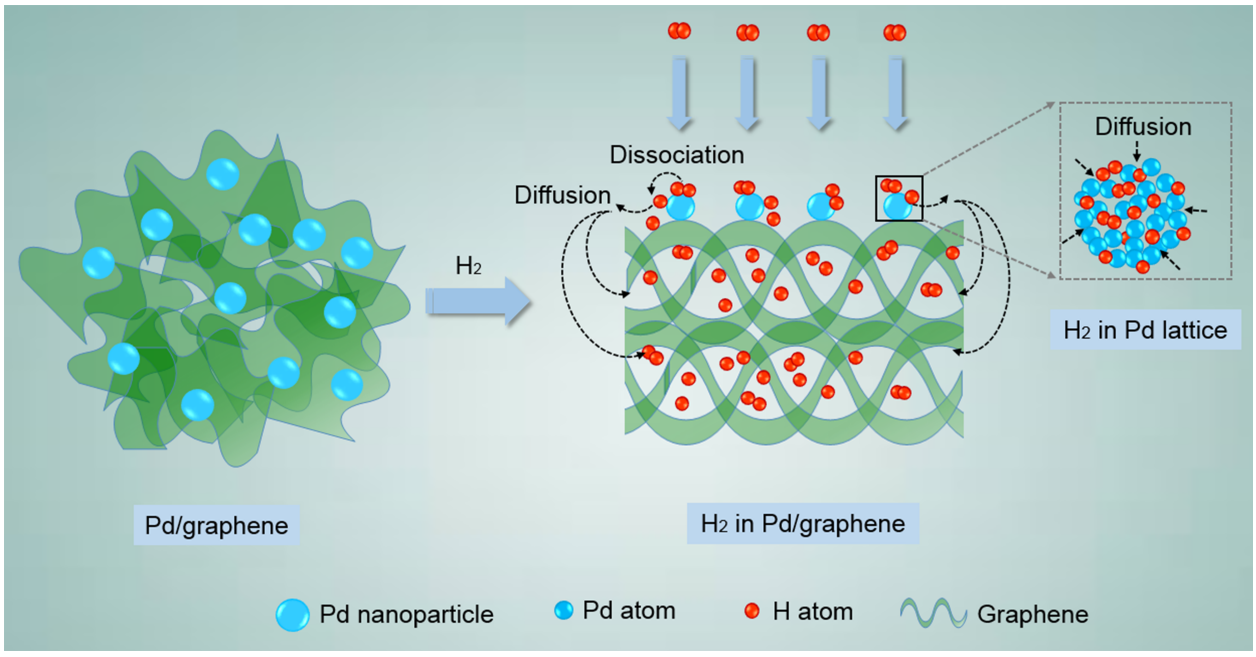

Fig. 6.6 Hydrogen storage mechanism of the Pd/graphene sorbent.

Nevertheless, the usage of TGA is not a commonly used methodology to determine the hydrogen storage capacities, and the experiment could violate the Van't Hoff Law as described in the section 4.4.5.

6.5 Conclusions

The Pd/graphene nanocomposites were developed for hydrogen storage. The spherical shaped Pd nanoparticles have an average size of 5-45 nm and are homogeneously distributed within the graphene matrix. The Pd nanoparticles are bound to the graphene structure through the Pd-C and Pd-O-C bonds. The nanocomposites were charged with hydrogen and at a hydrogen charging pressure of 50 bar, they could achieve a hydrogen storage density of 6.7 wt.% in the 1%Pd/graphene. As increased the pressure to 60 bar, the hydrogen uptake capacity was as high as 8.67 wt.% in the 1%Pd/graphene nanocomposite and 7.16 wt.% in the 5%Pd/graphene nanocomposite.

CHAPTER 7

CONCLUSIONS AND FUTURE RESEARCH

7.1 Summary

1. A laboratory apparatus has been designed, built and applied for the hydrogen charging process with a maximum operating temperature of 300°C and the pressure of 2000/137.9 (psi/bar). Each test allows a specimen with volume up to 166 mL. After hydrogen charging, the specimens are transferred to a TGA apparatus for the determination of hydrogen storage.
2. The transfer process exposes the specimens to air at ambient conditions. This process could cause errors in the amount of storage. The relevant factors include the adsorption of water and gas impurities, slight oxidation of hydrogen and metal, escape of hydrogen from sorbents at ambient conditions. Therefore, a series of blank tests were conducted by using TGA to eliminate the possible errors.
3. The modified Hummers method was developed to prepare graphene oxide that was subsequently reduced to graphene during the synthesis of metal/graphene. The graphene fine powder can be described by a 3D interconnected network with microscale lateral sized sheets. It has a specific average surface area of ~751.9 m^2/g with an average pore width of ~3.3 nm, a pore volume of 0.6 cm^3/g and an interlayer distance of ~0.38 nm. The loose sheets are fluffy, paper-like, wrinkled, folded with the elements C and O homogeneously distributed over the surface and a C/O atomic ratio of 6.14 (86 at.% :14 at.%). The graphene reveals the presence of carbon containing groups, including carbon ring C-C/C=C, C-O, C=O, and O-C=O bonds. This chemically prepared graphene shows a sp^2 hybridized graphitic structure with disorders/defects on the planes.
4. Two approaches were applied to synthesize the Ni/graphene composites. The first method was in situ chemical reduction of $Ni(OAc)_2$ in graphene gel, and the resultant precursor was freeze-dried and further converted to Ni/graphene by hydrogen thermal treatment. In the

second method, the $Ni(OAc)_2$-graphene solid powder was reduced by hydrogen thermal treatment.

5. In the Ni/graphene with a Ni loading amount of 5 at.%, the Ni has average crystal sizes of 7 - 9 nm. The elements C, O and Ni uniformly spread over the composites with an atomic ratio of 83.8 at.% : 11 at.% : 5.3 at.%, respectively. Moreover, Ni particles were well distributed in the graphene matrix and have a grain size of ~10 nm. Compared to the pure Ni particles of ~250 nm, the size of Ni particles in the composite was significantly diminished, suggesting that the formation of Ni clusters was prevented.
6. With the loading of Ni, graphene still remains the fluffy sheet network, but has a weakened sp^2 hybridization and a comparatively strengthened sp^3-bonded carbon. The Ni d orbitals could have hybridized with C π orbitals or O p orbitals on the graphene surface via the formation Ni-C and Ni-O-C bonds.
7. When charged at room temperature and atmospheric hydrogen pressure, the Ni/graphene (at.% Ni) yielded a hydrogen capacity of 0.14 wt.%. When increased to 60 bar, the sorbent reached a hydrogen gravimetric density of 1.18 wt.%. The sorbent released hydrogen at an operating temperature below 150°C and completed the release at 250°C. This system exhibits attractive features like storage of hydrogen at room temperature and low activated temperature for hydrogen release.
8. Pd/graphene (1 at.% Pd and 5 at.% Pd) were synthesized by hydrogen thermal treatment of the precursor $Pd(OAc)_2$/graphene obtained from the mixture of $Pd(OAc)_2$ ethanol solution with graphene gel.
9. In the Pd/graphene with a Pd loading amount of 5 at.%, the elements C, O and Pd are consistently dispersed over the composites with atomic ratios of 81.9 at.%, 13.8 at.%, 4.2 at.%, respectively. The spherical shaped Pd nanoparticles of 5~45 nm were homogeneously distributed over the graphene matrix. Compared to the pure Pd particles of ~300 nm, the Pd particles in the composite were significantly decreased in size, reflecting that graphene could effectively improve the dispersion of Pd particles and prevent the particle aggregation.
10. With the loading of Pd, the graphene also has the fluffy sheet network, while the Pd chemical state indicates a modification of electronic structure between the Pd and graphene, in which

electron density was presumably pulled towards the defects and oxygen-containing groups in the graphene via Pd-C and Pd-O-C bonds.

11. The Pd/graphene system shows attractive features like high gravimetric density, ambient conditions of hydrogen uptake and low temperature of hydrogen release. When charged with hydrogen at 50 bar, the material yielded a hydrogen capacity of 6.7 wt.% in the 1%Pd/graphene composite. When increased to 60 bar, the gravimetric density of hydrogen reached 8.67 wt.% in the 1%Pd/graphene and 7.16 wt.% in the 5%Pd/graphene.
12. Based on the structural characterizations and property determinations, four categories of hydrogen uptake were proposed: (1) Hydrogen molecules bound to the metal atoms. (2) The hydrogen atom attached to metal nanoparticles as a metal hydride. (3) Atomic hydrogen trapped at the unsaturated sites of graphene (hydrogenation of graphene). (4) Molecular hydrogen trapped in the porous graphene support.

7.2 Conclusions

Ni/graphene and Pd/graphene nanocomposites were synthesized and optimized for the usage of hydrogen storage. The Ni/graphene (5 at.% Ni) was determined to have a hydrogen capacity of 0.14 wt.% at room temperature and 1 bar of hydrogen. It had a hydrogen uptake density of 1.18 wt.% at 60 bar of hydrogen. The hydrogen release could take place at an operating temperature below 150°C, and the process completes within 250°C.

Especially, at room temperature, the Pd/graphene (1 at.% Pd) could yield a hydrogen gravimetric density of 6.7 wt.% at 50 bar of hydrogen. At the hydrogen charging pressure of 60 bar, the capacities reached 8.67 wt.% in the 1%Pd/graphene (1 at.% Pd) composite and 7.16 wt.% in the 5%Pd/graphene (5 at.% Pd). The composites could discharge hydrogen below 100°C and complete the process within 200°C.

7.3 Contribution to original knowledge

1. Design and construction of an apparatus for hydrogen storage determination

   It is the first time a custom-made apparatus was combined with a TGA technique to determine the hydrogen uptake capacities in materials. The self-constructed apparatus allows

a high operating temperature of 300°C and pressure of 2000/137.9 (psi/bar) and enables a sample volume as high as 166 mL for each test.

2. Development and optimization of the synthesis of composites

   Novel synthesis methods were developed to homogenously deposit the metal nanoparticles (Ni, Pd) into the graphene matrix. These approaches could effectively disperse the nano-size metal particles. They are affordable and can be simply applied for the production of large quantity of metal/graphene.

3. Investigation of the electronic structure of composites

   The electronic structures of composites were explored by using synchrotron techniques for the first time. They reveal an interaction between metal and graphene, and that facilitates the optimization of synthesis and the investigation of hydrogen storage performance.

4. Determination of the hydrogen storage property of Pd/graphene composite

   The composite allows ambient conditions of hydrogen uptake and low temperature of hydrogen release. In particular, this system shows attractive gravimetric densities of hydrogen capacities of 6.7 wt.% in the Pd/graphene (1 at.% Pd) at a hydrogen pressure of 50 bar, and 8.67 wt.% at 60 bar.

5. Suggestion of a hydrogen uptake mechanism

   Based on the properties and structural characterizations, this research experimentally suggested the hydrogen uptake behaviors in the composites that both metal and graphene play roles in the hydrogen uptake.

7.4 Limitations of the hydrogen storage measurements

In this project, the combination of hydrogen charging equipment with TGA apparatus is not a typical methodology for the determination of hydrogen storage properties as it violated the fundamental Van't Hoff Law for hydrogen desorption. After hydrogen charging process, the hydrogen charging pressure was released, which could desorb a certain amount of hydrogen from the sorbents. Besides, the hydrogen charged samples were took out and transferred to TGA for the measurement of hydrogen storage capacities. During the transfer process, the hydrogen charged samples were exposed to air, and it might result in a contamination of the samples. The

TGA measurement process could also cause a weight loss of the sorbents due to the argon flow or the reactions that take place within the hydrogen-charged samples.

7.5 Sieverts technique

In comparison to the methodology in this project, the gas sorption of Sieverts technique is a classic volumetric method to determine the Pressure–Composition Temperature (PCT) or Pressure–Composition Isotherm (PCI) properties of a solid state material[3,153]. The PCT/PCI curves are presented in Fig. 7.1a[153,195], in which the natural log of hydrogen pressure is versus the corresponding hydrogen concentration in a sorbent at a particular temperature. The Sieverts technique allows an in situ determination that directly estimates the isothermal hydrogen sorption process. The reversible storage capacity at a specific temperature can be determined by the width plateau in the PCT/PCI curves[3].

Moreover, the dehydrogenation in a Sieverts-type apparatus under 1 bar (or higher) H_2 pressure conforms to the Van't Hoff Law. The relevant plot could be used to evaluate the thermodynamic properties of a solid state system for practical storage purposes, including the enthalpy of hydride formation/decomposition (ΔH) and the entropy of hydriding/dehydriding process (ΔS)[3,153]. The Van't Hoff plot is a figure that depicts the natural log of plateau pressure as a function of inverse temperature as shown in Fig. 7.1b[153,195].

$$In\frac{P}{P_0} = \frac{\Delta H}{RT} - \frac{\Delta S}{R} \tag{7.1}$$

where,

P is the midplateau pressure,

P_0 is the atmospheric pressure

Δ H and Δ S are the enthalpy and entropy of formation/decomposition of hydride, respectively,

R is the universal gas constant (8.314472 $J \cdot K^{-1} \cdot mol^{-1}$),

T is the absolute temperature.

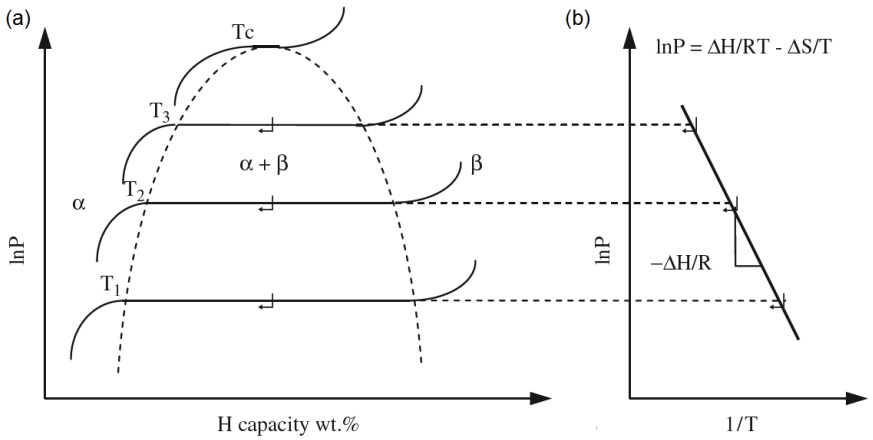

Fig. 7.1 (a) Pressure–Concentration–Temperature curves and (b) Van't Hoff plot[153,195].

Following Eq. 7.1, the intercept provides the entropy and the slope of the line yields the enthalpy[3]. ΔS determines the feasibility of hydrogen sorption process, while ΔH determines the operating temperature and pressure for a hydrogen storage system[3]. Therefore, these thermodynamic parameters can be used to assess the suitability of a material for hydrogen storage purpose. Consequently, the Sieverts technique provides a system for the in situ studies of hydrogen sorption process, which can be applied in the future work to accurately determinate the hydrogen storage properties of a metal-decorated graphene system regarding the PCT/PCI curves and thermodynamic parameters.

7.6 Suggestions for future work

1. To optimize the method for hydrogen storage determination

   A Sieverts type apparatus can be adopted for the in situ measurements of hydrogen storage properties and thermodynamic properties of the sorbents.

2. To perform cycling and isotherm tests, thermodynamic research and measurement of the times required for refueling

   The hydrogen charging/discharging cycles are crucial to the determination of the minimum life of sorbents. Isotherms are the plots of hydrogen uptake versus pressure at a fixed temperature. The ad/absorption and desorption isotherms show the reversibility of storage in the sample and correlate highly with thermodynamic properties. The future practical application requires a rapid refueling and release of hydrogen, thus, the hydrogen charging/discharging tests determine how fast a system can be refueled/powered.

3. To investigate various other metal/graphene systems

   The present work has focused on Ni/graphene and Pd/graphene composites. Some other metal/graphene systems, like Pt/graphene, Ti/graphene, and other theoretically predicted favorable systems can be investigated and used for hydrogen storage.

4. To experimentally explore the hydrogen storage mechanism

   The explanation of hydrogen uptake/release performances enables the optimization of sorbents. Synchrotron-based techniques can be used for in situ uptake/release processes, and should allow exploration of the further evolution of the electronic structure, and contribute to better understanding of the hydrogen storage in graphene composites.

REFERENCES

1. Rose, R. Fuel cells and hydrogen: The path forward; A comprehensive strategy for federal investment in fuel cell technology and fuel infrastructure. (2002).
2. Fuel cell technologies program. U.S. Department of Energy (2011).
3. Broom, D. P. Hydrogen storage materials: the characterisation of their storage properties. (Springer Science and Business Media, 2011).
4. Peigney, A., Laurent, C., Flahaut, E., Bacsa, R. R. and Rousset, A. Specific surface area of carbon nanotubes and bundles of carbon nanotubes. Carbon N. Y. 39, 507–514 (2001).
5. Ge, C., Lao, F., Li, W., Li, Y., Chen, C., Qiu, Y., Mao, X., Li, B., Chai, Z. and Zhao, Y. Quantitative analysis of metal impurities in carbon nanotubes: efficacy of different pretreatment protocols for ICPMS spectroscopy. Anal. Chem. 80, 9426–9434 (2008).
6. Pumera, M. Carbon nanotubes contain residual metal catalyst nanoparticles even after washing with nitric acid at elevated temperature because these metal nanoparticles are sheathed by several graphene sheets. Langmuir 23, 6453–6458 (2007).
7. Pumera, M. Graphene-based nanomaterials and their electrochemistry. Chem. Soc. Rev. 39, 4146–57 (2010).
8. Pumera, M. Graphene-based nanomaterials for energy storage. Energy Environ. Sci. 4, 668 (2011).
9. Rigo, V. A., Martins, T. B., Da Silva, A. J. R., Fazzio, A. and Miwa, R. H. Electronic, structural, and transport properties of Ni-doped graphene nanoribbons. Phys. Rev. B 79, 75435 (2009).
10. Wei, G., Miao, Y.E., Zhang, C., Yang, Z., Liu, Z., Tjiu, W.W. and Liu, T. Ni-doped graphene/carbon cryogels and their applications as versatile sorbents for water purification. Appl. Mater. Interfaces 5, 7584–7591 (2013).
11. Ouyang, L.Z., Yang, X.S., Zhu, M., Liu, J.W., Dong, H.W., Sun, D.L., Zou, J. and Yao, X.D. Enhanced Hydrogen Storage Kinetics and Stability by Synergistic. J. Phys. Chem. C

118, 7808–7820 (2014).

12. Wang, Y., Guo, C.X., Wang, X., Guan, C., Yang, H., Wang, K. and Li, C.M. Hydrogen storage in a Ni–B nanoalloy-doped three-dimensional graphene material. Energy Environ. Sci. 4, 195–200 (2011).

13. Zheng, L., Li, Z., Bourdo, S., Watanabe, F., Ryerson, C.C. and Biris, A.S. Catalytic hydrogenation of graphene films. Chem. Commun. (Camb). 47, 1213–5 (2011).

14. Adams, B. D. and Chen, A. The role of palladium in a hydrogen economy. Mater. Today 14, 282–289 (2011).

15. Yamauchi, M., Kobayashi, H. and Kitagawa, H. Hydrogen storage mediated by Pd and Pt nanoparticles. ChemPhysChem 10, 2566–2576 (2009).

16. Cappillino, P.J., Sugar, J.D., Hekmaty, M.A., Jacobs, B.W., Stavila, V., Kotula, P.G., Chames, J.M., Yang, N.Y. and Robinson, D.B. Nanoporous Pd alloys with compositionally tunable hydrogen storage properties prepared by nanoparticle consolidation. J. Mater. Chem. 22, 14013–14022 (2012).

17. Li, G., Kobayashi, H., Dekura, S., Ikeda, R., Kubota, Y., Kato, K., Takata, M., Yamamoto, T., Matsumura, S. and Kitagawa, H. Shape-dependent hydrogen-storage properties in Pd nanocrystals: Which does hydrogen prefer, octahedron (111) or cube (100)? J. Am. Chem. Soc. 136, 10222–10225 (2014).

18. Campesi, R., Cuevas, F., Gadiou, R., Leroy, E., Hirscher, M., Vix-Guterl, C. and Latroche, M. Hydrogen storage properties of Pd nanoparticle/carbon template composites. Carbon N. Y. 46, 206–214 (2008).

19. Contescu, C.I., Van Benthem, K., Li, S., Bonifacio, C.S., Pennycook, S.J., Jena, P. and Gallego, N.C. Single Pd atoms in activated carbon fibers and their contribution to hydrogen storage. Carbon N. Y. 49, 4050–4058 (2011).

20. Lee, H., Ihm, J., Cohen, M. L. and Louie, S. G. Calcium-decorated graphene-based nanostructures for hydrogen storage. Nano Lett. 10, 793–798 (2010).

21. Züttel, A. Materials for hydrogen storage. Mater. today. 6, 24–33 (2003).

22. National Research Council. The hydrogen economy: opportunities, costs, barriers, and R&D needs. (National Academy Press, 2004).

23. Klebanoff, L. Hydrogen storage technology: materials and applications. (CRC Press, 2012).

24. Von Helmolt, R. and Eberle, U. Fuel cell vehicles: Status 2007. J. Power Sources 165, 833–843 (2007).

25. Walker, G. Solid-state hydrogen storage: materials and chemistry. (Elsevier, 2008).

26. Orimo, S.I., Nakamori, Y., Eliseo, J. R., Züttel, A. and Jensen, C. M. Complex hydrides for hydrogen storage. Chem. Rev. 107, 4111–4132 (2007).

27. Sandrock, G. A panoramic overview of hydrogen storage alloys from a gas reaction point of view. J. Alloys Compd. 293–295, 877–888 (1999).

28. Corey, R.L., Ivancic, T.M., Shane, D.T., Carl, E.A., Bowman Jr, R.C., Bellosta von Colbe, J.M., Dornheim, M., Bormann, R., Huot, J., Zidan, R. and Stowe, A.C. Hydrogen motion in magnesium hydride by NMR. J. Phys. Chem. C 112, 19784–19790 (2008).

29. Thomas, K. M. Hydrogen adsorption and storage on porous materials. Catal. Today 120, 389–398 (2007).

30. Yürüm, Y., Taralp, A. and Veziroglu, T. N. Storage of hydrogen in nanostructured carbon materials. Int. J. Hydrogen Energy 34, 3784–3798 (2009).

31. Van Den Berg, A. W. C., Bromley, S. T. and Jansen, J. C. Thermodynamic limits on hydrogen storage in sodalite framework materials: a molecular mechanics investigation. Microporous Mesoporous Mater. 78, 63–71 (2005).

32. Langmi, H. W., Ren, J., North, B., Mathe, M. and Bessarabov, D. Hydrogen storage in metal-organic frameworks: a review. Electrochim. Acta 128, 368–392 (2014).

33. Makowski, P., Thomas, A., Kuhn, P. and Goettmann, F. Organic materials for hydrogen storage applications: from physisorption on organic solids to chemisorption in organic molecules. Energy Environ. Sci. 2, 480–490 (2009).

34. Scientific background on the nobel prize in physics 2010: graphene. The Royal Swedish Academy of Sciences (2010).

35. http://www.thenanoage.com/carbon.htm.

36. Boehm, H. P., Clauss, A., Fischer, G. O. and Hofmann, U. Das Adsorptionsverhalten sehr dünner Kohlenstoff-Folien. J. Inorg. Gen. Chem. 316, 119–127 (1962).

37. Mouras S, Hamm A., D. D.; C. J. C. Synthesis of first stage graphite intercalation compounds with fluorides. Rev. Chim. minérale 24, (1987).

38. Stankovich, S., Dikin, D.A., Dommett, G.H., Kohlhaas, K.M., Zimney, E.J., Stach, E.A., Piner, R.D., Nguyen, S.T. and Ruoff, R.S. Graphene-based composite materials. Nature 442, 282–286 (2006).

39. Novoselov, A. K. G. and K. S. The rise of graphene. Nat. Mater. 6, 183–191 (2007).

40. Russell, P. The band theory of graphite. J. Chem. Inf. Model. 53, 1689–1699 (2013).

41. Bonuu, H. P. Surface properties of extremely thin graphite lamellae. 12, 1–8 (1958).

42. Kostya Novoselov, Andre Geim, S.V. Morozov, D. J. Electric field effect in atomically thin carbon films. Science. 306, 666–669 (2004).

43. Kim, S.J., Choi, T., Lee, B., Lee, S., Choi, K., Park, J.B., Yoo, J.M., Choi, Y.S., Ryu, J., Kim, P. and Hone, J. Ultraclean patterned transfer of single-layer graphene by recyclable pressure sensitive adhesive films. Nano Lett. 15, 3236–3240 (2015).

44. McCann, E. and Koshino, M. The electronic properties of bilayer graphene. Rep. Prog. Phys. 76, 056503 (2013).

45. Tan, P., Han, W., Zhao, W. and Wu, Z. The shear mode of multilayer graphene. Nat. Mater. 11, 294–300 (2012).

46. Terrones, M., Botello-Méndez, A.R., Campos-Delgado, J., López-Urías, F., Vega-Cantú, Y.I., Rodríguez-Macías, F.J., Elías, A.L., Munoz-Sandoval, E., Cano-Márquez, A.G., Charlier, J.C. and Terrones, H. Graphene and graphite nanoribbons: Morphology, properties, synthesis, defects and applications. Nano Today 5, 351–372 (2010).

47. Pei, S. and Cheng, H. M. The reduction of graphene oxide. Carbon N. Y. 50, 3210–3228 (2012).

48. Avdoshenko, S. M., Ioffe, I. N., Cuniberti, G., Dunsch, L. and Popov, A. A. Organometallic complexes of graphene: Toward atomic spintronics using a graphene web. ACS Nano 5, 9939–9949 (2011).

49. Cheng, H., Hu, C., Zhao, Y. and Qu, L. Graphene fiber: a new material platform for unique applications. NPG Asia Mater. 6, e113 (2014).

50. Cao, X., Yin, Z. and Zhang, H. Three-dimensional graphene materials: preparation, structures and application in supercapacitors. Energy Environ. Sci. 7, 1850–1865 (2014).

51. Yang, Y., Rigdon, W., Huang, X. and Li, X. Enhancing graphene reinforcing potential in composites by hydrogen passivation induced dispersion. Sci. Rep. 3, 1–7 (2013).

52. Yang, Y., Rigdon, W., Huang, X. and Li, X. Highly compressible 3D periodic graphene aerogel microlattices. Nat. Commun. 6, 1–8 (2015).

53. Xu, F., Yu, H., Sadrzadeh, A. and Yakobson, B. I. Riemann surfaces of carbon as graphene nanosolenoids. Nano Lett. 34–39 (2015).

54. Gao, W. The chemistry of graphene oxide. Graphene Oxide Reduct. Recipes, Spectrosc. Appl. 61–95 (2015).

55. Lerf, A., He, H., Forster, M. and Klinowski, J. Structure of Graphite Oxide Revisited. J. Phys. Chem. B 102, 4477–4482 (1998).

56. Avouris, P. and Dimitrakopoulos, C. Graphene: synthesis and applications. Mater. today 15, 86–97 (2012).

57. Jayasena, B. and Subbiah, S. A novel mechanical cleavage method for synthesizing few-layer graphenes. Nanoscale Res. Lett. 6, 1–7 (2011).

58. Bao, C., Song, L., Xing, W., Yuan, B., Wilkie, C.A., Huang, J., Guo, Y. and Hu, Y. Preparation of graphene by pressurized oxidation and multiplex reduction and its polymer nanocomposites by masterbatch-based melt blending. J. Mater. Chem. 22, 6088–6096 (2012).

59. Liu, X., Giordano, C. and Antonietti, M. A facile molten-salt route to graphene synthesis. Small 10, 193–200 (2014).

60. Mahanandia, P., Simon, F., Heinrich, G. and Nanda, K. K. An electrochemical method for the synthesis of few layer graphene sheets for high temperature applications. Chem. Commun. (Camb). 50, 4613–5 (2014).

61. Tang, L., Li, X., Ji, R., Teng, K.S., Tai, G., Ye, J., Wei, C. and Lau, S.P. Bottom-up synthesis of large-scale graphene oxide nanosheets. J. Mater. Chem. 22, 5676–5683 (2012).

62. Kim, K.S., Zhao, Y., Jang, H., Lee, S.Y., Kim, J.M., Kim, K.S., Ahn, J.H., Kim, P., Choi, J.Y. and Hong, B.H. Large-scale pattern growth of graphene films for stretchable transparent electrodes. Nature 457, 706–710 (2009).

63. Park, S., Ruoff, R. S. and Engineering, M. Chemical methods for the production of graphenes. Nat. Nanotechnol. 4, 217–224 (2009).

64. Kymakis, E., Stratakis, E., Stylianakis, M. M., Koudoumas, E. and Fotakis, C. Spin coated graphene films as the transparent electrode in organic photovoltaic devices. Thin Solid Films 520, 1238–1241 (2011).

65. Kim, D.Y., Sinha Ray, S., Park, J.J., Lee, J.G., Cha, Y.H., Bae, S.H., Ahn, J.H., Jung, Y.C., Kim, S.M., Yarin, A.L. and Yoon, S.S. Self-healing reduced graphene oxide films by supersonic kinetic spraying. Adv. Funct. Mater. 24, 4986–4995 (2014).

66. Zhu, Y., Murali, S., Stoller, M.D., Velamakanni, A., Piner, R.D. and Ruoff, R.S. Microwave assisted exfoliation and reduction of graphite oxide for ultracapacitors. Carbon N. Y. 48, 2118–2122 (2010).

67. Garaj, S., Hubbard, W. and Golovchenko, J. A. Graphene synthesis by ion implantation. Appl. Phys. Lett. 97, 2–4 (2010).

68. Lu, X., Yu, M., Huang, H. and Ruoff, R. S. Tailoring graphite with the goal of achieving single sheets. Nanotechnology 10, 269–272 (1999).

69. Li, D., Müller, M. B., Gilje, S., Kaner, R. B. and Wallace, G. G. Processable aqueous

dispersions of graphene nanosheets. Nat. Nanotechnol. 3, 101–5 (2008).

70. Lu, X., Yu, M., Huang, H. and Ruoff, R. S. Graphene and graphene oxide: Synthesis, properties, and applications. Adv. Mater. 22, 3906–3924 (2010).

71. Huang, X., Qi, X., Boey, F. and Zhang, H. Graphene-based composites. Chem. Soc. Rev. 41, 666–686 (2012).

72. Wang, Feng, Yuanbo Zhang, Chuanshan Tian, Caglar Girit, Alex Zettl, Michael Crommie, and Y. Ron Shen. Gate-Variable Optical Transitions in Graphene. Science. 320, 206–209 (2008).

73. Pop, E., Mann, D., Wang, Q., Goodson, K. and Dai, H. Thermal conductance of an individual single-wall carbon nanotube above room temperature. Nano Lett. 6, 96–100 (2005).

74. Balandin, A.A., Ghosh, S., Bao, W., Calizo, I., Teweldebrhan, D., Miao, F. and Lau, C.N. Superior thermal conductivity of single-layer graphene. Nano Lett. 8, 902–907 (2008).

75. Ströbel, R., Jörissen, L., Schliermann, T., Trapp, V., Schütz, W., Bohmhammel, K., Wolf, G. and Garche, J. Hydrogen adsorption on carbon materials. J. Power Sources 84, 221–224 (1999).

76. Chambers, A., Park, C., Baker, R. T. K. and Rodriguez, N. M. Hydrogen Storage in Graphite Nanofibers. J. Phys. Chem. B 102, 4253–4256 (1998).

77. Murasawa, N., Koseki, H., Li, X.-R., Iwata, Y. and Sakamoto, T. Study on thermal behaviour and risk assessment of biomass fuels. Int. J. Energy Eng. 2, 242–252 (2012).

78. Chambers, A., Park, C., Baker, R. T. K. and Rodriguez, N. M. Hydrogen storage in a Ni–B nanoalloy-doped three-dimensional graphene material. Energy Environ. Sci. 4, 195 (2011).

79. Park, H. L. and Chung, Y. C. Hydrogen adsorption on Li metal in boron substituted graphene: Ab initio approach. INEC 2010-2010 3rd Int. Nanoelectron. Conf. Proc. 35, 917–918 (2010).

80. Parambhath, V. B., Nagar, R. and Ramaprabhu, S. Effect of nitrogen doping on hydrogen

storage capacity of palladium decorated graphene. Langmuir 28, 7826–7833 (2012).

81. Hussain, T., De Sarkar, A. and Ahuja, R. Strain induced lithium functionalized graphane as a high capacity hydrogen storage material. Appl. Phys. Lett. 101, (2012).

82. Cui, S., Zhao, N., Shi, C., Feng, C., He, C., Li, J. and Liu, E. Effect of hydrogen molecule dissociation on hydrogen storage capacity of graphene with metal atom decorated. J. Phys. Chem. C 118, 8–13 (2013).

83. Ao, Z. M., and F. M. P. High-capacity hydrogen storage in Al-adsorbed graphene. Phys. Rev. B 81, 205406–(1–7) (2010).

84. Kim, G. and Jhi, S. H. Ca-decorated graphene-based three-dimensional structures for high-capacity hydrogen storage. J. Phys. Chem. C 113, 20499–20503 (2009).

85. Hussain, T., Pathak, B., Ramzan, M., Maark, T. A. and Ahuja, R. Calcium doped graphane as a hydrogen storage material. Appl. Phys. Lett. 100, 12–17 (2012).

86. Wong, J., Yadav, S., Tam, J. and Veer Singh, C. A van der Waals density functional theory comparison of metal decorated graphene systems for hydrogen adsorption. J. Appl. Phys. 115, 224301–(1–11) (2014).

87. Sigal, A., Rojas, M. I. and Leiva, E. P. M. Interferents for hydrogen storage on a graphene sheet decorated with nickel: A DFT study. Int. J. Hydrogen Energy 36, 3537–3546 (2011).

88. Choi, M. H., Min, Y. J., Gwak, G. H., Paek, S. M. and Oh, J. M. A nanostructured Ni/graphene hybrid for enhanced electrochemical hydrogen storage. J. Alloys Compd. 610, 231–235 (2014).

89. Sigal, A., Rojas, M. I. and Leiva, E. P. M. Hydrogen storage in graphene decorated with Pd and Pt nano-particles using an electroless deposition technique. Sep. Purif. Technol. 82, 210–215 (2011).

90. Chen, C.H., Chung, T.Y., Shen, C.C., Yu, M.S., Tsao, C.S., Shi, G.N., Huang, C.C., Ger, M.D. and Lee, W.L. Hydrogen storage performance in palladium-doped graphene/carbon composites. Int. J. Hydrogen Energy 38, 3681–3688 (2013).

91. Fair, K.M., Cui, X.Y., Li, L., Shieh, C.C., Zheng, R.K., Liu, Z.W., Delley, B., Ford, M.J.,

Ringer, S.P. and Stampfl, C. Hydrogen adsorption capacity of adatoms on double carbon vacancies of graphene: A trend study from first principles. Phys. Rev. B - Condens. Matter Mater. Phys. 87, 1–7 (2013).

92. Contescu, C.I., Van Benthem, K., Li, S., Bonifacio, C.S., Pennycook, S.J., Jena, P. and Gallego, N.C. Single Pd atoms in activated carbon fibers and their contribution to hydrogen storage. Carbon N. Y. 49, 4050–4058 (2011).

93. Gong, C., Lee, G., Shan, B., Vogel, E.M., Wallace, R.M. and Cho, K. First-principles study of metal-graphene interfaces. J. Appl. Phys. 108, (2010).

94. Khomyakov, P.A., Giovannetti, G., Rusu, P.C., Brocks, G.V., Van den Brink, J. and Kelly, P.J. First-principles study of the interaction and charge transfer between graphene and metals. Phys. Rev. B - Condens. Matter Mater. Phys. 79, 1–12 (2009).

95. Valencia, H., Gil, A. and Frapper, G. Trends in the hydrogen activation and storage by adsorbed 3d transition metal atoms onto graphene and nanotube surfaces: A dft study and molecular orbital analysis. J. Phys. Chem. C 119, 5506–5522 (2015).

96. Hussain, T., Pathak, B., Ramzan, M., Maark, T. A. and Ahuja, R. Calcium doped graphane as a hydrogen storage material. Appl. Phys. Lett. 100, 183902 (2012).

97. Giovanni, M., Poh, H.L., Ambrosi, A., Zhao, G., Sofer, Z., Šaněk, F., Khezri, B., Webster, R.D. and Pumera, M. Noble metal (Pd, Ru, Rh, Pt, Au, Ag) doped graphene hybrids for electrocatalysis. Nanoscale 4, 5002–5008 (2012).

98. Lee, J., Novoselov, K. S. and Shin, H. S. Interaction between Metal and Graphene : Graphene. ACS Nano 5, 608–612 (2013).

99. Wang, W.X., Liang, S.H., Yu, T., Li, D.H., Li, Y.B. and Han, X.F. The study of interaction between graphene and metals by Raman spectroscopy. J. Appl. Phys. 109, 07C501-(1-3) (2011).

100. Xu, Z. and Buehler, M. J. Interface structure and mechanics between graphene and metal substrates: a first-principles study. J. Phys. Condens. Matter 22, 485301 (2010).

101. Reunchan, P. and Jhi, S.-H. Metal-dispersed porous graphene for hydrogen storage. Appl.

Phys. Lett. 98, 093103–(1–3) (2011).

102. Wang, L. and Yang, R. T. New sorbents for hydrogen storage by hydrogen spillover – a review. Energy Environ. Sci. 1, 268–279 (2008).

103. Chen, H. and Yang, R. T. Catalytic effects of TiF3 on hydrogen spillover on Pt/carbon for hydrogen storage. Langmuir 26, 15394–8 (2010).

104. Lachawiec, A. J., Qi, G. and Yang, R. T. Hydrogen Storage in Nanostructured Carbons by Spillover : Bridge-Building Enhancement. 11418–11424 (2005).

105. Prins, R. Hydrogen spillover. Facts and fiction. Chem. Rev. 112, 2714–38 (2012).

106. Yang, R. T. and Wang, Y. Catalyzed hydrogen spillover for hydrogen storage. J. Am. Chem. Soc. 131, 4224–6 (2009).

107. Stadie, N. P., Purewal, J. J., Ahn, C. C. and Fultz, B. Measurements of hydrogen spillover in platinum doped superactivated carbon. Langmuir 26, 15481–5 (2010).

108. Lee, K., Kim, Y.H., Sun, Y.Y., West, D., Zhao, Y., Chen, Z. and Zhang, S.B. Hole-Mediated Hydrogen Spillover Mechanism in Metal-Organic Frameworks. Phys. Rev. Lett. 104, 236101 (2010).

109. Conner, W. C. and Falconer, J. L. Spillover in Heterogeneous Catalysis. Chem. Rev. 95, 759–788 (1995).

110. Bandosz, T. J. and Ania, C. O. Surface chemistry of activated carbons and its characterization. 159–229 (2006).

111. Kim, Y., Lee, J., Yeom, M.S., Shin, J.W., Kim, H., Cui, Y., Kysar, J.W., Hone, J., Jung, Y., Jeon, S. and Han, S.M. Strengthening effect of single-atomic-layer graphene in metal-graphene nanolayered composites. Nat. Commun. 4, 1–7 (2013).

112. Bao, C., Song, L., Xing, W., Yuan, B., Wilkie, C.A., Huang, J., Guo, Y. and Hu, Y. Preparation of graphene by pressurized oxidation and multiplex reduction and its polymer nanocomposites by masterbatch-based melt blending. J. Mater. Chem. 22, 6088-6096 (2012).

113. Fan, F., Zhou, C., Wang, X. and Szpunar, J. A. Layer-by-Layer assembly of a self-healing anticorrosion coating on magnesium alloys. ACS Appl. Mater. Interfaces 7, 27271−27278 (2015).

114. Ikeo, N., Iijima, Y., Niimura, N., Sigematsu, M., Tazawa, T., Matsumoto, S., Kojima, K. and Nagasawa, Y. Handbook of X-ray Photoelectron Spectroscopy. (1991).

115. Downes, A. and Elfick, A. Raman spectroscopy and related techniques in biomedicine. Sensors 10, 1871–1889 (2010).

116. Winter, C. Hydrogen as an Energy Carrier. (Springer Berlin Heidelberg, 1988). doi:10.1007/978-3-642-61561-0

117. Crabtree, G. W., Dresselhaus, M. S. and Buchanan, M. V. The hydrogen economy. IEEE Eng. Manag. Rev. 34, 39–44 (2004).

118. Poh, H. L., Šaněk, F., Sofer, Z. and Pumera, M. High-pressure hydrogenation of graphene: towards graphane. Nanoscale 4, 7006–7011 (2012).

119. Zhu, M., Wang, H., Ouyang, L. Z. and Zeng, M. Q. Composite structure and hydrogen storage properties in Mg-base alloys. Int. J. Hydrogen Energy 31, 251–257 (2006).

120. Panella, B., Hirscher, M. and Roth, S. Hydrogen adsorption in different carbon nanostructures. Carbon N. Y. 43, 2209–2214 (2005).

121. Kemp, K.C., Seema, H., Saleh, M., Le, N.H., Mahesh, K., Chandra, V. and Kim, K.S. Environmental applications using graphene composites: water remediation and gas adsorption. Nanoscale 5, 3149–71 (2013).

122. Lee, D. H., Kim, J. C., Shim, H. W. and Kim, D. W. Highly reversible Li storage in hybrid NiO/Ni/graphene nanocomposites prepared by an electrical wire explosion process. ACS Appl. Mater. Interfaces 6, 137–142 (2014).

123. Yang, J., Zhang, E., Li, X., Yu, Y., Qu, J. and Yu, Z.Z. Direct Reduction of Graphene Oxide by Ni Foam as a High- Capacitance Supercapacitor Electrode. ACS Appl. Mater. Interfaces 8, 2297−2305 (2015).

124. Li, G., Kobayashi, H., Taylor, J.M., Ikeda, R., Kubota, Y., Kato, K., Takata, M.,

Yamamoto, T., Toh, S., Matsumura, S. and Kitagawa, H. Hydrogen storage in Pd nanocrystals covered with a metal-organic framework. Nat. Mater. 13, 802–806 (2014).

125. Newville, B. R. and M. Athena, Artemis, Hephaestus: data analysis for X-ray absorption spectroscopy using IFEFFIT. J. Synchrotron Radiat. 12, 537–541 (2005).

126. Rahmanian, N., Hamishehkar, H., Dolatabadi, J. E. N. and Arsalani, N. Nano graphene oxide: A novel carrier for oral delivery of flavonoids. Colloids Surfaces B Biointerfaces 123, 331–338 (2014).

127. Moon, I. K., Lee, J., Ruoff, R. S. and Lee, H. Reduced graphene oxide by chemical graphitization. Nat. Commun. 1, 73 (2010).

128. Perera, S.D., Mariano, R.G., Vu, K., Nour, N., Seitz, O., Chabal, Y. and Balkus Jr, K.J. Hydrothermal synthesis of graphene-TiO_2 nanotube composites with enhanced photocatalytic activity. ACS Catal. 2, 949–956 (2012).

129. Ugeda, M.M., Fernández-Torre, D., Brihuega, I., Pou, P., Martínez-Galera, A.J., Pérez, R. and Gómez-Rodríguez, J.M. Point Defects on Graphene on Metals. Phys. Rev. Lett. 107, 116803 (2011).

130. Barathi, M., Krishna Kumar, a. S., Kumar, C. U. and Rajesh, N. Graphene oxide–aluminium oxyhydroxide interaction and its application for the effective adsorption of fluoride. RSC Adv. 4, 53711–53721 (2014).

131. Wall, M. Raman spectroscopy optimizes graphene characterization. Adv. Mater. Process. 170, 35–38 (2012).

132. Prieto, P., Nistor, V., Nouneh, K., Oyama, M., Abd-Lefdil, M. and Díaz, R. XPS study of silver, nickel and bimetallic silver–nickel nanoparticles prepared by seed-mediated growth. Appl. Surf. Sci. 258, 8807–8813 (2012).

133. Zhou, G., Paek, E., Hwang, G. S. and Manthiram, A. Long-life Li/polysulphide batteries with high sulphur loading enabled by lightweight three-dimensional nitrogen/sulphur-codoped graphene sponge. Nat. Commun. 6, 7760 (2015).

134. Yang, D., Velamakanni, A., Bozoklu, G. and Park, S. Chemical analysis of graphene

oxide films after heat and chemical treatments by X-ray photoelectron and Micro-Raman spectroscopy. Carbon N. Y. 47, 145–152 (2009).

135. Wu, Z., Huang, X.L., Wang, Z.L., Xu, J.J., Wang, H.G. and Zhang, X.B. Electrostatic induced stretch growth of homogeneous β-Ni(OH)2 on graphene with enhanced high-rate cycling for supercapacitors. Sci. Rep. 4, 3669 (2014).

136. Maclennan, A., Banerjee, A., Hu, Y., Miller, J. T. and Scott, R. W. J. In Situ X-ray Absorption Spectroscopic Analysis of Gold–Palladium Bimetallic Nanoparticle Catalysts. ACS Catal. 3, 1411–1419 (2013).

137. Sham, T. K., Naftel, S. J. and Coulthard, I. M3,2-edge x-ray absorption near-edge structure spectroscopy: An alternative probe to the L3,2-edge near-edge structure for the unoccupied densities of d states of 5d metals. J. Appl. Phys. 79, 7134 (1996).

138. Penner-Hahn, J. E. X-ray absorption spectroscopy. Compr. Coord. Chem. II 2, 159–186 (2004).

139. Gougoussis, C., Calandra, M., Seitsonen, A., Brouder, C., Shukla, A. and Mauri, F. Intrinsic charge transfer gap in NiO from Ni K-edge x-ray absorption spectroscopy. Phys. Rev. B - Condens. Matter Mater. Phys. 79, 45118 (2009).

140. Wang, H., Miller, J.T., Shakouri, M., Xi, C., Wu, T., Zhao, H. and Akatay, M.C. XANES and EXAFS studies on metal nanoparticle growth and bimetallic interaction of Ni-based catalysts for CO_2 reforming of CH_4. Catal. Today 207, 3–12 (2013).

141. Agegnehu, A.K., Pan, C.J., Rick, J., Lee, J.F., Su, W.N. and Hwang, B.J. Enhanced hydrogen generation by cocatalytic Ni and NiO nanoparticles loaded on graphene oxide sheets. J. Mater. Chem. 22, 13849 (2012).

142. Li, Y., Yu, Y., Wang, J.G., Song, J., Li, Q., Dong, M. and Liu, C.J. CO oxidation over graphene supported palladium catalyst. Appl. Catal. B Environ. 125, 189–196 (2012).

143. Wu, T., Wang, X., Qiu, H., Gao, J., Wang, W. and Liu, Y. Graphene oxide reduced and modified by soft nanoparticles and its catalysis of the Knoevenagel condensation. J. Mater. Chem. 22, 4772 (2012).

144. Stankovich, S., Dikin, D.A., Piner, R.D., Kohlhaas, K.A., Kleinhammes, A., Jia, Y., Wu, Y., Nguyen, S.T. and Ruoff, R.S. Synthesis of graphene-based nanosheets via chemical reduction of exfoliated graphite oxide. Carbon N. Y. 45, 1558–1565 (2007).

145. Piccolo, L., Piednoir, A. and Bertolini, J. C. Absorption and oxidation of hydrogen at Pd and Pd-Au (111) surfaces. Surf. Sci. 600, 4211–4215 (2006).

146. Chao, B. and Klebanoff, L. in Hydrogen Storage Technology 109–132 (Taylor and Francis, 2012). doi:doi:10.1201/b13685-8

147. Huot, J. in Hydrogen Technology 474–477 (Springer-Verlag Berlin Heidelberg, 2008).

148. Ahn, Channing, and J. P. Storage Materials Based on Hydrogen Physisorption. Hydrogen Storage Technology: Materials and Applications (Taylor and Francis, 2012).

149. Cho, E.S., Ruminski, A.M., Aloni, S., Liu, Y.S., Guo, J. and Urban, J.J. Graphene oxide/metal nanocrystal multilaminates as the atomic limit for safe and selective hydrogen storage. Nat. Commun. 7, 10804 (2016).

150. Gadipelli, S. and Guo, Z. X. Graphene-based materials: Synthesis and gas sorption, storage and separation. Prog. Mater. Sci. 69, 1–60 (2015).

151. Mukherjee, S., Ramalingam, B. and Gangopadhyay, S. Hydrogen spillover at sub-2 nm Pt nanoparticles by electrochemical hydrogen loading. J. Mater. Chem. A 2, 3954 (2014).

152. Bhowmick, R., Rajasekaran, S., Friebel, D., Beasley, C., Jiao, L., Ogasawara, H., Dai, H., Clemens, B. and Nilsson, A. Hydrogen Spillover in Pt-Single-Walled Carbon Nanotube Composites : Formation of Stable C-H Bonds. J. Am. Chem. Soc. 5580–5586 (2011).

153. Varin, Robert A., Tomasz Czujko, and Z. S. W. Nanomaterials for solid state hydrogen storage. (Springer Science & Business Media, 2009).

154. Johansson, T. B. Renewable energy: sources for fuels and electricity. (Island Press, 1992).

155. Kverndokk, M. H. and S. Resource and energy economics. Elsevier 18, 1–114 (1996).

156. Hua, T.Q., Ahluwalia, R.K., Peng, J.K., Kromer, M., Lasher, S., McKenney, K., Law, K. and Sinha, J. Technical assessment of compressed hydrogen storage tank systems for

automotive applications. Int. J. Hydrogen Energy 36, 3037–3049 (2011).

157. Schlapbach, L. and Züttel, A. Hydrogen-storage materials for mobile applications. Nature 414, 353–358 (2001).

158. Silvera, I. The solid molecular hydrogens in the condensed phase: Fundamentals and static properties. Rev. Mod. Phys. 52, 393–452 (1980).

159. Li, S., Zhao, H. and Jena, P. Ti-doped nano-porous graphene: A material for hydrogen storage and sensor. Front. Phys. 6, 204–208 (2011).

160. Vinayan B, Sethupathi K, R. S. Hydrogen Storage Studies of Palladium Decorated Nitrogen Doped Graphene Nanoplatelets. J. Nanosci. Nanotechnol. 12, 6608–14. (2012).

161. Cabria, I., M. Isla, M. J. Lopez, J. I. Martınez, L. M. Molina, J. A. A. Hydrogen and Hydrogen Clusters Across Disciplines. Nanoclusters: A Bridge Across Disciplines. 1., 299 (2010).

162. Dimitrakakis, G. K., Tylianakis, E. and Froudakis, G. E. Pillared graphene: a new 3-D network nanostructure for enhanced hydrogen storage. Nano Lett. 8, 3166–3170 (2008).

163. Youn, I.S., Kim, D.Y., Singh, N.J., Park, S.W., Youn, J. and Kim, K.S. Intercalation of transition metals into stacked benzene rings: a model study of the intercalation of transition metals into bilayered graphene. J. Chem. Theory Comput. 8, 99–105 (2012).

164. Cho, Y., Choi, Y. C. and Kim, K. S. Graphene spin-valve device grown epitaxially on the Ni (111) substrate: a first principles study. J. Phys. Chem. C 115, 6019–6023 (2011).

165. Zheng, L., Li, Z., Bourdo, S., Watanabe, F., Ryerson, C.C. and Biris, A.S. Catalytic hydrogenation of graphene films. Chem. Commun. (Camb). 47, 1213–5 (2011).

166. Tiwari, J.N., Nath, K., Kumar, S., Tiwari, R.N., Kemp, K.C., Le, N.H., Youn, D.H., Lee, J.S. and Kim, K.S. Stable platinum nanoclusters on genomic DNA-graphene oxide with a high oxygen reduction reaction activity. Nat. Commun. 4, 2221 (2013).

167. Zhou, J.G., Wang, J., Sun, C.L., Maley, J.M., Sammynaiken, R., Sham, T.K. and Pong, W.F. Nano-scale chemical imaging of a single sheet of reduced graphene oxide. J. Mater. Chem. 21, 14622–14630 (2011).

168. Zhou, J., Wang, J., Liu, H., Banis, M.N., Sun, X. and Sham, T.K. Imaging nitrogen in individual carbon nanotubes. J. Phys. Chem. Lett. 1, 1709–1713 (2010).

169. Zhou, J., Wang, J., Hu, Y., Regier, T., Wang, H., Yang, Y., Cui, Y. and Dai, H. Imaging state of charge and its correlation to interaction variation in an LiMn(0.75)Fe(0.25)PO(4) nanorods-graphene hybrid. Chem. Commun. (Camb). 49, 1765–7 (2013).

170. Wang, J., Zhou, J., Hu, Y. F. and Regier, T. Chemical interaction and imaging of single Co_3O_4/graphene sheets studied by scanning transmission X-ray microscopy and X-ray absorption spectroscopy. Energy Environ. Sci. 6, 926–934 (2013).

171. Tiwari, J.N., Kemp, K.C., Nath, K., Tiwari, R.N., Nam, H.G. and Kim, K.S. Interconnected Pt-nanodendrite/DNA/reduced-graphene-oxide hybrid showing remarkable oxygen reduction activity and stability. ACS Nano 7, 9223–31 (2013).

172. Liu, G., Wang, Y., Qiu, F., Li, L., Jiao, L. and Yuan, H. Synthesis of porous Ni@rGO nanocomposite and its synergetic effect on hydrogen sorption properties of MgH2. J. Mater. Chem. 22, 22542 (2012).

173. Giovanni, Marcella, Hwee Ling Poh, Adriano Ambrosi, Guanjia Zhao, Zdeněk Sofer, Filip Šaněk, Bahareh Khezri, Richard D. Webster, and Martin Pumera. Noble metal (Pd, Ru, Rh, Pt, Au, Ag) doped graphene hybrids for electrocatalysis. Nanoscale 4, 5002 (2012).

174. Mayavan, S., Sim, J.-B. and Choi, S.-M. Simultaneous reduction, exfoliation and functionalization of graphite oxide into a graphene-platinum nanoparticle hybrid for methanol oxidation. J. Mater. Chem. 22, 6953 (2012).

175. Kim, Y., Lee, J., Yeom, M.S., Shin, J.W., Kim, H., Cui, Y., Kysar, J.W., Hone, J., Jung, Y., Jeon, S. and Han, S.M. Strengthening effect of single-atomic-layer graphene in metal-graphene nanolayered composites. Nat Commun 4, 2114 (2013).

176. Ao, Z. M., and F. M. P. High-capacity hydrogen storage in Al-adsorbed graphene. Phys. Rev. B - Condens. Matter Mater. Phys. 81, 1–7 (2010).

177. J. F. Moulder, J. C. and R. C. K. Handbook of X-ray photoelectron spectroscopy: a

reference book of standard spectra for identification and interpretation of XPS data. (Physical Electronics Division, Perkin-Elmer Corporation, 1995).

178. Zhou, C., Wang, J. and Szpunar, J. a. X-ray chemical imaging and the electronic structure of a single nanoplatelet Ni/graphene composite. Chem. Commun. (Camb). 50, 2282–5 (2014).

179. Zhou, C., Szpunar, J. A. and Cui, X. Synthesis of Ni/Graphene Nanocomposite for Hydrogen Storage. ACS Appl. Mater. Interfaces 8, 15232−15241 (2016).

180. Wang, L., Lee, K., Sun, Y.Y., Lucking, M., Chen, Z., Zhao, J.J. and Zhang, S.B. Graphene oxide as an ideal substrate for hydrogen storage. ACS Nano 3, 2995–3000 (2009).

181. Chen, H., Yu, H., Zhang, Q., Liu, B., Liu, P., Zhou, X., Han, Z. and Zhou, S. Enhancement in dehydriding performance of magnesium hydride by iron incorporation : A combined experimental and theoretical investigation. 322, (2016).

182. Gutés, A., Hsia, B., Sussman, A., Mickelson, W., Zettl, A., Carraro, C. and Maboudian, R. Graphene decoration with metal nanoparticles: Towards easy integration for sensing applications. Nanoscale 4, 438 (2012).

183. Zhang, H., Hines, D. and Akins, D. L. Synthesis of a nanocomposite composed of reduced graphene oxide and gold nanoparticles. Dalton Trans. 43, 2670–5 (2014).

184. Sun, S. and Wu, P. Competitive surface-enhanced Raman scattering effects in noble metal nanoparticle-decorated graphene sheets. Phys. Chem. Chem. Phys. 13, 21116 (2011).

185. Zheng, G. and Altman, E. I. Oxidation of Pd(111). Surf. Sci. 462, 151–168 (2000).

186. Grochala, W. and Edwards, P. P. Thermal decomposition of the non-interstitial hydrides for the storage and production of hydrogen. Chem. Rev. 104, 1283–1315 (2004).

187. Liu, W. and Aguey-Zinsou, K.-F. Size effects and hydrogen storage properties of Mg nanoparticles synthesised by an electroless reduction method. J. Mater. Chem. A 2, 9718 (2014).

188. Wang, L., Stuckert, N. R., Chen, H. and Yang, R. T. Effects of Pt particle size on

hydrogen storage on Pt-doped metal-organic framework IRMOF-8. J. Phys. Chem. C 115, 4793–4799 (2011).

189. Meitzner, G. and Sinfelt, J. H. X-ray absorption studies of the electronic structures of Pd-Ag and Pd-Au alloys. Catal. Letters 30, 1–10 (1995).

190. D. H. Pearson, C. C. Ahn, and B. F. White lines and d-electron occupancies for the 3d and 4d transition metals. Phys. Rev. B 47, 8471–8478 (1993).

191. Wang, J., Zhou, J., Hu, Y. and Regier, T. Chemical interaction and imaging of single Co_3O_4/graphene sheets studied by scanning transmission X-ray microscopy and X-ray absorption spectroscopy. Energy Environ. Sci. 6, 926-934 (2013).

192. Ting, V. P., Cuesta, A. J. R.-, Bimbo, N., Sharpe, J. E. and Timothy, J. Direct evidence for solid-like hydrogen in a nanoporous carbon hydrogen storage material at supercritical temperatures. ACS Nano 9, 8249–8254 (2015).

193. Wu, H.Y., Fan, X., Kuo, J.-L. and Deng, W. Q. DFT Study of Hydrogen Storage by Spillover on Graphene with Boron Substitution. J. Phys. Chem. C 115, 9241–9249 (2011).

194. Lueking, A. D., Psofogiannakis, G. and Froudakis, G. E. Atomic Hydrogen Di ff usion on Doped and Chemically Modi fi ed Graphene. (2013).

195. Schlapbach, Louis, and A. Z. Hydrogen-storage materials for mobile applications. Nature 414, 353–358 (2001).

196. Broom, D. The accuracy of hydrogen sorption measurements on potential storage materials. Int. J. Hydrogen Energy 32, 4871–4888 (2007).

197. Broom, D. P. Hydrogen sorption measurements on potential storage materials-experimental methods and measurement accuracy. JRC Eur. Comm. 86 (2008).

198. Lemmon, E. W., Huber, M. L. and Leachman, J. W. Revised standardized equation for hydrogen gas densities for fuel consumption applications. J. Res. Natl. Inst. Stand. Technol. 113, 341–350 (2008).

199. Xu, W.C., Takahashi, K., Matsuo, Y., Hattori, Y., Kumagai, M., Ishiyama, S., Kaneko, K. and Iijima, S. Investigation of hydrogen storage capacity of various carbon materials. Int.

J. Hydrogen Energy 32, 2504–2512 (2007).

200. Zhou, L. and Zhou, Y. Determination of compressibility factor and fugacity coe cient of hydrogen in studies of adsorptive storage. 26, 597–601 (2001).

201. Poirier, E., Chahine, R., Tessier, a. and Bose, T. K. Gravimetric and volumetric approaches adapted for hydrogen sorption measurements with in situ conditioning on small sorbent samples. Rev. Sci. Instrum. 76, 55101 (2005).

202. Blackman, J. M., Patrick, J. W. and Snape, C. E. A reliable method for the determation of hydrogen storage capacity at high pressure and its application to carbon materials. 49, 207–209 (2004).

203. Poirier, E., Chahine, R., Be, P., Lafi, L. and Chandonia, P. A. Hydrogen Adsorption Measurements and Modeling on Metal-Organic Frameworks and Single-Walled Carbon Nanotubes. Langmuir 8784–8789 (2006).

204. Léon, A. ed. Hydrogen technology: mobile and portable applications. (Springer Science and Business Media, 2008).

205. Zlotea, C., Sahlberg, M., Özbilen, S., Moretto, P. and Andersson, Y. Hydrogen desorption studies of the Mg24Y5–H system: Formation of Mg tubes, kinetics and cycling effects. Acta Mater. 56, 2421–2428 (2008).

206. Zeppelin, F. von, Haluška, M. and Hirscher, M. Thermal desorption spectroscopy as a quantitative tool to determine the hydrogen content in solids. Thermochim. Acta 404, 251–258 (2003).

207. Alexander, L. and Klug, H. P. Determination of crystallite size with the x-ray spectrometer. J. Appl. Phys. 21, 137–142 (1950).

208. Rogério dos Santos Alves and Alex Soares de Souza. The Scherrer Formula for X-Ray Particle Size Determination. Igarss 2014 56, 1–5 (2014).

209. Cancado, L.G., Takai, K., Enoki, T., Endo, M., Kim, Y.A., Mizusaki, H., Jorio, A., Coelho, L.N., Magalhaes-Paniago, R. and Pimenta, M.A. General equation for the determination of the crystallite size La of nanographite by Raman spectroscopy. Appl.

Phys. Lett. 88, 1–4 (2006).

210. Chabal, M. A. ; Y. J. A Review on Reducing Graphene Oxide for Band Gap Engineering. J. Mater. Sci. Res. 2, 201 2 (2012).

211. Hussein, G. ; Nohman, A. ; Attyia, K. Characterization of the decomposition course of nickel acetate tetrahydrate in air. J. Therm. Anal. 42, 1155–1165 (1994).

212. Ham, H., Van Khai, T., Park, N.H., So, D.S., Lee, J.W., Na, H.G., Kwon, Y.J., Cho, H.Y. and Kim, H.W. Freeze-drying-induced changes in the properties of graphene oxides. Nanotechnology 25, 1–8 (2014).

213. Mohandes, F. and Salavati-Niasari, M. Freeze-drying synthesis, characterization and in vitro bioactivity of chitosan/graphene oxide/hydroxyapatite nanocomposite. RSC Adv. 25993–26001 (2014).

214. Yi, C. W. and Szanyi, J. Pd overlayer on oxygen pre-covered graphene/Ru(0001): Thermal stability. Surf. Sci. 648, 271–277 (2016).

APPENDIX A. CUSTOM-MADE APPARATUS FOR HYDROGEN STORAGE DETERMINATION

A.1 Equipment and components

The designed custom-made apparatus is equipped with a pressure regulator, a sample vessel, a rupture disc, a heater, a pumping system with a vacuum gauge, a pressure gauge, a temperature controller with a ceramic insulated thermocouple, a filter, and a mass spectrometer. All tubes, valves, connectors and fittings were purchased from Swagelok. The high operating pressure and temperature as well as the potential corrosion exposure requires that all the reactors, valves, connectors and fittings should be made of 316 stainless steel; and all the valves are bellows-sealed with the maximum working temperature of 343°C and pressure of 240 bar. The main components and their characteristics are listed in Table A.1 and Table A.2.

Table A.1 Main components of the custom-made apparatus.

No	Item	Part number	Company	Description
1	hydrogen tank	HY 5.0UH-T, UHP Grade 99.999%	Praxair	research grade, 50 L, 2400/183 (psi/bar)
2	helium tank	HE 6.0 RS-T50	Praxair	research grade, 50 L, 2640/183 (psi/bar)
3	tube	SS-T2-S-028-20	Swagelok	316 SS seamless tubing, 1/8 in. OD x 0.028 in. wall x 20 feet 8500/586 (psi/bar)
4	pressure regulator	KPP1RSH422P2A030	Swagelok	316 SS, 3600/248 (psi/bar), maximum inlet pressure 4000/275 (psi/bar), gauge designator with inlet and outlet pressure
				Continued on next page

Table A.2 Continued from previous page.

No	Item	Part number	Company	Description
5	bellows-sealed Valve	SS-4UG-V51-VS	Swagelok	316 SS, secondary packed bellows-sealed valve, silver-plated gasket, spherical stem tip, 1/4 in. female VCR fitting, polyimide insert, -20/-28 to 650/343 (°F/°C), 2500/172 (psi/bar)
6	pressure reactor (Vessel heater)	854HC	Parr instrument	115/400 (volt, max/watts)
7	sample vessel	453HC-316-0719842151	Parr instrument	316 SS, 662/350 (F/°C), 3000/206 (psi/bar), 250 mL
8	gasket	457HC2	Parr instrument	350°C
9	filter	SS-4FW-VCR-2	Swagelok	stainless steel all-welded in-line filter, 1/4 in. male VCR, 2 μm 482°C, 3280/225 (psi/bar)
10	mass spectrometer	RGA100 (Residual Gas Analyzers)	Stanford Research System (SRS)	___
11	temperature controller	210/TIMER-K	J-KEM Scientific	50-1200°C
12	thermocouple	XC-20-K-24	Omega	980°C
13	vacuum pump	___	___	10^{-7} Torr
14	rupture disc	526HCPG	Parr instrument	3000/206.8 (psi/bar)
15	pressure gauge	PPC5352	Winters Instrument	-40-93°C, 2000/137.9 (psi/bar)

Fig. A.1 (top) schematically displays the system. Fig. A.1 (bottom) shows the picture of the system. The function of each component is described:

1. Valves A and B control the hydrogen inlet and outlet, respectively, allowing the introduction/removal of gas.
2. Valve C controls the connection between the mass spectrometer and the vessel. Valves D and E control the vacuum outlets.
3. The fine powder sample sits in the sample vessel with a filter preventing the sample from escape.
4. Extremely tight bellow-valves are carefully polished allowing tight connections of components.
5. The vacuum unit consists of a primary pump and a turbo-molecular pump. This vacuum unit eliminates the impurities and contamination in the system.
6. The temperature of vessel is controlled by a temperature controller unit. In case when the real temperature of the sample differs from that of the heater, a thermocouple is fixed to the reactor wall and used to monitor the temperature of the sample vessel.
7. The sand is placed surrounding the sample vessel to cover the gap between the vessel and the heater, which further minimizes the temperature gradients and keeps a steady temperature.

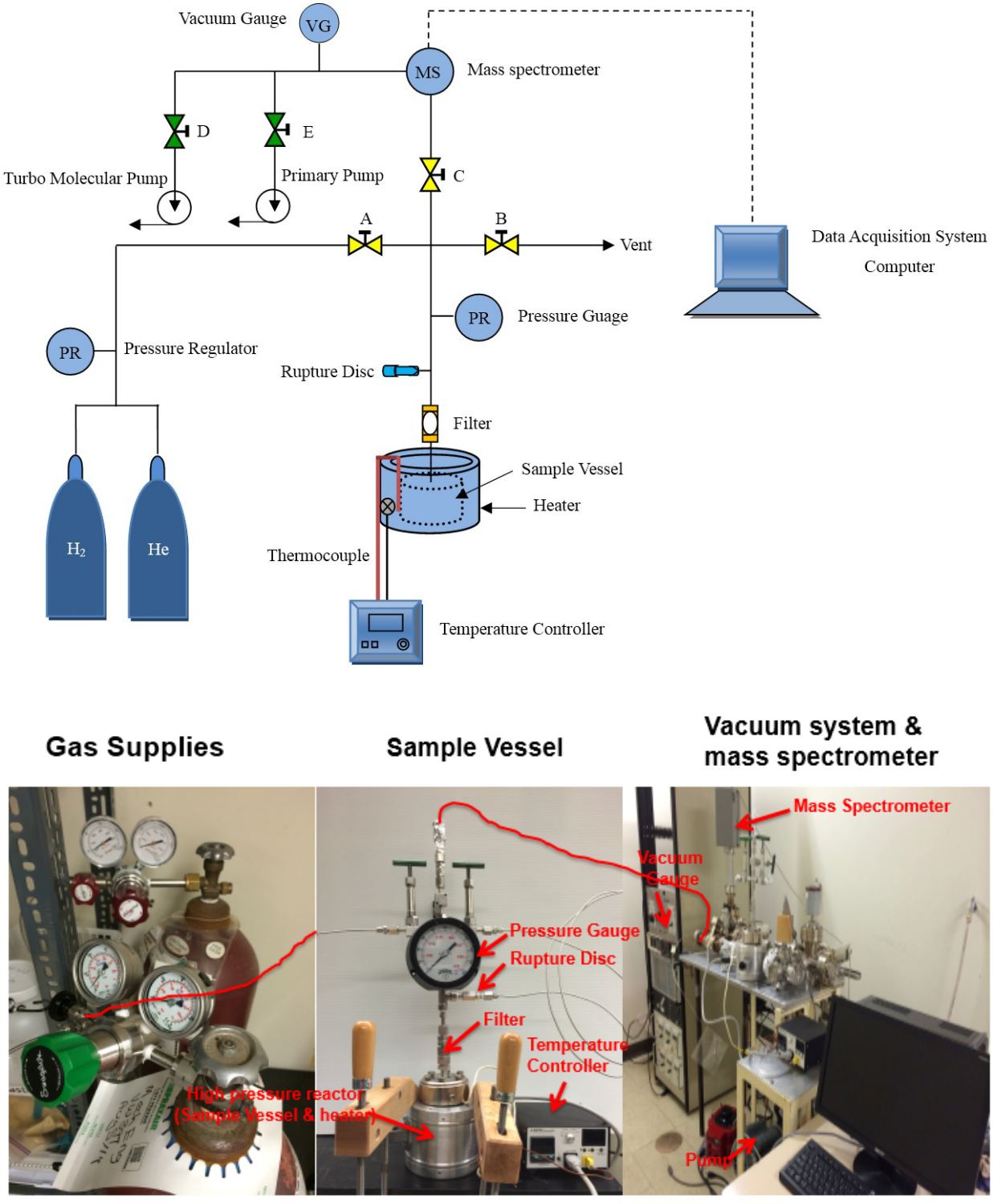

Fig. A.1 Custom-made apparatus for the hydrogen storage determination: (top) schematic view and (bottom) digital image.

Pressure and temperature limits

On the basis of the pressure limit of each component and the temperature limit of the sample cell, the maximum operating pressure is restricted below 2000/137.9 (psi/bar) and temperature below 300°C. For practical application, the parameters in this project are set to the operating values as shown in Table A.3.

Table A.3 Limits of the operating pressure and temperature in this project.

Pressure and Temperature Limits	
maximum working pressure	maximum working temperature
60 bar	300°C

Operation procedures

To perform a single sorption experiment, the following protocol is applied.

1. Prior to a hydrogen adsorption experiment, the whole apparatus is evacuated to a pressure level of 10^{-2} Pa by using the primary pump and turbomolecular pump. The sample vessel with a dry and empty sample (~2 g, fine powder) is heated up to a degassing temperature of 300°C for 1 h. The evacuation and heating are conducted simultaneously to remove any remaining gases and impurities from the vessel.
2. After that, the evacuation and heating are switched off, and the enclosure is cooled down to a constant activation temperature (RT to 300°C).
3. The valve A remains open with the valves B-E closed, allowing the sample vessel filled with hydrogen. At the stabilized temperature, hydrogen is introduced to the sample until the pressure reaches an initial steady pressure P_0.
4. The valve A is then closed to isolate the sample vessel. Then the experiment begins.
5. The temperature and pressure are constantly monitored and accurately measured.
6. At each constant operating temperature and initial pressure, any drop in pressure over

time is read, which is related to the amount of hydrogen uptake by the sample.

7. When the pressure reaches stable with no detectable variation, the hydrogen charging process stops.
8. To determine a full pressure-composition sorption isotherm, the above-described procedures are repeated by pressurizing the sample vessel with various initial pressures and at a constant temperature.
9. To determine the most favorable charging temperature, the above-described procedures are repeated by varying the operating temperature (RT to 300°C) at a constant initial pressure.
10. For desorption, the desorbed hydrogen from the hydrogen-charged sample leads to an increase of pressure in the vessel. The amount of hydrogen release is then determined as a function of pressure.

This volumetric measurement tool can measure in situ full isotherms, and that will enable the determination of reversibility and perform various cycling test.

The hydrogen uptake capacity is calculated using the real gas law with precise H_2 compressibility factor, Z (P, T)[1,196–199],

$$PV = nZRT \tag{A.1}$$

where P is the pressure, V is the volume, n is the number of moles, Z is the gas compressibility corresponding to the particular pressure and temperature of each measurement, R is the universal gas constant and T is the temperature. For each test, the amount of moles stored is given by

$$\Delta n = \frac{P_0 V}{Z_0 RT} - \frac{P_t V}{Z_t RT} \tag{A.2}$$

Where T is assumed to be the constant measurement temperature, P_0 and P_t are the initial and final pressures at isotherm point, and Z_0 and Z_t are the hydrogen compressibilities at the temperature T and the pressures P_0 and P_t, respectively. The values of T and P_0 are the starting points in the measurement. V is the dead space volume and equals to the volume of sample cell

minus the volume occupied by the sample[196,198,200]. V can be calibrated and directly measured by using non-interacting helium. The hydrogen uptake amount is calculated and converted to the weight percent, the ratio of the hydrogen uptake amount to the hydrogen-charged sorbent mass.

During the measurement process, some errors may result from some experimental issues, mainly including leakage[196], sample pre-treatment[147], degassing, gas purity (99.999%)[196], equilibrium[147], temperature measurement and control[147,199,201], measurement sensitivity[202], dead space[203], venting system[204]. Therefore, the corresponding corrections should be made to avoid these errors for an accurate data collection.

Besides, the mass spectrometer can be used as a complementary technique, and further confirms the desorption process[141,205–207]. Basically, after hydrogen charge, the vessel is evacuated to remove the free hydrogen from the dead space. The thermally desorbed hydrogen from the sample is continuously transported to the mass spectrometer in a constant helium flow[147,197]. The flux of desorbed hydrogen is then monitored as a function of temperature. This thermal desorption can be used for the quantitative determination of hydrogen discharge, and also to determine the desorption temperature.

Safety concerns

1. Powder and gas control

   Power and gas supplies should be disconnected before maintenance or cleaning.
2. Moving cylinder

   The pressure regulator should be uninstalled from the gas cylinder. Then the cylinder is tightly closed before moving to the fume hood.
3. Sample amount

   The sample volume in the sample cell should be less than two third volume of the cell (<166 mL).
4. Cleaning and maintenance

   Regular cleaning is required.
5. Sample degassing

Turbomolecular pump and baking can be used to ensure a clean system, and avoid any contaminations of the adsorbent during hydrogen uptake process[147]. That is, prior to each measurement, the setup is evacuated to a pressure level of 10^{-2} Pa; and the sample is heated up to 300°C for 1 h.

6. Gas purity

   The hydrogen and helium supplies are of high purity grades (99.999%)[196].

7. Leakage-free detection

   Hydrogen leakage is the main problem for the system[196]. The accumulative leakage could be undetectable over time and incorrectly counted into the calculation of hydrogen uptake amount[196]. Therefore, low leakage rate valves are used to prevent a fast leakage. Regarding the slow leakage, the connections are tightly polished before every measurement with the tightness checked by using a liquid leakage detector. Further before each experiment, a leakage test is performed by verifying the stability of pressure: Blank tests are performed by pressurizing the system either with hydrogen or with helium for a period of 6 h at 60 bar. Any leakage can be detected by the gas pressure measurement, and the leakage can be sealed.

8. Leakage vent

   The sample vessel along with the heater is placed in a fume hood. To avoid the hazards to human beings and lab environment, any minor or unexpected leakage of hydrogen should be directed outside of the room through fume hood[204].

9. Safety rupture disc

   A safety rupture disc is installed to the setup in case when the dangerous pressure exceeds the pressure limit of the sample vessel.

10. Temperature control

    Hydrogen release from the host material is an exoergic process. To avoid an extremely high temperature, a thermocouple is attached to monitor the temperature of the sample cell. Thus, the experiment can be terminated once the temperature approaches a dangerous level.

APPENDIX B. SUPPORTING INFORMATION

Supporting Information of Chapter 4

Synthesis of Ni/Graphene Nanocomposite for Hydrogen Storage

Chunyu Zhou[*,†], Jerzy A. Szpunar[†] and Xiaoyu Cui[‡]

[†]Department of Mechanical Engineering, University of Saskatchewan, Saskatoon, SK, S7N 5A9, Canada.

[‡]Canadian Light Source Inc., Saskatoon, SK, S7N 2V3, Canada.

Corresponding Author

Chunyu Zhou

Department of Mechanical Engineering, College of Engineering,

University of Saskatchewan, 57 Campus Drive, Saskatoon SK S7N 5A9, Canada.

*Email: chunyu.zhou@usask.ca

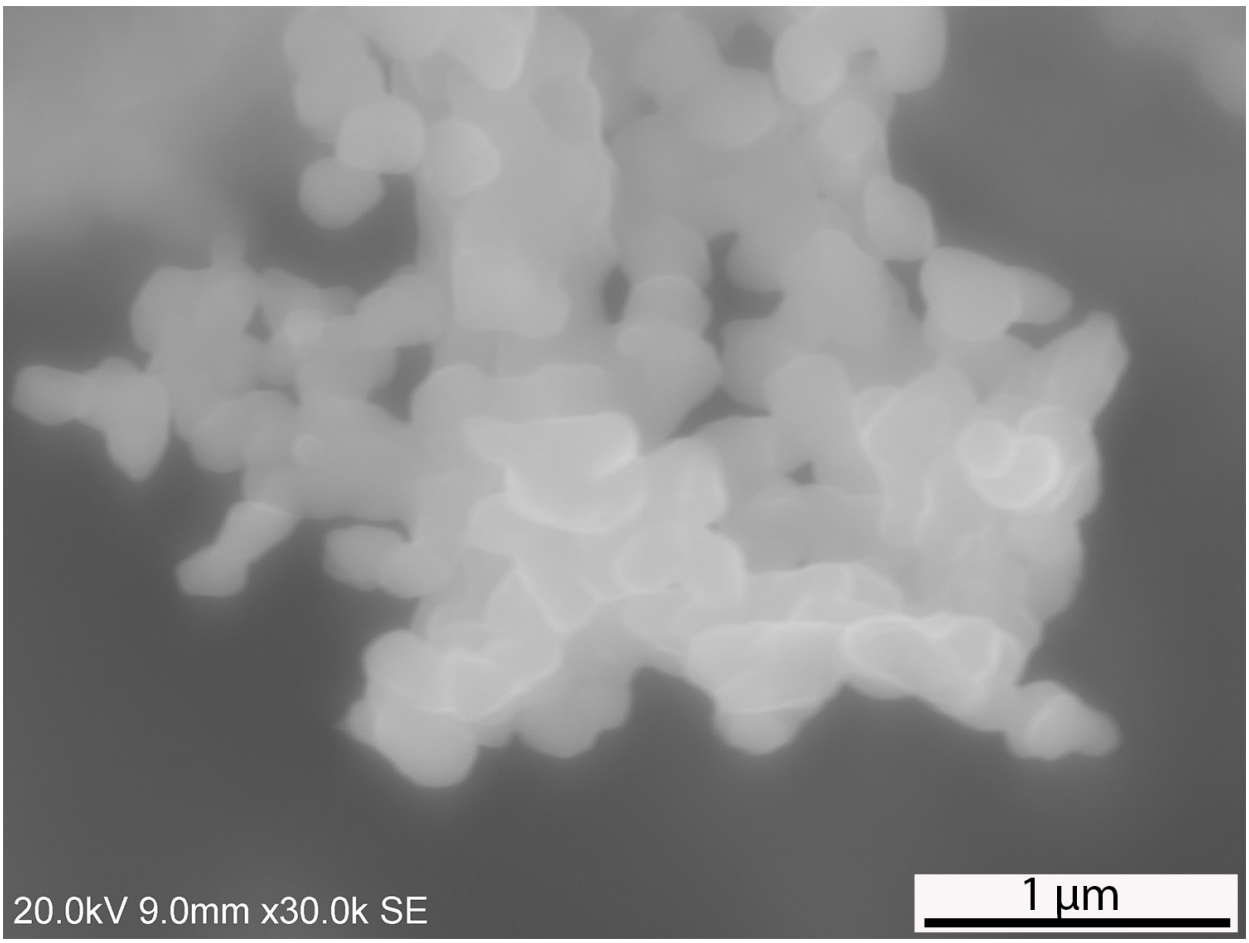

Fig. B.1 SEM micrograph of the bare metallic Ni that was prepared from hydrogen thermal treatment.

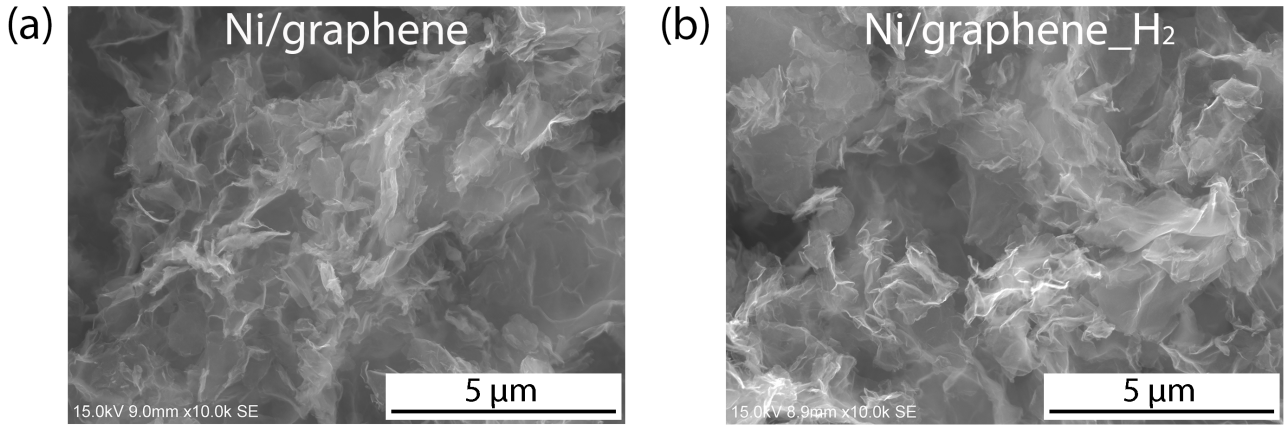

Fig. B.2 SEM micrograph of Ni/graphene composites before and after hydrogen charge: (a) Ni/graphene_0 bar and (b) Ni/graphene_60 bar.

Supporting Discussion

The Scherrer analysis of the XRD broadened peaks allows the determination of the crystal size of nanocrystals in solid powder with the domain size smaller than 100 nm[122,208–210]. Using the spectrum of Ni/graphene, the crystallite size of Ni nanoparticles was measured by evaluating the Scherrer relation $\tau = K\lambda/\beta\cos\theta$ to be 7-9 nm.

where:

τ is the mean size of the crystallites, which may be smaller or equal to the grain size;

K is a crystallite shape factor, with a value close to unity and the typical value of about 0.9;

λ is the X-ray radiation wavelength of radiation [λ(Cr)=0.229 nm];

β is the line broadening of full width at half maximum (FWHM) of Ni(111) or Ni (200) in radians; θ is the Bragg angle and the peak position in degrees.

Supporting Information of Chapter 5

X-ray Chemical Imaging and Electronic Structure of a Single Nanoplatelet Ni/graphene Composite

Chunyu Zhou[1], Jian Wang[2], and Jerzy A. Szpunar[1]

[1] Department of mechanical Engineering, University of Saskatchewan, Saskatoon, Canada

[2] Canadian Light Source Inc., University of Saskatchewan, Saskatoon, Canada

Corresponding Author

Jerzy A. Szpunar

[1]Department of Mechanical Engineering, University of Saskatchewan, Saskatoon,

SK, S7N 5A9, Canada.

*E-mail: jerzy.szpunar@usask.ca

Jian Wang

[2]Canadian Light Source Inc., Saskatoon, SK, S7N 2V3, Canada.

*E-mail: jian.wang@lightsource.ca

Synthesis of Ni/graphene precursor

The precursor of Ni/graphene composite was synthesized by a pressurized multiplex reduction of graphene oxide[58] and simultaneously a reduction of Ni compounds by hydrazine hydrate. Briefly, graphene oxide (2 g) was dispersed in deionized water (50 mL) that was put in a beaker Teflon reactor (80 mL). By magnetic stirring, nickel acetate hydrate (200 mg) was added. 10 min later, hydrazine hydrate (2.5 mL) was dropwise added to the blend. Then the autoclave with the beaker Teflon reactor was tightly covered, fastened, and placed in an oven. The pressurized multiplex reduction was carried out at 110°C for 1 h. Subsequently, the mixture was washed with diluted hydrochloric acid for three times and then washed with deionized water for multiple times. A vacuum filtration was used for the filtration in order to remove the residual impurities. The precursor of Ni/graphene composite was finally obtained from the freeze-drying of filtrate for 12 h.

Thermal treatment of precursor

The precursor was thermally treated and converted to the Ni/graphene composite. The schematic reactor part of the furnace is shown in Fig. B.3. Prior to thermal processing, the instrument was tested to be leakage free with a liquid leak detector for 10 min. Then the quartz tube was purged with argon (99.99%, purity) at 50 mL/min to remove the impurities in the tube[173]. 10 min later, the system was heated to 800°C for the exfoliation of graphite oxide and decomposition of $Ni(OAc)_2$ in argon atmosphere[174,210]. When the temperature reached 800°C, the temperature control was switched to 500°C, and the test remained at this temperature for 1 h. Meanwhile, the gas input was switched from argon to hydrogen (99.99%, purity) with a flow rate of 50 mL/min. Hydrogen served as a reductant agent and converted the NiO to Ni particles that deposited on the graphene nanoplatelets.

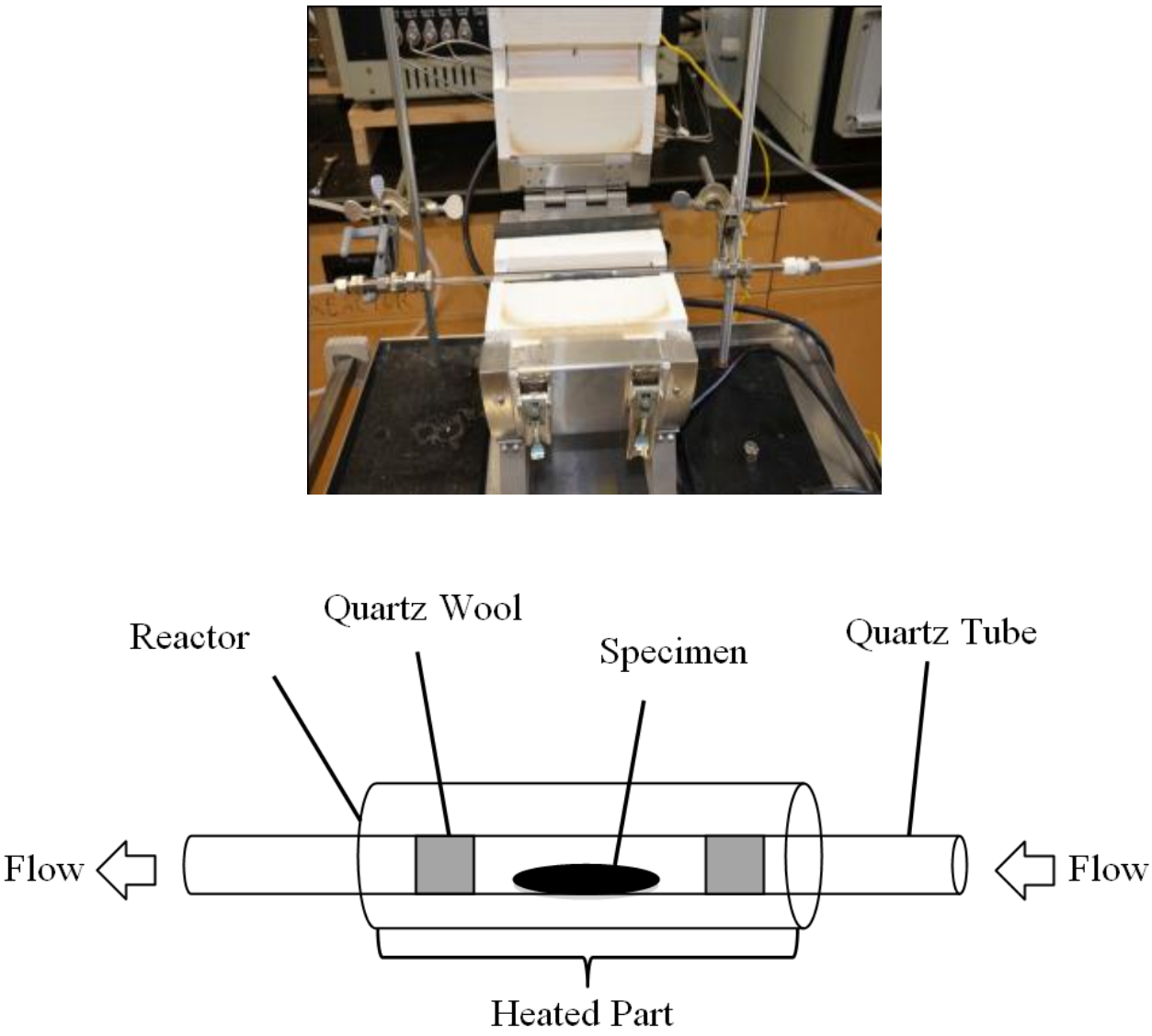

Fig. B.3 Digital image (top) and schematic diagram (bottom) of the reactor part for the thermal treatment.

The thermal treatment involved a series of reactions, including the decomposition and reduction of $Ni(OAc)_2 \cdot xH_2O$ and the exfoliation and reduction of graphite oxide. In particular, $Ni(OAc)_2 \cdot xH_2O$ was initially dehydrated at 160 °C, then decomposed at 500 °C, and eventually converted to Ni and NiO[211]. Meanwhile, graphite oxide powder was thermally exfoliated to graphene oxide nanoplatelets; and the oxygen-containing groups on the nanoplatelets were thermally removed, resulting in the reduced graphene oxide. During this process, the Ni particles

were attached to the graphene nanoplatelets, yielding the Ni/graphene composite in powder. The following chemical equations demonstrate the processes of the decomposition and hydrogen reduction of $Ni(OAc)_2 \cdot xH_2O$. The reactions occurred at 160°C, 363°C and 500°C, respectively[211].

$$Ni(OAc)_2 \cdot xH_2O\ (s) \rightarrow Ni(CH_3COO)_2\ (s) + xH_2O \quad \text{(B.1)}$$

$$Ni(CH_3COO)_2\ (s) \rightarrow CH_3COCH_3\ (g) + NiCO_3\ (s) \rightarrow CO_2\ (g) + NiO\ (s) \quad \text{(B.2)}$$

$$NiO\ (s) + H_2\ (g) \rightarrow Ni\ (g) + H_2O\ (s) \quad \text{(B.3)}$$

Electronic structure

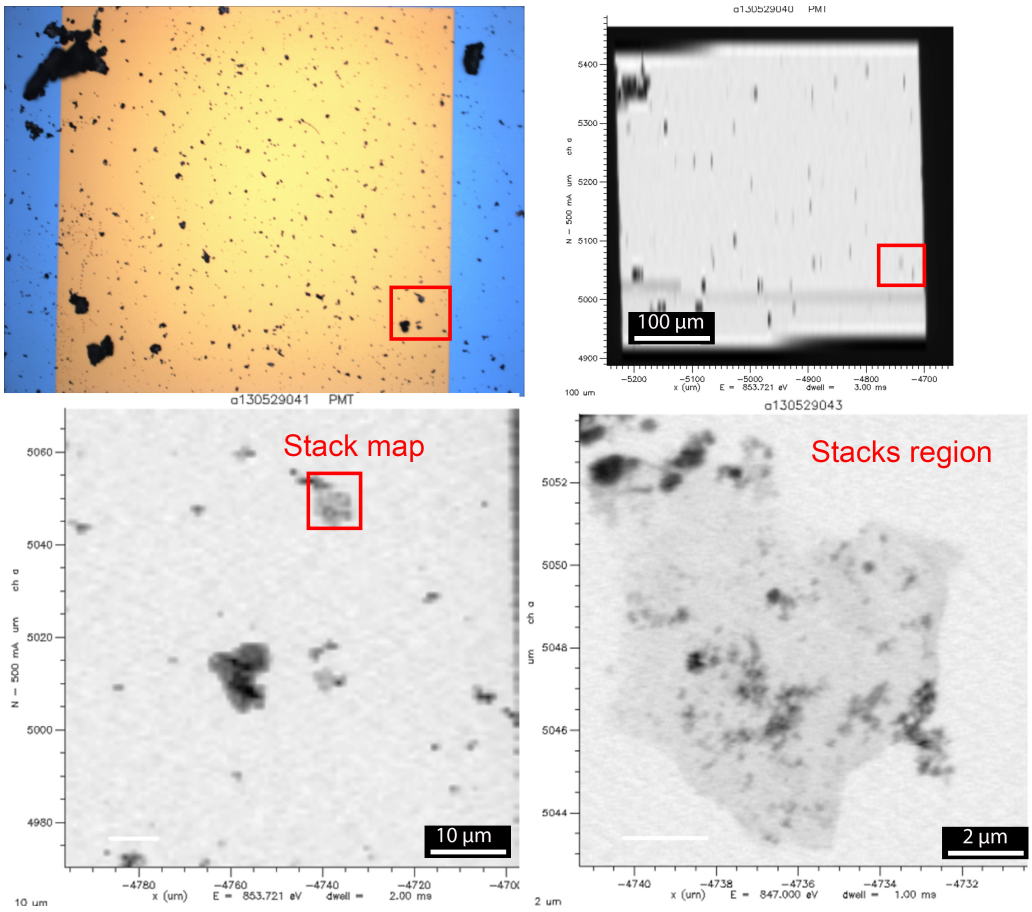

Fig. B.4 STXM chemical imaging of the Ni/graphene sample.

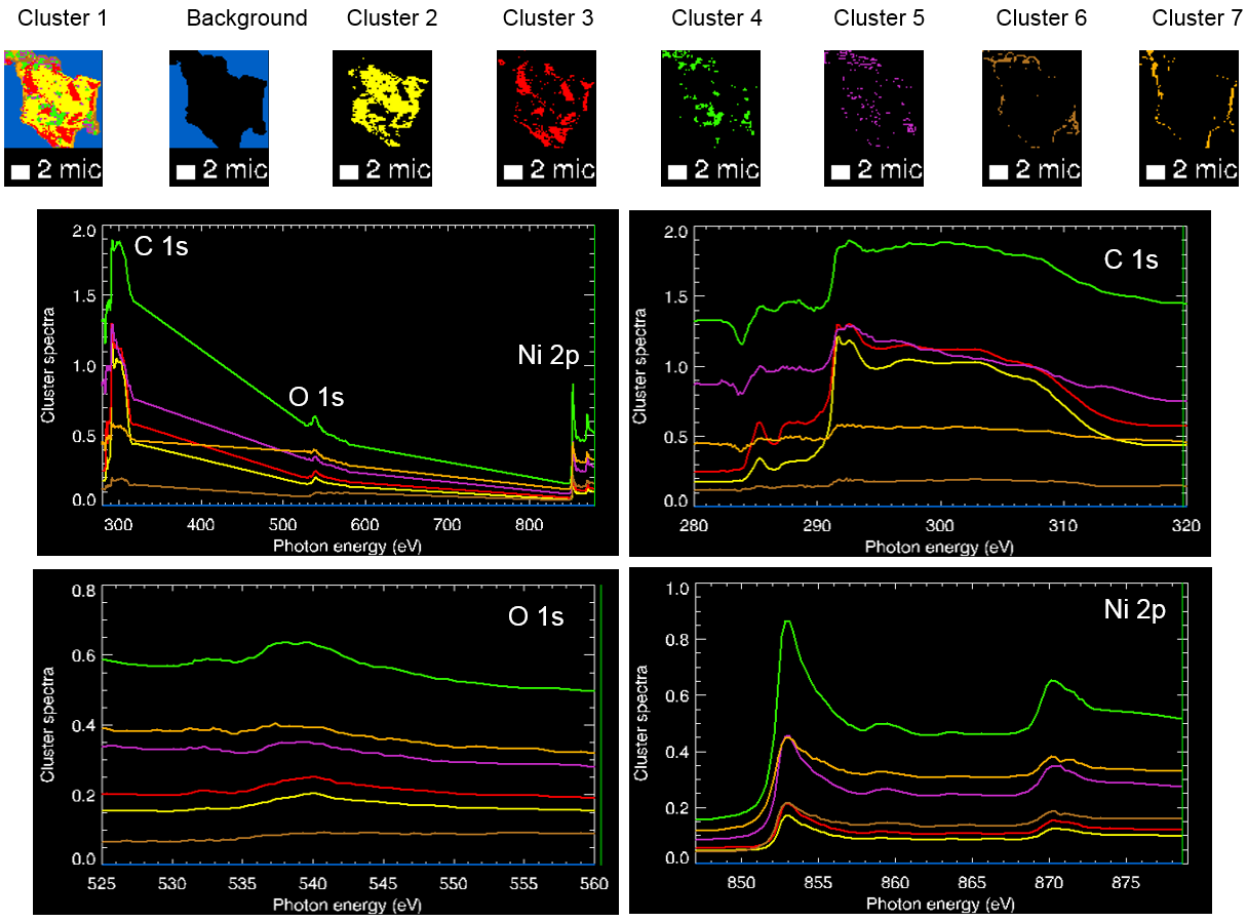

Fig. B.5 STXM XANES C 1s, O 1s and Ni 2p spectra of the single Ni/graphene nanoplatelet.

Characterizations of phase and morphologies

An X-ray diffractometer (XRD, Bruker D8) equipped with a Cu Kα tube (λ=0.1542 nm) was used to determine the crystal structures and composition of the samples, including the as-purchased $Ni(OAc)_2$, Ni obtained from the thermal treatment of $Ni(OAc)_2$ (500°C in H_2 for 1 h), Ni/graphene precursor, and the as-prepared Ni/graphene composite from the thermal treatment of precursor (RT to 800°C in Ar, then 500°C in H_2 for 1 h).

The XRD patterns in Fig. B.6a show that all peaks in the spectrum of as-purchased $Ni(OAc)_2$ disappeared after the thermal treatment at 500°C in H_2 atmosphere for 1 h. It suggests that the as-purchased $Ni(OAc)_2$ was successfully converted to the Ni particles during the thermal processing. The XRD patterns in Fig. B.6b illustrate that the Ni/graphene composite was obtained from the

thermal processing of the precursor. Compared to the spectrum of pure Ni in Fig. B.6a, an additional weak peak of the carbon (002) plane appeared in Fig. B.6b, confirming the existence of graphite-like structure.

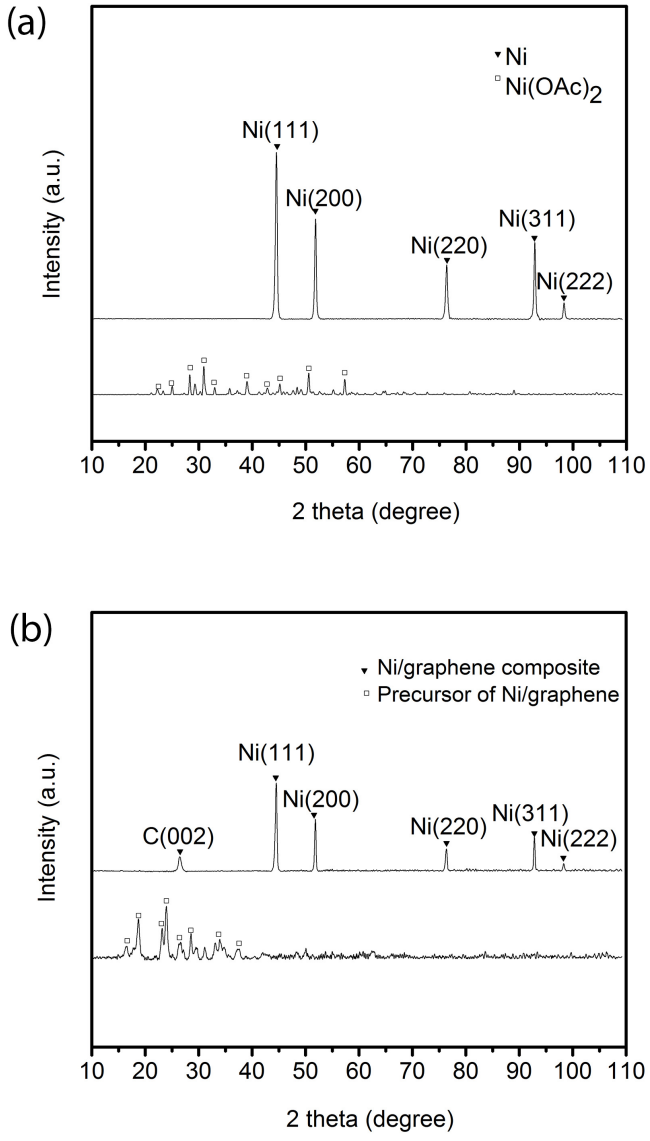

Fig. B.6 XRD patterns of samples before and after thermal processing: (a) as-purchased $Ni(OAc)_2$ and Ni; (b) Ni/graphene precursor and Ni/graphene from thermal processing (RT to 800°C in Ar, 500°C in H_2 for 1 h).

A scanning electron microscopy (SEM, FEI XL30) was performed to characterize the modification of graphene by Ni. The morphologies of graphene, $Ni(OAc)_2$, Ni, and Ni/graphene composite is shown in Fig. B.7. After the thermal treatment of the as-purchased $Ni(OAc)_2$ in hydrogen at 500°C for 1 h, Ni was obtained with significant decrease in particle size (Fig. B.7b and $Ni(OAc)_2$, inset).

Compared to the pure graphene sheet in Fig. B.7a, we observe that the Ni particles were homogeneously distributed over the graphene nanoplatelets, as shown in Fig. B.7c. The modified graphene system still remains structurally stable after the thermal treatment, which enables a high specific surface area of the composite that allows sufficient anchoring sites for the Ni particles. A higher magnification image (Fig. B.7d) further suggests a uniform distribution of the nano-sized Ni particles over the surface of graphene. This nanostructured composite can accommodate active sites for both atomic and molecular hydrogen, which should further contribute to an enhancement of hydrogen uptake capacities compared to the storage in pure graphene and bare metal.

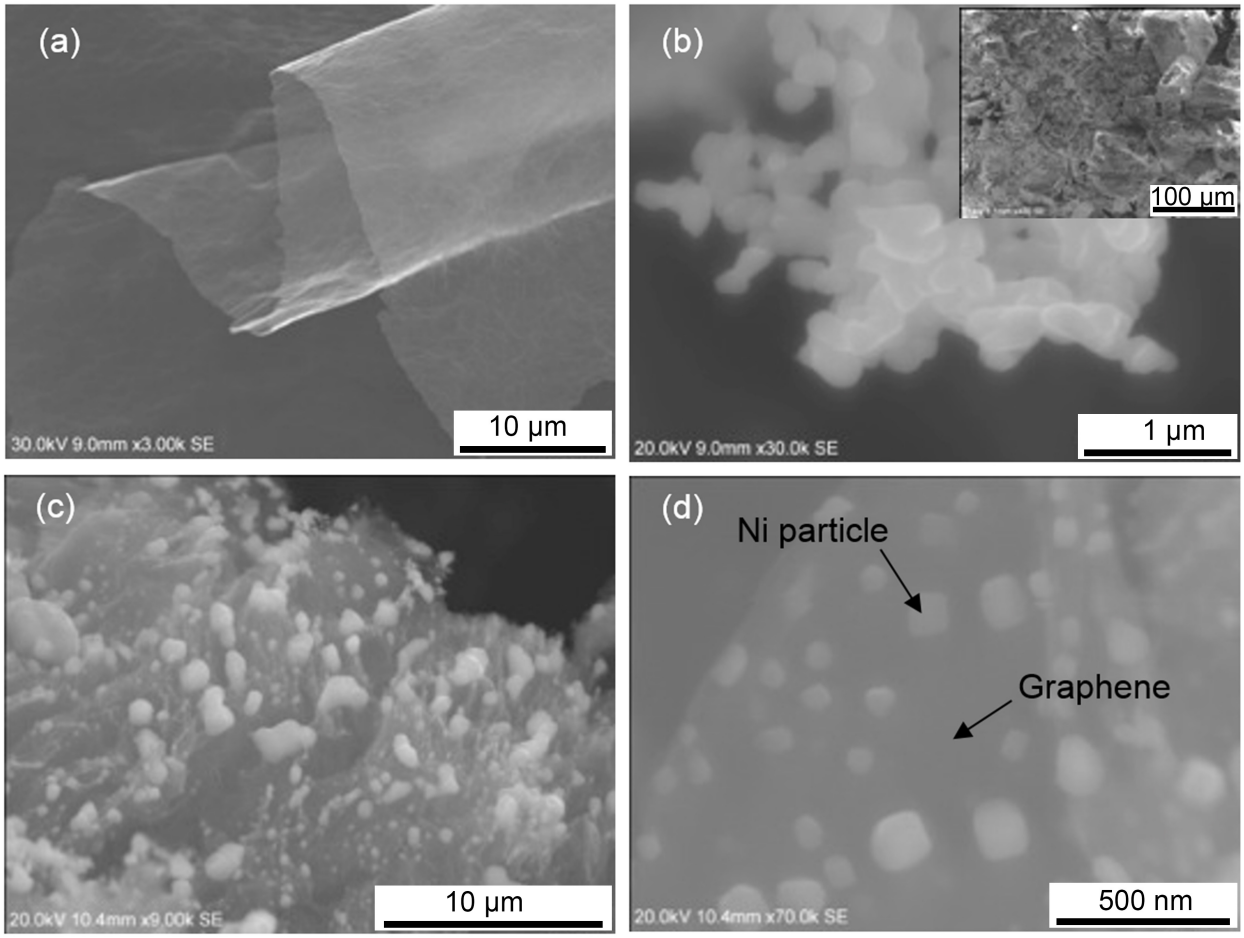

Fig. B.7 SEM images of graphene oxide, Ni and Ni/graphene composite: (a) graphene; (b) Ni (inset, $Ni(OAc)_2$); (c) and (d) low and high magnification of Ni/graphene composite from thermal processing (RT to 800°C in Ar, 500°C in H_2 for 1 h).

Supporting Information of Chapter 6

Hydrogen storage performance in Pd/graphene nanocomposites

Chunyu Zhou and Jerzy A. Szpunar

Department of Mechanical Engineering, University of Saskatchewan, Saskatoon, SK, S7N 5A9, Canada

Corresponding Author

Chunyu Zhou

Department of Mechanical Engineering, College of Engineering,

University of Saskatchewan, 57 Campus Drive, Saskatoon SK S7N 5A9, Canada.

*Email: chunyu.zhou@usask.ca

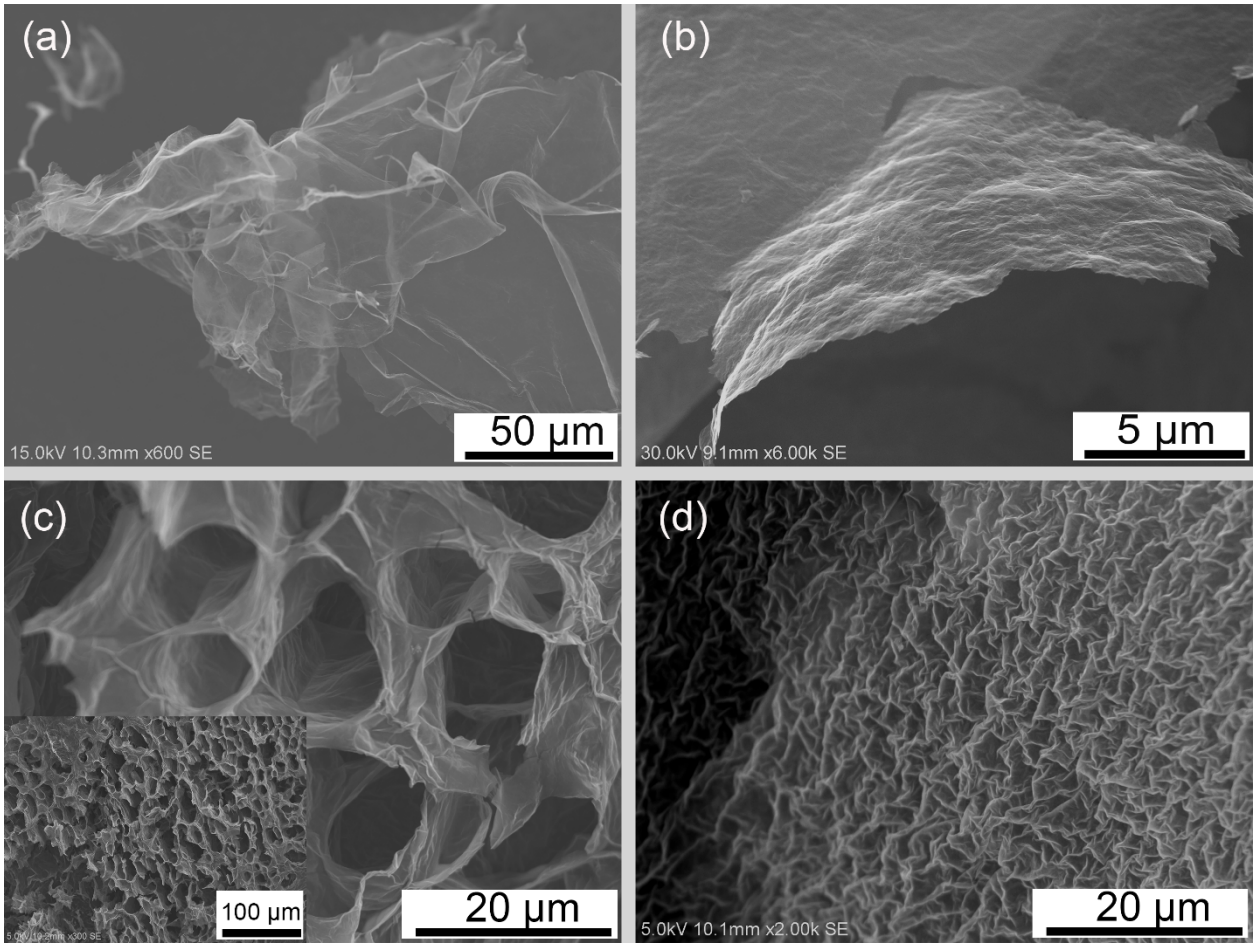

Fig. B.8 SEM micrographs of the as-prepared graphene.

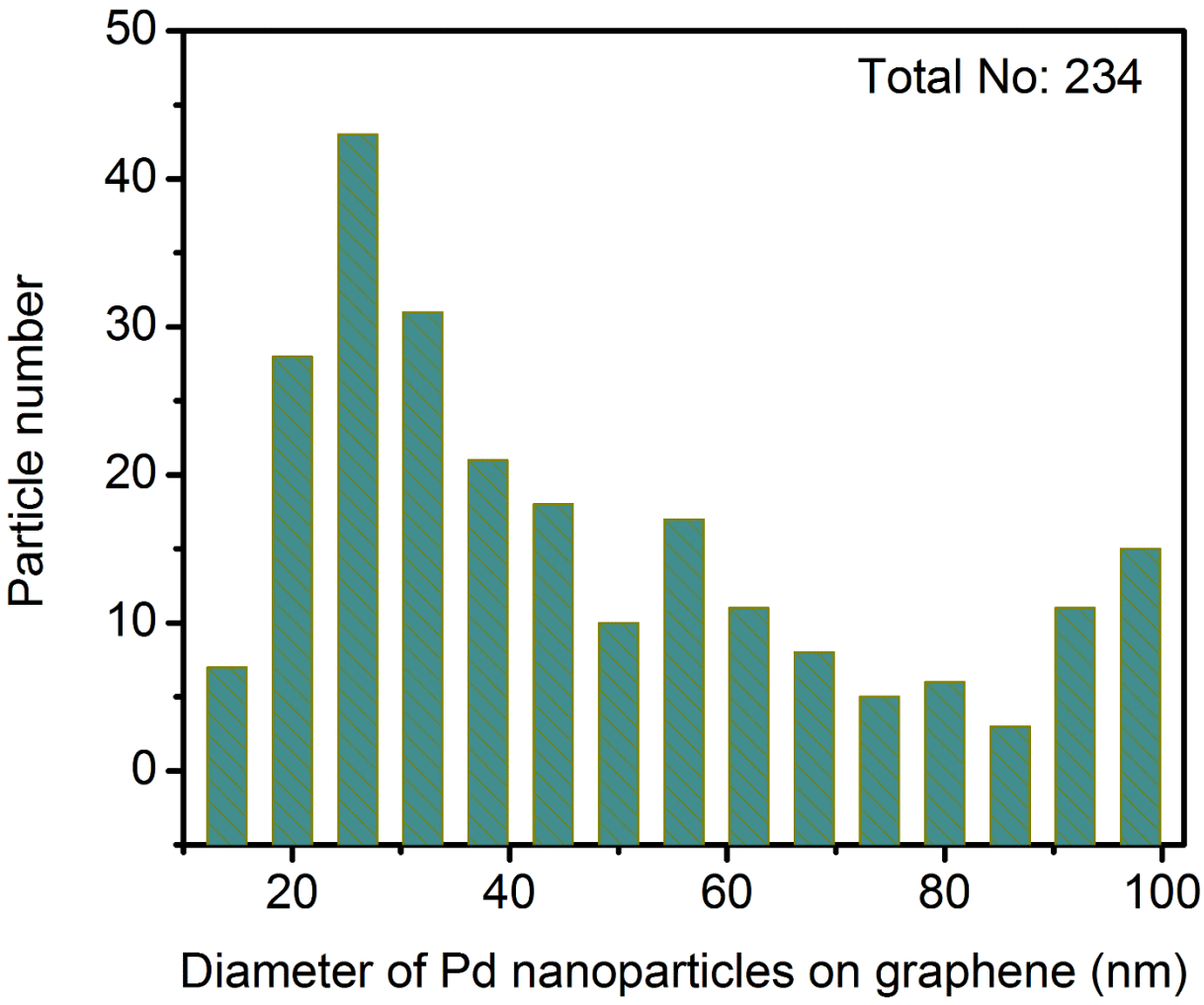

Fig. B.9 Particle size distribution of Pd nanoparticles on graphene sheets by SEM observation.

One can see in Fig. B.10a left, the pure graphene has significantly wrinkled, crumpled and folded structure with a microscale lateral dimension, indicating a high specific surface area. In Fig. B.10a right, the Pd compound had a bulk strip shape with a particle size of tens of microns. In Fig. B.10b, the $Pd(OAc)_2$ appeared to be well dispersed in the graphene matrix. The mechanical treatments and the usage of ethanol could disperse the Pd particles in graphene during the mixing step of the synthesis, and the freeze drying was also crucial to prevent the graphene sheets from agglomeration[212,213]. Consequently, the surface of the graphene sheet was entirely loaded with homogeneously dispersed $Pd(OAc)_2$ particles that were starfish shaped (Fig. B.10b) with a smaller particle size of less than 1 micron. Compared to the as-received sample, the significantly

decreased size of $Pd(OAc)_2$ particles implied that graphene substrate likely contributes to the dispersion of the compound. In addition, the starfish shaped $Pd(OAc)_2$ particles were partially attached to the graphene surface, as marked in the red square, while the rest evenly penetrated into the crumpled, wrinkled and folded graphene structure, as marked in the blue circle.

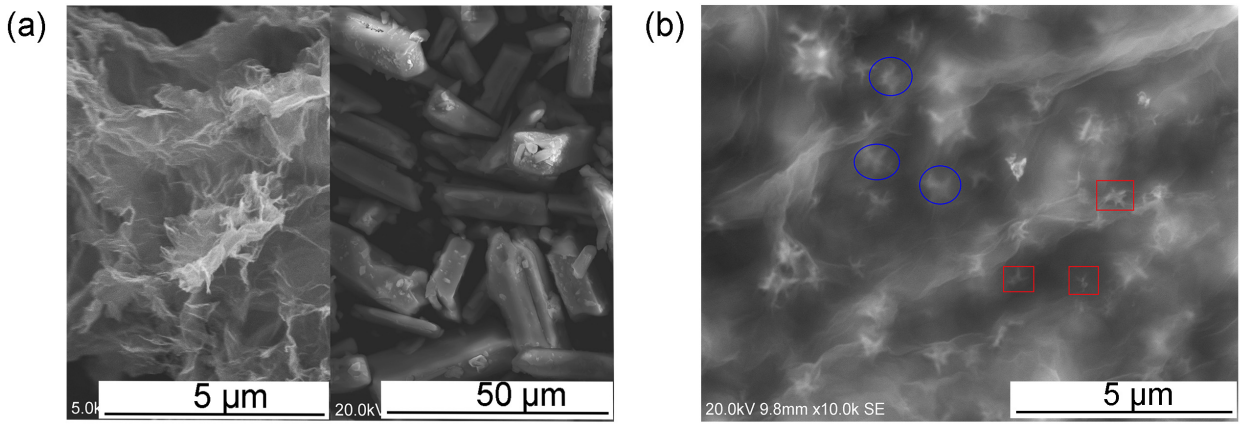

Fig. B.10 Morphology observations. SEM images of (a) as-prepared graphene (left), $Pd(OAc)_2$ (right), and (b) precursor $Pd(OAc)_2$/graphene.

After the thermal reduction at 300°C, the oxygen groups could be partially removed from the graphene sheets in the sorbents. To determine the amount of the remaining oxygen in the sorbent, we have conducted the EDS test on the 1%Pd/graphene composite as displayed in Fig. B.11. The yellow square area has the atomic percentages of oxygen and palladium of ~11.5 at.% and 0.8 at.%, respectively. This residual oxygen in the oxygen-containing groups could anchor the metal nanoparticles onto the graphene substrate[214] perhaps via the formation of Pd-O-C bond[178], which could further facilitate the stability of the Pd nanoparticles/clusters in the sorbents for a stable cycling of hydrogen storage.

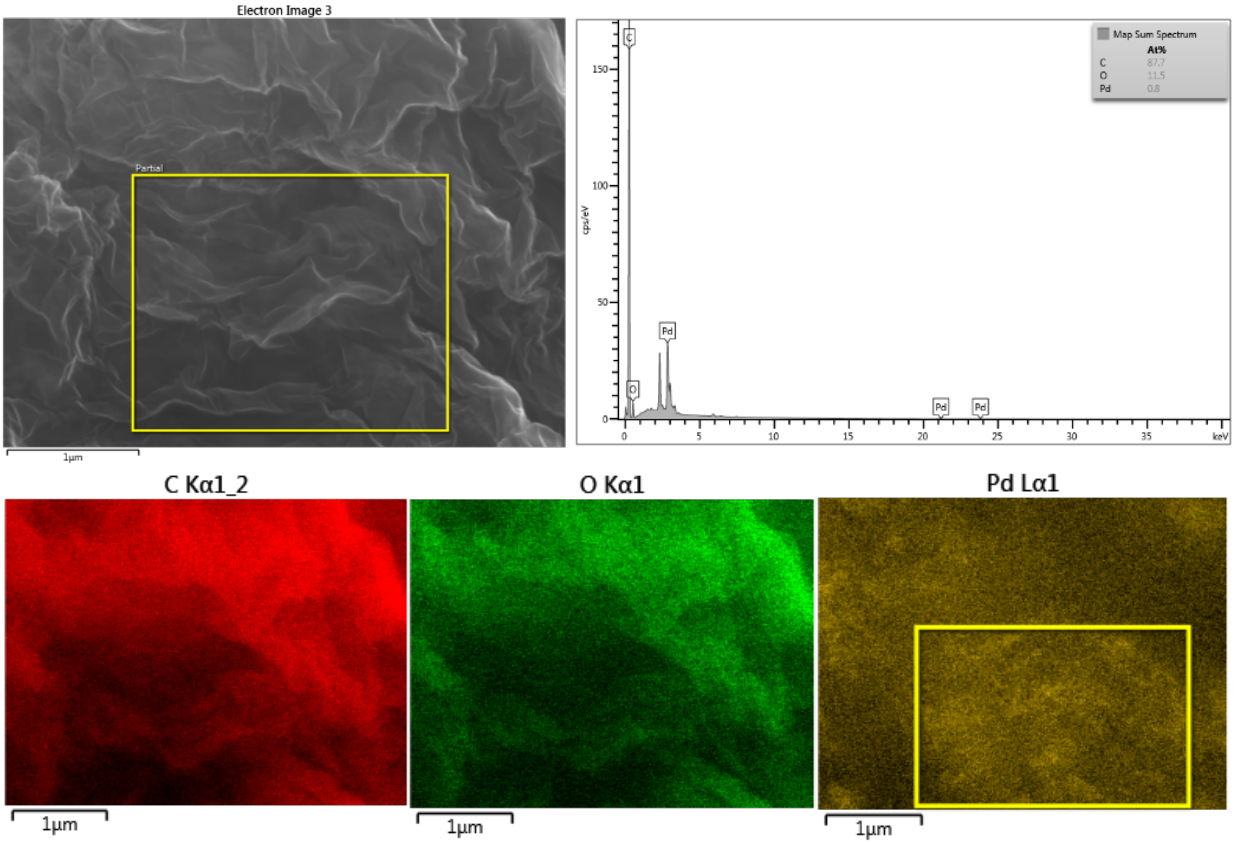

Fig. B.11 EDS mapping of the 1%Pd/graphene nanocomposite.

The SEM image in Fig. B.12a shows a fluffy structure of graphene with microscale lateral size. A corresponding EDS spectrum shows the C and O on the graphene surface with a C/O atomic ratio of 6.14 (86 at.%; 14 at.%). The EDS elemental mapping illustrates that these elements are homogeneously distributed on the surface of graphene flakes. In Fig. B.12b, SEM observation displays the fluffy structure of Pd/graphene nanocomposite, and EDS spectrum reveals the elements of C, O and Pd with a C/O/Pd atomic ratio to be 81.9 at.% : 13.8 at.% : 4.2 at.%. This result is consistent with the component atomic ratio used for the synthesis (Pd : C = 0.053; 5 at.% ; 95 at.%). In addition, the EDS elemental mapping implies that the C, O, and Pd, are uniformly spread over the nanocomposite.

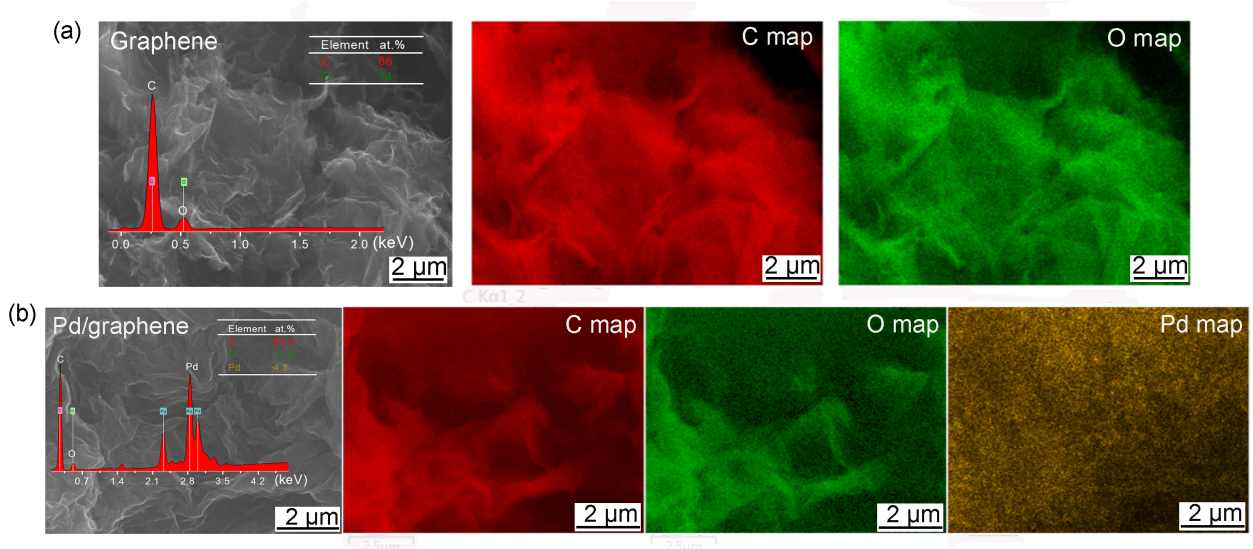

Fig. B.12 Elemental distribution of graphene and Pd/graphene nanocomposite. EDS spectrum and elemental mapping of (a) graphene and (b) 5%Pd/graphene nanocomposite.

Table B.1 Raman spectroscopy of the graphene and Pd/graphene nanocomposites (Gaussian function fitting).

Material	D band	G band	I_D (a.u.)	I_G (a.u.)	I_D/I_G
	Position (cm^{-1})				
1%Pd/graphene	1353.08	1586.15	615.47	524.02	1.17
5%Pd/graphene	1356.54	1592.50	146.43	160.65	0.91
Graphene	1362.88	1595.38	298.92	335.84	0.89

We used XRD to detect the crystal phases in the samples. Fig. B.13 displays the XRD pattern of the as-prepared Pd/graphene nanocomposite (blue line). For comparison, we collected the XRD patterns of $Pd(OAc)_2$/graphene (red line), and metallic Pd (green line) that was prepared by following the same thermal reduction procedures as the reference samples.

Two characteristic diffraction peaks appear in both spectra of Pd/graphene nanocomposite (blue line) and metallic Pd (green line), i.e., diffraction planes of (111) and (200) located at 2θ = 61.3° and 72.1° respectively, representing the presence of metallic Pd in the sample. In Pd/graphene XRD pattern (blue line), the complete absence of $Pd(OAc)_2$ pattern suggests a successful conversion of the Pd compound to the metallic Pd in the graphene matrix. In addition, the broadening of diffraction peaks in the nanocomposite, compared to those in metallic Pd, indicates a decreased Pd crystallite size, the average crystal size of Pd is calculated to be in the range of 9.8 ~13.5 nm using the Scherrer equation[128] based on the broadening of (111) peak.

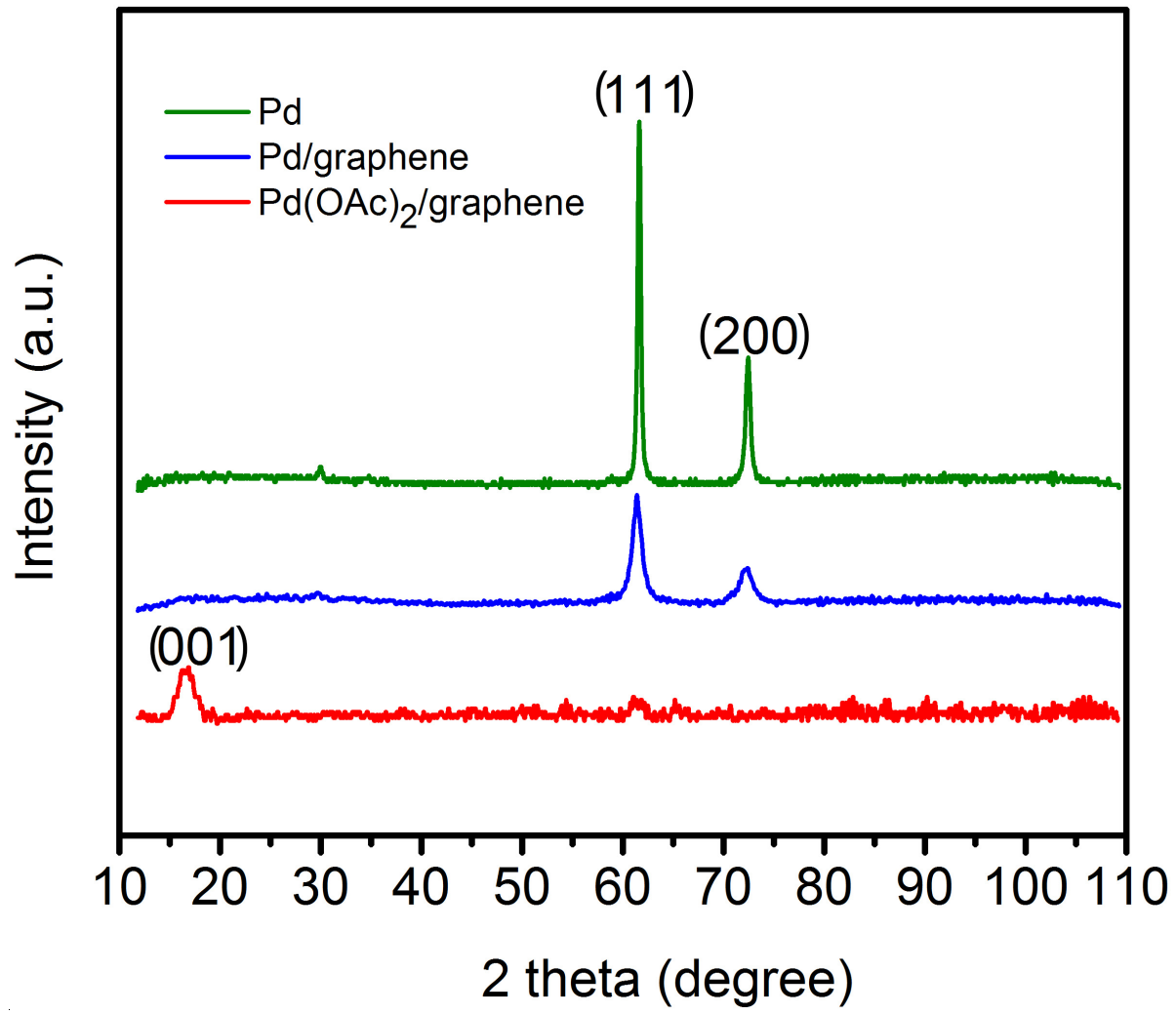

Fig. B.13 XRD (Cr Kα tube, λ=0.229 nm) patterns of metallic Pd, the as-prepared precursor $Pd(OAc)_2$/graphene and Pd/graphene nanocomposite.

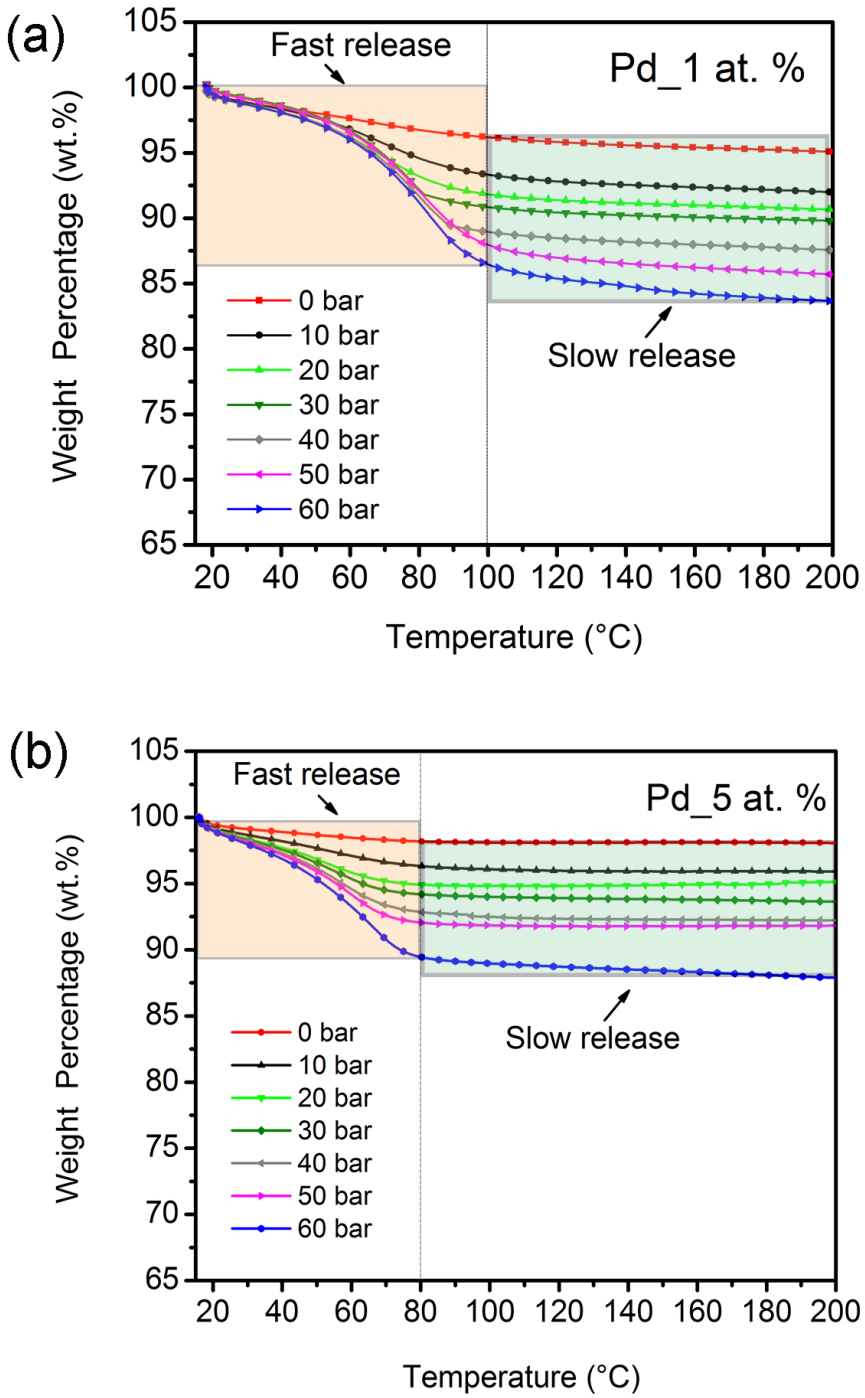

Fig. B.14 Thermogravimetric analysis. Hydrogen storage capacities in the Pd/graphene nanocomposites with a loading amount of (a) Pd 1 at.% and (b) Pd 5 at.% that were charged with hydrogen at pressures from 10 to 60 bar.

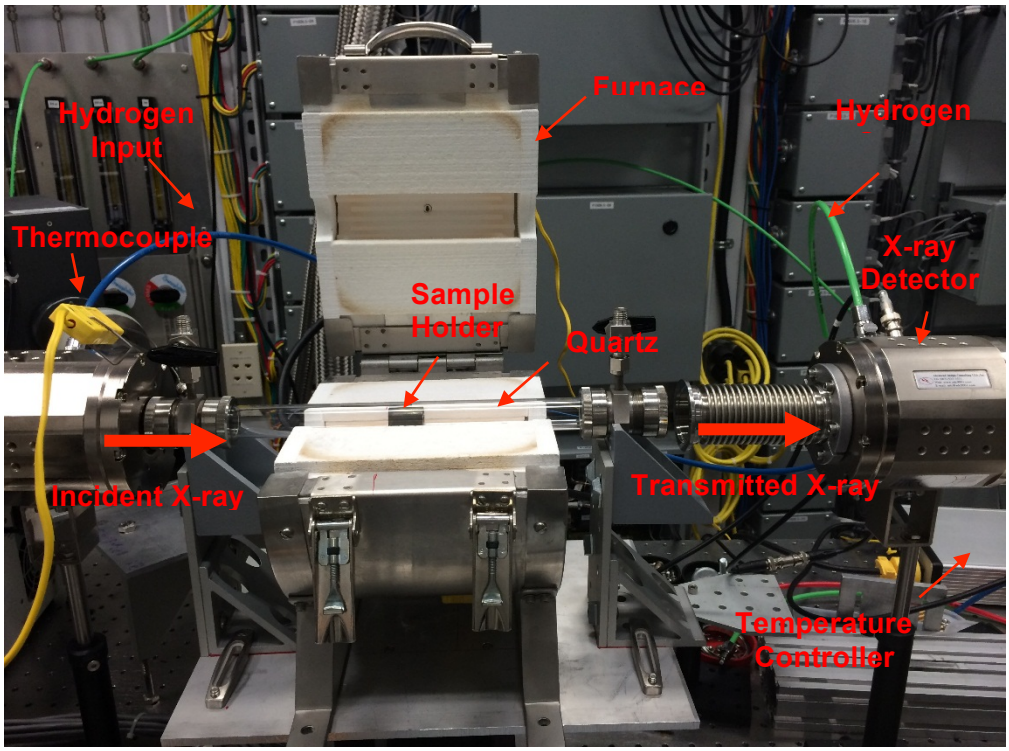

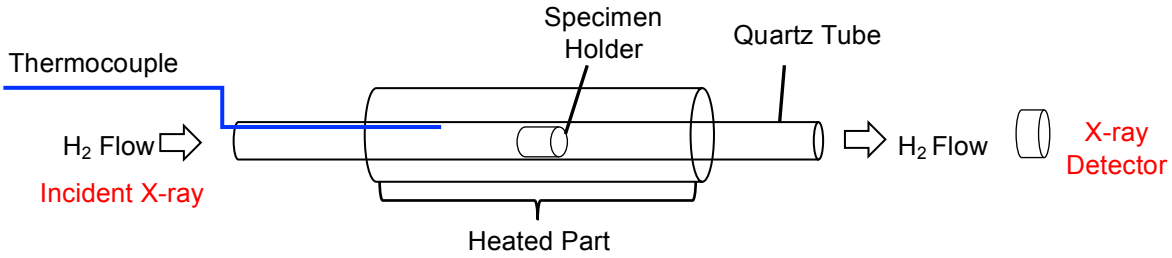

Fig. B.15 In-situ hydrogen reduction and X-ray absorption spectroscopy (XAS) characterization of Pd/graphene on SXRMB 06B1-1 beamline at the Canadian Light Source (CLS).

APPENDIX C. COPRYRIGHT PERMISSION

For previously published manuscripts that form a part of a thesis, written permission from the publisher (copyright holder) is required by the College of Graduate Studies and Research (CGSR).

Copyright Permission for manuscript 1 and 3 (Chapter 4 and Chapter 6)

"Use in Theses/Dissertations

The following wording is from the ACS Thesis/Dissertation Policy and the ACS Journal Publishing Agreement:

Reuse/Republication of the Entire Work in Theses or Collections: Authors may reuse all or part of the Submitted, Accepted or Published Work in a thesis or dissertation that the author writes and is required to submit to satisfy the criteria of degree-granting institutions. Such reuse is permitted subject to the ACS' "Ethical Guidelines to Publication of Chemical Research"; the author should secure written confirmation (via letter or email) from the respective ACS journal editor(s) to avoid potential conflicts with journal prior publication*/embargo policies. Appropriate citation of the Published Work must be made**. If the thesis or dissertation to be published is in electronic format, a direct link to the Published Work must also be included using the ACS Articles on Request author-directed link.

* Prior publication policies of ACS journals are posted on the ACS website.

** "Reprinted with permission from [COMPLETE REFERENCE CITATION]. Copyright [YEAR] American Chemical Society." Insert the appropriate wording in place of the capitalized words. This credit line wording should appear on the first page of your ACS journal article.

If your university requires written permission and your manuscript has not yet received a DOI (published ASAP), send a request to copyright@acs.org that includes the manuscript number, the name of the ACS journal, your complete mailing address, your 24-hour fax number, and the date

that you need to receive our reply. For manuscripts in ASAP status, please use the RightsLink permission system to obtain permission."

6/15/2016 Rightslink® by Copyright Clearance Center

Copyright Clearance Center RightsLink®

Home | Create Account | Help | Live Chat

ACS Publications Most Trusted. Most Cited. Most Read.

Title: Synthesis of Ni/Graphene Nanocomposite for Hydrogen Storage

Author: Chunyu Zhou, Jerzy A. Szpunar, Xiaoyu Cui

Publication: Applied Materials

Publisher: American Chemical Society

Date: Jun 1, 2016

Copyright © 2016, American Chemical Society

LOGIN

If you're a copyright.com user, you can login to RightsLink using your copyright.com credentials. Already a RightsLink user or want to learn more?

PERMISSION/LICENSE IS GRANTED FOR YOUR ORDER AT NO CHARGE

This type of permission/license, instead of the standard Terms & Conditions, is sent to you because no fee is being charged for your order. Please note the following:

- Permission is granted for your request in both print and electronic formats, and translations.
- If figures and/or tables were requested, they may be adapted or used in part.
- Please print this page for your records and send a copy of it to your publisher/graduate school.
- Appropriate credit for the requested material should be given as follows: "Reprinted (adapted) with permission from (COMPLETE REFERENCE CITATION). Copyright (YEAR) American Chemical Society." Insert appropriate information in place of the capitalized words.
- One-time permission is granted only for the use specified in your request. No additional uses are granted (such as derivative works or other editions). For any other uses, please submit a new request.

BACK | CLOSE WINDOW

Copyright © 2016 Copyright Clearance Center, Inc. All Rights Reserved. Privacy statement. Terms and Conditions.
Comments? We would like to hear from you. E-mail us at customercare@copyright.com

Copyright Permission for manuscript 2 (Chapter 5)

Author reusing their own work published by the Royal Society of Chemistry

"You do not need to request permission to reuse your own figures, diagrams, etc, that were originally published in a Royal Society of Chemistry publication. However, permission should be requested for use of the whole article or chapter except if reusing it in a thesis. If you are including an article or book chapter published by us in your thesis please ensure that your co-authors are aware of this.

Reuse of material that was published originally by the Royal Society of Chemistry must be accompanied by the appropriate acknowledgement of the publication. The form of the acknowledgement is dependent on the journal in which it was published originally, as detailed in 'Acknowledgements'."

Rights retained by authors

"When the author accepts the exclusive licence to publish for a journal article, he/she retains certain rights that may be exercised without reference to the Royal Society of Chemistry.

- *Reproduce/republish portions of the article (including the abstract).*
- *Photocopy the article and distribute such photocopies and distribute copies of the PDF of the article for personal or professional use only (the Royal Society of Chemistry makes this PDF available to the corresponding author of the article upon publication. Any such copies should not be offered for sale. Persons who receive or access the PDF mentioned above must be notified that this may not be made available further or distributed.).*
- *Adapt the article and reproduce adaptations of the article for any purpose other than the commercial exploitation of a work similar to the original.*
- *Reproduce, perform, transmit and otherwise communicate the article to the public in spoken presentations (including those that are accompanied by visual material such as slides, overheads and computer projections).*

- *The author(s) must submit a written request to the Royal Society of Chemistry for any use other than those specified above.*
- *All cases of republication/reproduction must be accompanied by an acknowledgement of first publication of the work by the Royal Society of Chemistry, the wording of which depends on the journal in which the article was published originally. The acknowledgement should also include a hyperlink to the article on the Royal Society of Chemistry website.*
- *The author also has some rights concerning the deposition of the whole article."*